

DESIGN AND OPTIMIZATION OF A HIGH
TEMPERATURE REACTOR FOR THE PRODUCTION
OF II-VI COMPOUNDS VIA COMPUTER MODELS
AND STATISTICAL EXPERIMENTATION

By

CHRISTOPHER D. SHAY

Bachelor of Science

University of Texas at Dallas

Richardson, Texas

1991

Submitted to the Faculty of the
Graduate College of the
Oklahoma State University
in partial fulfillment of
the requirements for
the Degree of
MASTER OF SCIENCE
December, 1998

DESIGN AND OPTIMIZATION OF A HIGH
TEMPERATURE REACTOR FOR THE PRODUCTION
OF II-VI COMPOUNDS VIA COMPUTER MODELS
AND STATISTICAL EXPERIMENTATION

Thesis Approved:



Thesis Advisor



Co-Advisor



Committee Member



Dean of the Graduate College

PREFACE

The purpose of this research was to design a high-temperature, vapor phase reactor for the production of Group II-VI compounds for specialty applications. There is a reactor in use by the sponsor, but it suffers from poor process control that inevitably results in low product yield and waste generation. The reactor is unique in that it is diffusion mass transfer limited, as opposed to kinetically controlled. This situation necessitated extensive computational fluid dynamic (CFD) modeling to produce a proposal for an improved design. The model entailed the adaptation of expressions to account for the undetermined kinetics, as well as empirical coefficients to adequately describe critical secondary flow phenomena within the reactor.

A reactor design was proposed that fully addresses the technical and business hurdles posed by the process. The new reactor's operating and physical parameters were optimized via statistically designed experiments that were performed within the computer model. The product yield was maximized while achieving the desired batch output quantity and proper product distribution within the reactor. Additionally, functions were generated to allow for prediction of reactor performance across a range of input conditions.

There are several persons and organizations that deserve my gratitude for the successful completion of this work. My advisors, Drs. A.J. Johannes and Gary Foutch, provided invaluable assistance in areas not limited to research. Dr. AJ's frankness and wisdom were especially helpful in the course of this two-year journey, as was Dr. Foutch's attention to all the details and sense of personal dedication. Also, Dr. Afshin Ghajar's flexibility and sincere helpfulness are appreciated.

My fellow students, especially Trey Morrison, are due special mention. Trey's diligence and thoroughness provided balance to the research team to counteract my own deficiencies. Although he would invariably espouse points incongruous to mine, the many contrarities provided a great breadth of reasoning that is necessary in research and in life. Other characters to be thanked include Doug Ratzlaff and Siva Natarajan for their dedication to cultural enlightenment. The Eagle-Picher staff members; Mr. Tom Potts and Mr. Mark Dudley, are due thanks for their time and help, as well. To the other persons too numerous to mention that also deserve thanks, I shall express my gratitude individually.

Appreciation is due the entire faculty and staff at the School of Chemical Engineering. I have yet to encounter a group as committed to the teaching and assisting of others.

Financial assistance provided by Oklahoma State University, The Oklahoma Center for the Advancement of Science and Technology, and Eagle-Picher Technologies, Inc, is greatly appreciated.

TABLE OF CONTENTS

Chapter	Page
I. INTRODUCTION.....	1
Group II-VI Compounds and Applications.....	1
Current Synthesis Reactor and System.....	3
Analysis of Historical Performance of the System.....	5
Objectives.....	7
II. LITERATURE REVIEW.....	9
Introduction	9
Review of Production Methods.....	9
Bulk Synthesis.....	10
Growth of Single Crystals.....	12
Thin Film Methods and Device Fabrication.....	14
Physical Methods.....	15
Chemical (Reactive) Methods.....	16
Chemical Vapor Deposition (CVD).....	16
Examples.....	16
Deposition Processes and Theory.....	17
Mass Transport.....	19
Heat and Energy Considerations.....	20
Reaction Kinetics.....	21
Nucleation and Aerosol Dynamics.....	23
Types of Nucleation.....	23
Condensation Phenomena	24
Reactor Design Methods.....	27
Dimensionless Parameters.....	27
Other Design Calculations.....	29
Examples of Methods.....	29
Examples of Commercial Reactors and Processes	30
Reactor Models and Simulations.....	31
Elements of a Reactor Model.....	32

Chapter	Page
Examples of Numerical Methods.....	32
Computational Fluid Dynamic (CFD) Models...	33
Optimization of Reactors and Processes.....	35
Design of Experiments (DOE).....	35
Analysis of Variation (ANOVA).....	37
Response Surface Methodology (RSM).....	37
Examples of DOE/RSM Applied to Process Models and Simulators.....	38
Process Prediction and Optimization by Artificial Neural Networks (ANN).....	39
 III. RESEARCH AND OPTIMIZATION OF THE PRESENT SYSTEM.	 40
Introduction.....	40
Experimental Study.....	41
Basis for the Study.....	41
Dimensionless Parameter Analysis.....	41
Outline of ZnSe Experimental Study.....	44
Rationale for Establishment of Factor Levels...	46
Design Matrix.....	48
Design Grid.....	49
Experimental Design Results.....	52
Results Summary Method.....	53
Statistical Analysis of Run Data.....	54
Response Variables.....	55
Analysis of Non-Subjective Response Variables..	56
Other Non-Subjective Response Variables.....	62
Analysis of Subjective Response Variables.....	62
Follow-up Runs.....	64
Response Variable Linearity.....	64
Conclusions and Discussion.....	66
Summary of Results.....	66
Follow-up Analysis and Confirmation.....	69
Recommendations and Conclusions.....	71
Summary.....	73
 IV. PROPOSED NEW REACTOR DESIGN AND MODELING.....	 75
Introduction.....	75

Chapter	Page
Basis for the Design.....	75
Alternative Designs Considered.....	78
Overview of the New Design.....	79
New Design Research Objectives.....	82
CFD Modeling of Proposed New Design.....	82
Modeling Theory and Steps.....	82
Purpose and Classification of the Model.....	83
FLUENT CFD Basics.....	84
Summary of Governing Equations.....	86
Modeling Methods and Approach.....	89
Reactions and Kinetic Rate Forms.....	89
Transport Properties.....	92
Empirical Parameter Fitting.....	92
Summary of Assumptions.....	93
Modeling Results and Discussion.....	95
Conclusions and Recommendations.....	97
 V. NEW DESIGN OPTIMIZATION.....	 98
Introduction.....	98
FLUENT Model Experimental Designs.....	99
Design Optimization Study I.....	99
Results and Analysis.....	102
Reactor Sizing and Conversion.....	104
Preliminary Conclusions.....	105
Design Optimization Study II.....	105
Prediction of Plugging in the Steady-State Model	106
Results and Analysis.....	107
Confirmation Runs.....	112
FLUENT/UNS Profiles of the System.....	113
Discussion of New Design Results.....	122
Effect of Inert Carrier Gas.....	122
Using the Experimental Data for Process Prediction.....	123
Response Surfaces.....	123
Equations for the Surfaces.....	125
Summary of Steps for Establishing	
New Operating Conditions.....	126
 VI. CONCLUSIONS AND RECOMMENDATIONS.....	 128

Chapter	Page
BIBLIOGRAPHY.....	132
APPENDICES.....	141
APPENDIX A - DERIVED KINETIC AND THERMODYNAMIC PARAMETERS.....	141
APPENDIX B - DESIGN BASIS CALCULATIONS.....	145
APPENDIX C - FLUENT/UNS DOCUMENTATION OF EXPERIMENTS.....	151

LIST OF TABLES

Table		Page
2-1	Dimensionless Parameter Groups Characterizing Transport Phenomena in CVD.....	28
2-2	Comparison of Four Experimental Approaches.....	36
3-1	Reactor Tube Dimensions.....	46
3-2	Experimental Design Matrix.....	49
3-3 (a & b)	Factors and Interactions Symbols Key.....	51
3-4	Matrix Design Grid.....	51
3-5	Summary of Factor Levels.....	52
3-6	Results Criteria and Tabulation Method.....	53
3-7 (a & b)	Response Variables and Classifications for the Experimental Runs	55
3-8	Results for Yield Response Variable.....	56
3-9	Results for Wormhole Length Response Variable.....	61
3-10	Subjective Response Variables Results and Key.....	63
3-11	Product Color Response Variable Results.....	63
3-12	Product Consistency Response Variable Results.....	64
3-13	Follow-up Run Conditions.....	65
4-1	Summary of the Design Basis.....	78

Table		Page
4-2	Characteristics of the Proposed New Design.....	80
4-3	Key Kinetic and Transport Model Variables.....	94
4-4	Sample of Empirical Parameter Fitting Regimen.....	96
5-1	Design Optimization Study I Factors and and Levels.....	99
5-2	Rationale for Experimental Levels.....	100
5-3	Study I Background Variables.....	101
5-4	Study I Factor Results (Yield).....	102
5-5	Study I Interactions Results (Yield).....	104
5-6	Study II Factors and Levels.....	106
5-7	Study II Results (Yield).....	107
5-8	Study II Results (Plugging Factor).....	107
5-9	Optimum Reactor Dimensions and Conditions.....	113
A-1	Experimental Rate Data.....	143
A-2	Comparison of Calculated Activation Energies for ZnSe Reaction	144
B-1	Steady State Mole Fractions from FLUENT for Confirm05 Run	148
B-2	Inlet Volumetric Flow Rates for Confirm05 Run.....	148
B-3	Outflow Mole Fractions from FLUENT for Confirm05 Run.....	149
C-1	Study I Experimental Grid.....	152
C-2	FLUENT DDN Reactor Coordinates.....	154
C-3	FLUENT Nozzle Coordinates.....	155
C-4 (a & b)	Operating Parameters Flow Calculations.....	156

Table		Page
C-5	Operating Parameters Input Grid.....	158
C-6	Study I Run Data.....	159
C-7	Study I Factor Analysis.....	160
C-8	Study I Interactions Analysis.....	162
C-9	Study II FLUENT DDN Coordinates.....	164
C-10	Study II Factor Key.....	164
C-11	Study II Run Data and Results (Yield).....	165
C-12	Study II Run Data and Results (Plugging Factor).....	166
C-12	RSM Data Extracted from Study II Results.....	167

LIST OF FIGURES

Figure		Page
1-1	Sketch of Current Eagle-Picher Reactor.....	3
2-1	CVD Processes.....	18
2-2	Elements of a CVD Reactor Model.....	32
3-1	RT/AF Interaction Check	57
3-2	FT/XS Interaction Check.....	58
3-3	BRT/RT Interaction Check.....	58
3-4	FT/BR Interaction Check.....	58
3-5	XS/BR Interaction Check.....	58
3-6	Interaction of Boiling Rate and XS Se on Product Yield.....	59
3-7	Interaction of Reactor Tube and Boiler Ramp Time on Product Yield	60
3-8	Interactions Check for AF/BR on Wormhole Length.....	62
3-9	Linearity Check for XS Se Effects.....	65
4-1	New Reactor System Drawing.....	81
4-2	Steps to Creating Physical Model in FLUENT/UNS.....	85
5-1	Effect of Zinc Flow Rate on Yield.....	103
5-2	Effect of Nozzle Diameter an Product Yield.....	103

Figure	Page
5-3	Effect of Zinc Nozzle Diameter and Flow Rate on ZnSe Product Yield 108
5-4	Effect of Zinc Nozzle Diameter and Velocity on ZnSe Product Yield 109
5-5	Effect of Selenium Nozzle Diameter and Flow Rate on ZnSe Yield..... 110
5-6	Effect of Zinc Nozzle Diameter and Flow Rate on Plugging Factor..... 111
5-7	Effect of Selenium Nozzle Diameter and Flow Rate on Plugging Factor..... 111
5-8	Reactant Flow Rate Effects on ZnSe Product Yield..... 112
5-9	FLUENT Profiles of Zn Mole Fraction (optimized conditions)..... 115
5-10	FLUENT Profiles of Se Mole Fraction (optimized conditions)..... 116
5-11	FLUENT Profiles of ZnSe Mole Fraction(optimized conditions)..... 117
5-12	FLUENT Profiles of ZnSe Mole Fraction (unoptimized conditions)..... 118
5-13	FLUENT Profiles of Velocity Vectors (optimized conditions)..... 119
5-14	FLUENT Profiles of Velocity Vectors (unoptimized conditions)..... 120
5-15	FLUENT Temperature Profiles..... 121
5-16	Response Surface for Effect of Reactant Flow Rates at Constant Inlet Diameters on Product Yield..... 124
5-17	Response Surface for Effect of Nozzle Diameter and Total Flow Rate on the Plugging Factor..... 125
5-18	Steps to Establishing New Operating Conditions..... 127

NOMENCLATURE

Symbols

-	At the low level setting
+	At the high level setting
a	Radius of falling aerosol particle, m
A	Cross-sectional area, m^2
A_E	Activation energy, J/kmol
AF	Argon Flow, ml/min
BR	Boiling Rate, in terms of $^{\circ}C$ setpoint
BRT	Boiler Ramp Time, hrs
C	Total molar concentration, moles/ m^3
c_A	Concentration of A, moles/L, kg/m^3
c	Concentration, moles/L
CD	Cooldown Time
cP	Centipoise
C_p	Constant pressure heat capacity, J/mol-K
eV	Energy band gap, electron-volts
D	Diameter, m
D_m	Mass diffusivity, m^2/sec
D_{ij}	Diffusivity of component i in component j, m^2/sec
D_i^T	Effective thermal binary diffusivity, $kg/m-sec$
e	Exponential
F	FLUENT body force term, N/m^2
F_{A0}	Feed rate of component A, moles/sec
FR	Flow Rate, mol/sec
FRS	Flow Rate Selenium, mol/sec

FRZ	Flow Rate Zinc, mol/sec
FT	Furnace Temperature, K
g_c	Gravitational constant, 9.8 m/sec^2
G	Gibbs free energy, J/kmol
h_j	FLUENT notation for enthalpy of j^{th} component, J/kmol
H	Enthalpy, J/Kmol
ΔH_{rxn}	Heat of reaction, J/kmol
ΔH_f	Heat of formation, J/kmol
J	Formation rate of critical nuclei, 1/sec
J_j	FLUENT notation for diffusion of j^{th} component, m^2/sec
\mathbf{J}_i	Diffusive flux of component i, $\text{kg/m}^2\text{-sec}$
\mathbf{j}_i^C	Concentration driven component of diffusive flux of i, $\text{kg/m}^2\text{-s}$
\mathbf{j}_i^T	Temperature driven component of diffusive flux of i, $\text{kg/m}^2\text{-s}$
k	Rate constant, L/mol-s
k	FLUENT molecular conductivity, W/m-K
k_r	Thermal diffusion ratio, dimensionless
k_{ij}^T	Thermodiffusion ratio, dimensionless
k_c	Thermal conductivity, $\text{kg-m/s}^3\text{-K}$, W/m-K
k_o	Pre-exponential factor
K	Temperature, kelvin
K_{eq}	Equilibrium constant, 1/sec
K_n	Knudsen number, dimensionless
L	Volume, m^3
\dot{m}_i	Mass flow rate of component i, g/sec
M_i	Molecular weight of component i, kg/kmol
M	Molar concentration, moles/liter
\dot{m}	Molar flow rate of component i, mol/sec
NA	Nozzle Angle, degrees
ND	Nozzle Diameter, mm
NDS	Nozzle Diameter of Selenium inlet, mm
NDZ	Nozzle Diameter of Zinc inlet, mm

NP	Nozzle Position (distance from centerline), mm
N_A	Avogadro's number, 6.023×10^{23}
N's	Number of nines of purity, %
N_{Re}	Reynolds number, dimensionless
p_∞^T	Saturated vapor pressure at temperature T, Pa
P	Partial pressure, Pa
p	Pressure, Pa
Pe_m	Mass Peclet number, dimensionless
\dot{q}'''	FLUENT notation for volumetric heat source term, $J/m^3\text{-sec}$
Q_0	Dimensionless mass transfer rate
r	FLUENT notation for radial coordinate
$-r_A$	Rate of disappearance of component A, mol/sec
RL	Reactor Length, mm
RT	Reactor Tube
R^2	Regression coefficient
$-R_A$	Rate of disappearance of component A, mol/sec
Ra	Rayleigh number, dimensionless
R	Gas constant, $8.314 \text{ m}^3\text{-Pa/mol-K}$
Re	Reynolds number, dimensionless
\mathcal{R}_j^G	Gas phase reaction j
S	FLUENT modulus of the mean rate-of-strain tensor
S	Entropy, kJ/kg-K
S	Saturation ratio, dimensionless

Sc	Schmidt number, dimensionless
S _h	FLUENT heat of reaction, J/kmol
Sm	FLUENT accumulation term
t	Time, sec
T	Temperature, K
T ^{ref}	Reference Temperature, K
u	FLUENT notation for velocity, m/sec
v	Velocity, m/sec
ν	Kinematic viscosity, m ² /sec
V	Volume, m ³
V _o	Volumetric flow rate, m ³ /sec
v _{ij} ^G	Stoichiometric coefficient of i th species in j th reaction
Wt	Weight of product, grams
x _i	Mass fraction of component i
x	FLUENT notation for axial coordinate, m
X _A	Conversion of A, %
XS	Excess Selenium, moles
y _i	Mole fraction of component i
ZT	Zone Temperature, K

Greek Letters

α	Effective Prandtl numbers, dimensionless
α _c	Critical nucei constant, dimensionless
α _t	Thermal diffusivity, kg/m-sec
β	Volume expansion coefficient, 1/K
Δ	Change in
Δ	Low – High Factor Effect
ε	Rate of dissipation of turbulent kinetic energy, W
ε _A	Expansion coeffiecient, dimensionless

δ	Standard molar volume gas constant, m ³ /mole
γ	Pressure parameter, dyns/cm
ρ	Density, kg/m ³
∂	Partial derivative
ψ_{AB}	FLUENT binary diffusivity coefficient, m ² /sec
σ	Population standard deviation
τ	Momentum flux, N/m ²
τ	Reactor residence time, sec
μ	Viscosity, cP
μ_{eff}	FLUENT effective viscosity, kg/m-s
μ_{mol}	FLUENT molecular viscosity, kg/m-s
∇	Tensor notation symbol
ω	Mass fraction
ω_i	Normalized factor effect, dimensionless
Σ	Summation

Subscripts and Superscripts

C	Concentration, moles/L
o	Initial
l	Final
o	At reference conditions
°	Degree, K
eg	At equilibrium
g	Gas phase
G	Gas phase
i	Component i
∞	A point at an infinite distance
j	Component j
T	Thermally driven

Diacritical Marks

→	The vector of
.	Rate of
—	Average

Abbreviations

2D	Two-dimensional
3D	Three-dimensional
AACVD	Aerosol Assisted Chemical Vapor Deposition
ANOVA	Analysis of Variation
AVG	Average
C	Centigrade
CAD	Computer Aided Design
CBD	Chemical Bath Deposition
CFD	Computational Fluid Dynamics
DOE	Design of Experiments
E-P	Eagle-Picher Industries, Inc.
g	grams
HPCVD	High Pressure Chemical Vapor Deposition
IR	Infrared
kgs	kilograms
K	Kelvin
LCVD	Laser-induced Chemical Vapor Deposition
LED	Light Emitting Diode
LFAR	Laminar Flow Aerosol Reactor
ln	Natural logarithm
LPCVD	Low Pressure Chemical Vapor Deposition
LPMOCVD	Low Pressure Metallorganic Chemical Vapor Deposition

MBE	Molecular Beam Epitaxy
mid	Midpoint Run
ml	milliliters
MOCVD	Metallorganic Chemical Vapor Deposition
mol	Mole
MOVPE	Metallorganic Vapor Phase Epitaxy
PCVD	Photo-assisted Chemical Vapor Deposition
PECVD	Plasma Enhanced Chemical Vapor Deposition
PFC	Plugging Factor Criteria
PFR	Plug Flow Reactor
RSM	Response Surface Methodology
SCTCVD	Supercritical fluid Transport Chemical Vapor Deposition
SCVT	Seeded Chemical Vapor Transport
SEM	Scanning Electron Microscopy
SPC	Statistical Process Control
SPVT	Seeded Physical Vapor Transport
UNS	Unstructured

CHAPTER I

INTRODUCTION

Group II-VI Compounds and Applications

The focus of this work is the design and optimization of a high temperature reactor for the production of Group II-VI compounds by Eagle-Picher (E-P) Industries, Incorporated. Specifically, the compounds include zinc and cadmium sulfides and selenides. The basis of this research will primarily rely upon zinc selenide as the compound of interest for modeling purposes and represents the greatest commercial potential for E-P, Inc.

Group II-VI compounds have several properties that lend themselves to unique applications. The dominant property that enables this class of compounds to be adapted for opto-electronic applications is their direct energy band gap (Marfaing, 1991). The band gap is defined as the gap between conducting and valence electronic energy bands. Group II-VI compounds occupy two ranges on a scale of energy gap vs. lattice constant when compared to other semiconductors. The low-energy materials in the infrared (IR) wavelength range are well suited for IR detectors and IR laser emitters. The high-energy gap materials include the zinc and cadmium sulfides and selenides that reside in the visible wavelength range. High band gap materials are actively sought for use in devices for emission of light at a specific wavelength light in the blue-green range of the spectrum. Zinc selenide has an energy band gap of 2.7eV and 480 nm and hence an ideal

emitter of blue light. These high band gap materials are the least developed and thus provide the impetus for this research.

The zinc selenide product is a powder that is eventually converted by proprietary crystal growth methods to a single crystal substrate. The methods of crystal growth include the Bridgman technique, as well as various casting and recrystallization techniques. The multi-zone capsule growth method, as outlined by Burr and Woods (1971), is an example of one such technique. The single crystal substrates are then incorporated into several devices of commercial interest. There is a particularly high potential for the use of ZnSe substrates as light emitting diodes (LEDs) employed in laser optical devices. ZnSe is used in high-powered CO₂ lasers due to its low absorption at specific wavelengths. It also has uses in medical, industrial, and military applications such as thermometry, spectroscopy, and High Resolution Forward Looking Infrared Radar (FLIR), respectively (Morton Advanced Materials, 1998).

The advent of optical memory storage devices is an area of extremely high interest for application of ZnSe materials. The use of blue diode light as a means of reading optical memory (as opposed to IR light) has the potential of increasing the storage capacity of devices four-fold or more (Lerner, 1998). Additionally, specific wavelength LED technology may eventually evolve to a level where the diodes can be included in flat panel displays and in room lighting devices when combined with other primary color diodes. With a commercial potential of this magnitude, competition in this area is understandably fierce and currently revolves around diode unit cost and lifetime. A competing technology for a blue-green diode source material is gallium nitride that has a lifetime of approximately one thousand hours. Currently, ZnSe diodes have

demonstrated several hundred hours of continuous operation, but will need to operate for several thousand hours at a reduced per unit cost. Interest in reducing the cost of synthesizing the ZnSe powder is consequently an important element in the economic viability of the entire process.

Current Synthesis Reactor and System

The reactor and production system presently in use at Eagle-Picher is approximately 50 years old and is shown in Figure 1-1:

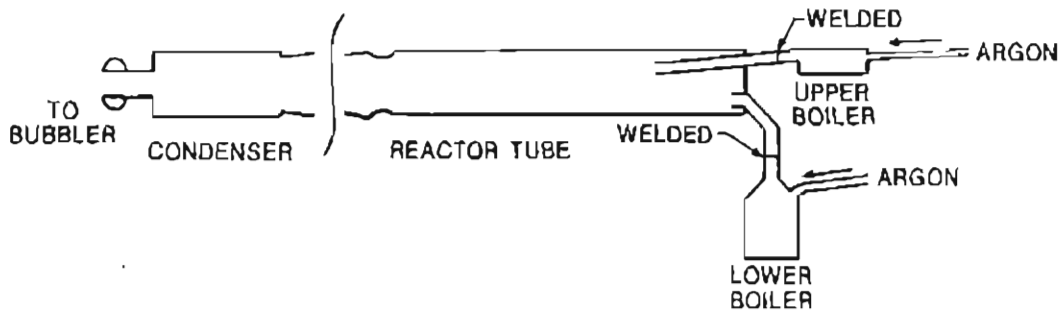


Figure 1-1. Sketch of Current Eagle-Picher Reactor (Source: Foutch, 1996)

The high-temperature quartz reactor system consists of two boilers where the solid reactants of zinc and selenium are introduced into the upper (horizontal) and the lower (vertically oriented) boilers, respectively and vaporized. The reactant vapors are

then carried into the high temperature (1000°C)-reactor tube by argon gas where they react and condense to form a ZnSe powder. Byproducts and unreacted starting materials flow into and condense in the jacketed condenser outside of the reactor zone. The effluent then passes through a bubbler solution to scrub the uncondensed materials from the inert carrier stream. The entire synthesis unit is quartz welded to provide a joint-free (with the exception of the ground glass joint condenser) closed system. Joint-free construction prevents the introduction of contaminants, especially oxygen, which can produce metal oxides and other impurities. The constituent parts of the reactor are all constructed in-house at E-P. The reactor tube is enclosed in a three zone furnace consisting of a Mullite™ tube surrounded by wire wrapped ceramic heating elements. The heating elements are insulated by firebrick and enclosed in a steel shell. A 240-volt three-phase rectifier supplies power to the furnace. The boilers are heated by 240-volt portable elements. The upper cylindrical heating element is slid around the boiler from the back and supported by a steel apparatus. The lower boiler is heated by a 'pot-shaped' element that is raised into place by a jack stand. Gaps between the boiler heaters and the furnace around the boiler transfer tubes are hand wrapped with insulating fiberfrax material prior to the beginning of each run. Temperature control is facilitated by thermocouples placed within the boiler and furnace elements that are in contact with the quartz surface of interest. The thermocouple settings and readouts are made via a system of digital and analog controllers. Thermocouple fouling by molten metals precludes temperature readings or control of either the starting materials or inside the reactor tube.

The reactor is appropriately termed an aerosol flow reactor. This type of reactor is characterized by the flow of aerated particles into a reacting zone where the products

are formed. An analogous reactor type that will be relied upon in this work is the chemical vapor deposition (CVD) reactor. In a typical CVD process, thin solid films are synthesized from the gas phase via chemical reaction and deposited on thin wafers located within the reactor (Hitchman and Jensen, 1993). While our process of interest is concerned with the deposition of bulk material within the reactor, many of the transport processes and chemical kinetic phenomena are similar, if not identical, to CVD processes.

The historical design basis for the reactor is difficult to establish. Little information exists within E-P as to the evolution of the system. A few facts are known, however. The horizontal orientation of the reactor is necessary to prevent void spaces from forming within the crystal structure of the product. The use of quartz as the material of construction is necessary due to its high purity and high temperature performance characteristics.

Analysis of Historical Performance of the Current System

In the present system, a batch synthesis run requires approximately three days turn-around-time per run due to lengthy steps in the set-up and breakdown procedures. These procedures involve welding of the boilers to the reactor inlet tubes prior to each run and the breakdown steps require disassembling of the reactor components by sawing. The reactor tube and boiler components are then cleaned with a concentrated mixture of sulfuric and nitric acids. The components are then dipped in a hydrofluoric acid bath to remove metal traces, rinsed with deionized water, and allowed to air dry. Each run results in approximately 700g of ZnSe product.

Current product specifications require five-nines (5N's or 99.999%) purity. The current system produces acceptable product purity, but anticipation of future trends indicates a probable need for 6N's purity.

Product production cost is an obvious concern and represents an area for design and process improvement. Analysis of historical data indicates an average yield based on zinc of only 40%. Further, the number of runs that are aborted approaches one for every five attempted. Aborted runs are most often due to plugging of inlet tubes by product material, which necessitates the shut down of the system to avoid over-pressurization. These aborted runs result in the waste of expensive high purity starting materials. Additionally, significant time losses occur as a result of the time necessary for the system to cool down as well as that required to breakdown and clean the reactor components.

The cause of the low yield and high run failure rate is primarily attributable to the low level of knowledge as to the actual process variables which inevitably results in poor process control. Successful setup and operation of the system is apparently heavily dependent upon operator experience. The process requires a bit of "wizardry" to produce a desirable quantity and quality of product. Historically, documentation of the process in terms of output data, observations, performance characteristics, and evolution of operating conditions was minimal. System operation has been geared toward the production of research quantities of high value materials. The commercial demand for the product has shifted towards a need for larger quantities of competitively priced material. Successful competition in the new marketplace will require a much greater level of process control.

Objectives

The need for a reactor with performance characteristics that will enhance the economic viability of the process is well founded. We are charged with developing a design that is capable of providing the following:

- 1) Reduced turnaround time.
- 2) Increased product output per run.
- 3) Improved product purity.
- 4) A high degree of process control.
- 5) Increased ease of operation.
- 6) Reduced labor costs.
- 7) 'Scale-ability' for future increases in production.
- 8) Adaptability for production of other Group II-VI compounds.
- 9) Improved safety characteristics.

The focus of this work is to provide assistance toward achieving these goals by accomplishment of the following objectives:

- 1) Conduct experimentation to analyze the present system and gain performance data that will aid in the design of a new reactor.
- 2) Submit recommendations as a result of the experimental analysis to enhance the performance of the present system.
- 3) Develop a concept that will meet all of the design objectives.
- 4) Develop a FLUENT™ Computational Fluid Dynamics (CFD) model of the new design concept.

- 5) Analyze the CFD model via a statistical Design of Experiments (DOE) study and validate the model by comparison and reconciliation with available data.
- 6) Optimize the new reactor design by use of DOE methods applied to the process variables within the CFD model.

CHAPTER II

LITERATURE REVIEW

Introduction

While there is little information in the literature related closely to this research; there is information available by analogy. The intent of this review is to provide a broad overview of specialized semiconductor vapor deposition processing. An initial review of related (some loosely so) alternative methods of production of similar compounds will lead into a discussion of various chemical vapor deposition technologies. From this fundamental ground, we will proceed into a review of the factors that regulate these processes and attempt to lay a basis from which to begin reactor design work. The literature related to design of high temperature vapor phase reactors, modeling and simulation will be reviewed. Statistical techniques to optimize reactor designs with computer models will also be explored.

Review of Production Methods

There are several alternatives for the synthesis of Group II-VI compounds as bulk powders, single crystals, and thin films. The emphasis of this work is the bulk synthesis of the various crystalline powders; however, various methods related to single crystal and thin film fabrication will be discussed as well. High temperature vapor phase synthesis from elemental metal reactants and wet solution methods are the two primary routes for

bulk synthesis. Methods for monocrystalline epitaxial growth for large single crystals include seeded physical vapor transport (SPVT) and seeded chemical vapor transport (SCVT). Thin film production methods for device fabrication can be grouped into the general categories of electrochemical, high temperature, and electrical field (electron beam and plasma). Many of the thin film methods are incorporated within Chemical Vapor Deposition (CVD) technology.

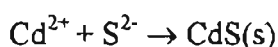
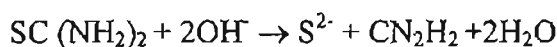
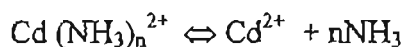
Bulk Synthesis

Group II-VI bulk synthesis can result from the transport of vaporized metal reactants through a reactor constructed of a suitable high-temperature material such as quartz by an inert carrier gas. Alternatively, hydrogen sulfide, or other gaseous metalorganic compounds of the Group VI metal, can react with vaporized Group II metal. An example is the reaction of dimethylzinc ($(\text{CH}_3)_2\text{Zn}$) and hydrogen sulfide (H_2S) to form zinc sulfide (ZnS). The vaporization of the reactants is followed by condensation of the product within a cooler reactor zone. This method approximates the present system in use at E-P. Literature related to system design, either batch or continuous, of this nature is scarce. The fifty-year evolution of the E-P design did not include publication of articles or patents and remains an in-house trade secret. Further, there is little research or production documentation available. One notable exception is the effect of reactor tube orientation. Brown (1964) experimented with synthesis of II-VI compounds in a vertical reactor and observed a greater tendency towards plugging of the inlets with product material. This orientation also is known to produce defects within the product crystal structure (Kucharczyk and Zabłudowska, 1986). The bases for other physical aspects of

the design are available piecemeal in the literature. The necessity for using quartz as the material for the reactant boilers and reactor tube is well founded. The high purity of quartz eliminates product contamination and also provides high thermal stability (Spirin et al., 1996). The quartz vessel allows for operation at high temperatures (up to 1500K) while maintaining low thermal expansivity, good thermal conductivity, and high tensile strength. Also, quartz allows for in-house fabrication of the various vessels, and pieces can be welded with relative ease.

The operating parameters were arrived at over a great length of time by analytic experimentation at E-P and have little basis in the literature. There are analogous references from crystal growth methods, especially those that employ the ampoule methods as outlined by Kucharczyk and Zabłudowska (1986). Although not directly transferable to our synthesis system, the trends related to residence time, carrier gas velocities, and cooling time provide a basis for gauging the effects on the product crystal quality, size and morphology (Foutch et al., 1995).

The second type of production method includes several wet chemistry techniques. These methods are usually performed by precipitation of the reaction product from either an organic or aqueous solution. Product purity is limited by the quality of the solutions, as well as the apparatus, therefore, the vapor methods usually yield higher purities. Chemical Bath Deposition (CBD) is one wet chemistry technique for the production of cadmium sulfide from cadmium salts in an ammonia medium (Chopra et al., 1982):



Wet methods permit production under ambient conditions and there exist schemes to enable control of product characteristics. Bredol et al. (1996) controlled the nucleus size of zinc sulfide by addition of the reactants to an organic phase that forms a “nuclei organosol” when added to an aqueous zinc salt solution. The ZnS precipitates on the nuclei by treatment with H₂S gas. Films of cadmium selenide were grown layer-by-layer from CBD solutions containing cadmium sulfate, sodium selenosulfate, and a sodium nitrilotriacetate (NTA) complexing agent (Cachet et al. 1996). Further, Cachet et al. (1997) achieved epitaxial growth of CdSe on (111) single crystal substrates of InP.

Growth of Single Crystals

There are numerous methods of preparing single crystal II-VI compounds. Only a few will be addressed here to illustrate the importance of transport processes in the production of these materials - regardless of final morphology.

Kucharczyk and Zabloudowska (1986) reviewed the methods of crystal preparation by first categorizing the crystallization as one-component or multi-component. The distinction is due to the composition of the mixture from which the crystals are grown. If the crystals are formed from a mixture where the compound is relatively pure, the method is termed “one-component.” “Multi-component” refers to a mixture of materials that includes the compound of interest. Further, the processes can be grouped by the phase transition involved in the crystallization, i.e.- solid to solid, gas to solid, or liquid to solid.

Korostelin et al. (1996a) described the methods of monocrystal formation from polycrystalline ZnSe using both SPVT and SCVT. The process uses helium for physical

transport, or an argon-helium mixture for chemical transport, of ZnSe within a sealed quartz growth ampoule enclosed in a furnace at approx. 1200°C. The cooler, lower end of the furnace contains a single crystal wafer of (111) ZnSe as the seed that is placed on a polished quartz rod. The authors grew crystals up to 50mm in diameter and found that the mass transport rate varies with the square of the ampoule radius, and concluded that there is a strong influence of diffusion on the mass transfer, i.e.- the growth is a diffusion limited process.

Crystallization from one-component molten material is known as the Bridgman – Stockbarger method. It involves drawing a cylindrical, pointed crucible through a highly controlled temperature gradient to produce monocrystals from a single, unidirectional nucleus contained in the point. The process is extremely sensitive to the temperature profile and crucible rate of travel (Kucharczyk and Zabłudowska, 1986). Deviations from ideal conditions caused variation in stoichiometric composition and crystal morphology. Kimura and Komiya (1973) note that the crucible can be modeled as a three phase equilibrium maintained between the melt, the diffusing gases, and the growing crystal.

Crystal growth from the vapor phase is referred to as the sublimation-condensation method. The method, with its heat and mass transfer considerations, is analogous to the process of this research. Transport of the vapor can be made by active (or dynamic) flow by using an inert carrier gas, or by static transfer. Static transfer relies on the high vapor pressures of molten II-VI materials, whereas dynamic transfer rates are augmented by the addition of the inert stream. Korostelin et al. (1996b) notes that the vapor phase method is “preferable to obtain pure and highly perfect single crystals.” In

an extension of their work, the authors found that the composition of the resulting crystals is dependent upon the growth conditions that vary with the steady-state composition of the vapor phase material. Their work centered on relating the flux of Cd and Zn to the diffusivities, partial pressures, physical properties, and the geometric factors related to the ampoule. Battat et al. (1976) assumed interfacial equilibrium to estimate diffusion-controlled mass transfer rates that limit the crystal growth rate.

In their review, Kucharczyk and Zabłudowska (1986) make note of two interesting observations relevant to vapor phase crystal growth: 1) the quality of the monocrystal is improved with longer residence time of the vapor(s). 2) Clark and Woods (1968) report that crystals produced in a vertically configured furnace contain a greater number of void defects that impact physical and electrical properties. Single crystals are also grown by homoepitaxial methods, where the growth occurs on a substrate of the same material as the crystal. Heteroepitaxial growth occurs on a substrate of a different material.

Thin Film Methods and Device Fabrication

The unique properties of deposited films can be utilized as decorative and protective coatings such as those used for reactor walls (Mattox, 1979), high-pressure valves (Pierson, 1981), and specialty bearings (Hinterman and Laeng, 1983). Many products such as machine parts and medical devices also require highly specialized coatings to improve strength, durability, and appearance characteristics. Electronic applications include fabrication of thin film transistors, capacitors, resistors, and solar devices, among others (Jackson, 1993). Optic-electronic applications, such as laser

storage devices, represent the greatest area of commercial potential as discussed in the introduction. These films also have unique photonic applications in long distance fiber optic systems with low optical loss characteristics (Dupois, 1984), as well as the next generation of computer and video displays.

Thin film synthesis methods can be grouped as either reactive or physical. In a reactive process, the film is deposited following a gas phase chemical reaction. Or, the film can be deposited directly from the source material in a physical process (Hitchman and Jensen, 1993). Examples of physical thin film methods include evaporation, sublimation, sputtering, and various high-energy routes such as pulsed laser deposition and Molecular Beam Epitaxy (MBE). The reactive methods include electrosynthesis of thin film layers and Chemical Vapor Deposition (CVD). CVD is the primary means that a chemical reaction in the gas phase can lead to epitaxial or non-epitaxial deposition of the thin film. Since they are analogous to our process, examples of each of these methods will be explored with particular attention to reactive CVD processes.

Physical Methods

Physical vapor deposition originates directly from an evaporating source of the same material contained in a Knudsen cell or open boat. The evaporation and sublimation of the source material can be facilitated by techniques such as MBE, where a molecular beam is formed by heating the material within an ultra-high vacuum (Dupuis, 1984; Jackson et al., 1987). Alternate means of obtaining the energy for evaporation include the use of a pulsed laser (Misiewicz et al., 1994) and high energy sputter deposition (Greene and Eltoukhy, 1981).

Chemical (Reactive) Methods

Many of the non-reactive methods of depositing thin films can be used to perform reactive vapor deposition of layers. For example, Nouhi and Stirn (1986) discuss the deposition of ZnSe films on glass substrates via reactive magnetron sputtering. Also, pulsed lasers, plasmas, and other photo-assisted means have been employed to enhance reactive CVD – e.g. plasma-enhanced chemical vapor deposition (PECVD).

While seldom used, electrochemistry is another technology that can be used to produce thin films by reaction. Harn et al. (1991) discuss the electrosynthesis of thin films of Group II-VI compound semiconductors. The authors differentiate the electrochemical methods as anodic or cathodic. The cathodic route involves reduction of both the Group II metal and the Group VI chalcogen (selenium) in either an aqueous or organic solvent. Alternatively, a film can be formed by anodization of the metal in a basic solution of the chalcogen – e.g. Cd metal in a 1M K₂Se and KOH solution. Using this method, the authors were successful in forming thin films of CdSe.

Chemical Vapor Deposition (CVD)

Examples

Thin films of Group II-VI compounds can be produced by numerous types of reactive chemical vapor deposition techniques; only a few of which will be discussed here. The metallorganic techniques discussed earlier can be applied to a dynamic flow horizontal reactor containing parallel rows of wafer substrates. Alternatively, deposition

can occur within a static flow “pancake reactor barrel” with flatly distributed wafer substrates. This method is referred to as metallorganic chemical vapor deposition (MOCVD). Su et al. (1997) fabricated thin films of ZnS on nine inch diagonal wafers from $(\text{CH}_3)_2\text{Zn}$ (DMZn) and H_2S in a low pressure horizontal reactor (LPMOCVD) with a dynamic carbon substrate. The authors found the deposition quality and uniformity was heavily dependent upon reactor temperature and pressure, substrate temperature, reactant flow rate, and nozzle widths. The use of organometallic precursors allows for operation at much lower temperatures. This method of MOCVD is distinct from MOPVD and MOVPE, which are physical deposition processes for thin film and reactive epitaxial growth methods, respectively (Moon and Houn, 1993). Other acronyms that are commonly used to describe CVD processes include: low pressure (LPCVD), high pressure (HPCVD), plasma-enhanced (PECVD), laser-induced (LCVD), and photo-assisted (PCVD) (Wahl, 1993). There are many lesser-used permutations of the CVD reactor including supercritical fluid transport (SCTCVD) and aerosol-assisted (AACVD) (XU et al., 1995). The authors note the advantages of aerosol aided CVD by improving the transport of compounds with low vapor pressures (non-metallorganics) and low thermal stabilities.

Deposition Processes and Theory

An introduction to CVD technology will illustrate the many of the same principles that govern our process. A thorough source of theoretical and applied information regarding CVD processing is available by Hitchman and Jensen (1993).

The authors summarize the essential steps of CVD technology by describing sequentially the mass transport steps:

- 1) *mass transport in the bulk gas flow region from the reactor inlet to the deposition zone;*
- 2) *gas phase reactions leading to the formation of film precursors and byproducts;*
- 3) *mass transport of film precursors to the growth surface;*
- 4) *adsorption of film precursors on the growth surface;*
- 5) *surface diffusion of film precursors to growth sites;*
- 6) *incorporation of film constituents into the growing film;*
- 7) *desorption of byproducts of the surface reactions; and*
- 8) *mass transport of byproducts away from the deposition zone towards the reactor exit.*

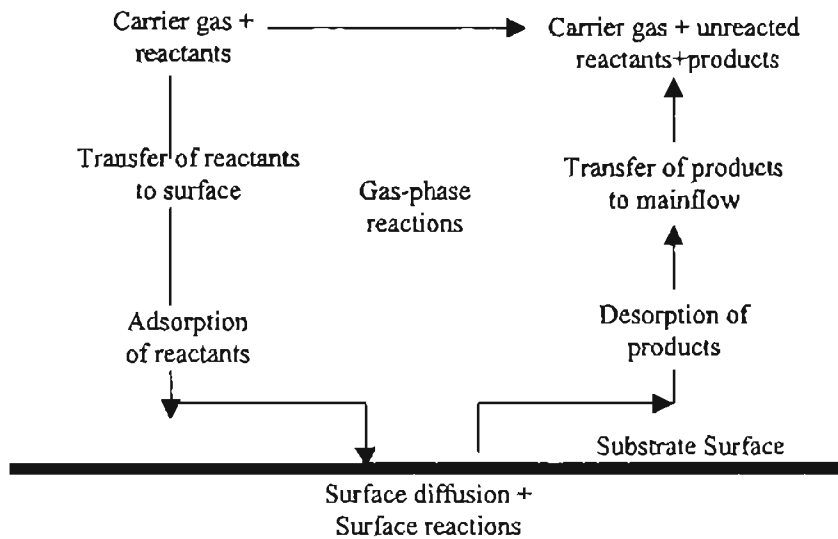


Fig. 2-1: CVD Processes (Source: Hitchman and Jensen, 1993, pg.13)

As with the process that is the focus of this work, each step in the CVD process is critical to the successful completion of a run. Note that the reactor walls or other particles, either in the bulk fluid or deposited as a layer, can act as a substrate in the Figure 2-1.

Mass Transport

Fluid flow and species transport is governed by the equations of conservation of mass (continuity) and momentum as given by Bird et al., (1960). These basic balance equations are relied upon for reactor modeling. Jensen (1993) notes that a pseudo-steady-state condition can be assumed for most CVD reactors. By analogy, this assumption appears to be applicable to our system as well. For the fluid flow; the x, y, and z velocity components are obtained by solution of the equation (in vector notation) for total momentum balance (Bird et al., 1960):

$$\rho(D\mathbf{v}/Dt) = -\nabla p - [\nabla \cdot \boldsymbol{\tau}] + \rho \mathbf{g} \quad (2-1)$$

The equation of continuity is given from conservation of mass by (Bird et al., 1960) and provides the local pressure:

$$\nabla \cdot (\rho \mathbf{v}) = 0 \quad (2-2)$$

The diffusive flux of a species i is due to the concentration and thermal driven components by (Jensen, 1993):

$$\mathbf{J}_i = \mathbf{j}_i^C + \mathbf{j}_i^T \quad (2-3)$$

Where the concentration flux is solved from the Stefan-Maxwell equation (Bird et al., 1960; Jensen, 1993):

$$\nabla \omega_i + \omega_i \nabla (\ln M) = \sum (1/\rho D_{ij}) [(M\omega_j/M_j) \mathbf{j}_j^C - (M\omega_j/M_i) \mathbf{j}_i^C] \quad (2-4)$$

The diffusion due to thermal forces is given by (Jensen, 1993):

$$\mathbf{j}_i^T = D_i^T \nabla (\ln T) \quad (2-5)$$

The effective thermal diffusivity, D_i^T , is estimated by (Kleijn et al., 1989; Jensen, 1993):

$$D_i^T = \Sigma (c^2/\rho) M_i M_j D_{ij} k_{ij}^T \quad (2-6)$$

The density of the reactor gases cannot be calculated by linear extrapolation due to the large gas expansion from the heat flux. Therefore, the density should be determined by the ideal gas law (Jensen, 1993):

$$\rho = (PM/RT) \quad (2-7)$$

Finally, the balance for each species includes contributions from diffusion, convection, and n^G gas reactions (Jensen, 1993):

$$\nabla \cdot (\rho v \nabla \omega_i) = -\nabla \cdot \mathbf{j}_i + \Sigma v_{ij}^G M_i \mathfrak{R}_j^G \quad \text{for } i = 1 \dots, S-1 \quad (2-8)$$

Where S is total number of species undergoing transport, and \mathfrak{R} is a surface or bulk phase reaction rate.

In addition to the above sources; a firm footing in the theoretical basis of mixing phenomena related to dispersion and diffusion in open systems can be gained from Nauman and Buffham's (1983) signature book on mixing in flow systems.

Heat and Energy Considerations

The two sources of energy that must be accounted for in the total energy balance for the reactor are the external heat sources that contribute via conduction, convection, and radiation, and the heat of reaction(s). The theses of Brent Foster (in progress) and Zeljko Nikolic (in progress) deal extensively with the heat transfer aspects of our process and will be deferred to for a complete description of those issues. We will concern ourselves here with the energy considerations relevant to the design of vapor deposition

reactors. Neglecting viscous energy terms; the energy balance taking into account n^G vapor phase reactions \mathcal{R} (Jensen, 1993):

$$\rho C_p \mathbf{v} \cdot \nabla T = \nabla \cdot (k \nabla T) - \sum [\mathbf{j}_i \cdot \nabla H_i + H_i \sum v_{ij}^s M_i \mathcal{R}_j^s] \quad (2-9)$$

Where k is the thermal conductivity of the gas species and C_p is the heat capacity at constant pressure of the gas species.

Reaction Kinetics

Considering that most gas phase reaction equations have little relation to the actual mechanism; it is essential to gather data or estimate kinetic expressions for each step in the mechanism. Further, there is a need to understand the surface reactions in addition to the gas phase reactions. There is, unfortunately, little data available in the literature as to kinetic parameters of high temperature gas phase or surface reactions. Notable exceptions are the well studied reactions for silane chemistry (White et al., 1985; Jasinski et al., 1987; and Moffat and Jensen, 1991) and GaAs free radical chemistry (Mountziaris and Jensen, 1991).

Due to the dearth of kinetic information, it is usually necessary to estimate the required parameters. Jensen (1993) summarizes the two primary means of accomplishing this task. The first route is to empirically fit the parameters of a simplified rate form to experimental data. Levenspiel (1972) outlines the steps involved in this approach. Essentially, the method entails fitting the temperature dependency of the rate constant to a plot of inverse temperature to obtain the activation energy from the slope. Various schemes with log plots of concentration versus time data are used to ascertain the overall

order. The rate constant k is obtained from the slope of such a plot, once a suitable linear log plot is found.

The second method involves the more rigorous approach of estimation of the kinetic parameters from transition state theory and statistical thermodynamics. Gavrishchuk and Dadanov (1990) estimated the value of rate constants for the deposition of ZnSe layers by using a mathematical model for the deposition process that accounts for the geometry of the material. Jackson et al. (1987) determined the rate of the growth of a physically deposited layer from constitutive relationships that describe incident fluxes towards the substrate, as well as adsorption and reflection of the species deposited.

Wang and Pollard (1995) present a methodology for the estimation of the rate constants of elementary surface reactions from statistical mechanics and transition state theory. They determine activation energies from bond dissociation energies and heats of adsorption. While rooted in thermodynamic theory, the method appears rather exhaustive; as a description of the surface structure and bonding configurations must be available. However, if thermodynamic data are available; the authors review the straightforward method of determining the equilibrium constant from:

$$K_{eq} = \exp\{-(\Delta H_{f,298}^{\circ} - T\Delta S_{298}^{\circ})/RT\} \quad (2-10)$$

Nucleation and Aerosol Dynamics

Product nucleation and aerosol dynamics play a critical role in the design of a deposition reactor. Specifically, the behaviors of particles dictate the performance of the system to a large extent.

Hitchman and Jensen (1993) are primarily concerned with the formation of thin films within reactors, but those processes are also relevant to the bulk deposition of powder product. Nucleation effects both the growth and the microstructure of the developing film. Hitchman and Jensen (1993) remark that the film characteristics are, “determined by surface diffusion and nucleation processes on the growth interface, which are influenced by the substrate temperature, reactor pressure, and gas-phase composition.” The process of this research involves the condensation of product nuclei on themselves as well as the reactor walls. It, therefore, can be described as a dual-substrate system. Alternatively, the process may be considered a three-phase reaction process. The reactor is an aerosol assisted chemical vapor deposition (AACVD) reactor for bulk synthesis. An alternative designation is a laminar flow aerosol reactor (LFAR). The various nucleation and aerosol related literature that has been researched will be reviewed.

Types of Nucleation

Reist (1993) thoroughly covers the many aspects related to aerosol dynamics. He describes the different types of nucleation as homogeneous or heterogeneous. He notes that the formation of an aerosol initially requires a surface for condensation – the

condensation nucleus. Homogeneous, or spontaneous, nucleation is the condensation of vapor molecules onto molecules of the same material. Conversely, heterogeneous nucleation is the condensation onto a dissimilar material. In our process, the bulk production of powders will involve both homogeneous and heterogeneous nucleation of particles onto themselves as well as the reactor walls as a substrate. Reist describes the steps necessary for nucleation as: 1) supersaturation of the vapor, 2) formation of small clusters of molecules that he calls, 'embryos,' and 3) the condensation of the supersaturated vapor onto these clusters. He further notes that heterogeneous nucleation only involves the first and third steps where in the case of the third step, the reactor walls fulfill the role as the substrate embryo or cluster.

Condensation Phenomena

Reist (1993) gives the saturation ratio of a vapor in a gas as:

$$S \equiv p/p_{\infty}(T) \quad (2-11)$$

Where p is the partial pressure of the vapor in the gas, and $p_{\infty}(T)$ is the saturated vapor pressure of the vapor over a volume of the liquid at temperature T . Further, he lists equations for the calculations of 'S' for adiabatically expanding gases from thermodynamic relationships based on Clausius-Clapeyron's equation. He states that when $S > 1$, the gas is supersaturated with vapor. The gas is saturated at $S = 1$ and is unsaturated at values less than 1. Reist states that once supersaturation is achieved, the formation rate of critical nuclei (in terms of the number of clusters reaching critical size per unit time) is given by the following expression developed by Pruppacher and Klett (1978):

$$J = (\alpha_c / \rho_w) (2N_A^3 M \gamma / \pi)^{1/2} (p_\infty / RT)^2 S \exp(-\Delta G / kT) \quad (2-12)$$

Where the required condition for spontaneous nucleation is $J \approx 1.0$. The author also discusses heterogeneous nucleation and gives an excellent review of kinetic gas theory, molecular speeds, mean free path calculations, drag coefficients, Stoke's Law, and particle diffusion from Fick's Law. He also includes a chapter devoted to coagulation of particles, which plays a role in most aerosol reactor processes.

Another source for aerosol dynamics information that emphasizes mathematical descriptions of the various phenomena is given by Wen (1996). Wen covers some interesting problems pertaining to the relationship between rate of mass transfer of aerosol particles and the reactor dimensionless parameters that will be addressed later. Specifically, he relates the aerosol mass transfer rate to the zero-Peclet number mass transfer rate Q_0 :

$$Q_0 = 4 \pi a D_m (C_1 - C_0) \quad (2-13)$$

Where a is the particle radius, D_m is the molecular diffusivity, D_0 is the vapor molecular diffusivity, C_1 is the concentration at the particle surface, and C_0 is the concentration at some distance from the particle. Pratsinis and Vemury (1996) also offer a review of recent progress in the area of particle formation in the synthesis of powders.

On a more practical front; there are several references to aerosol related issues that relate to chemical reactors. In these cases, the objective is often to produce very exact distributions of particles in high temperature reactors designed to produce ceramic particles from the gas phase. These phenomena are closely related to the present research, inasmuch that experimental data will attempt to associate reactor conditions to Scanning Electron Microscopy (SEM) analysis of product particles.

Pratsinis (1988) reviews the general dynamic equations for simultaneous aerosol nucleation, condensation, and coagulation in reactors and suggests that there are five dimensionless parameters that determine the particle characteristics. Kudas et al. (1987) conducted experiments that confirmed that aerosol dynamics in a tubular flow reactor are controlled by reactant mixing above the critical saturation ratio. Likewise, below the critical saturation ratio; the dynamics were not influenced by mixing since formation and growth of particles occurred primarily in the laminar region. They determined the particle size distributions for a range of mixing head configurations. Okuyama et al. (1992) measured the effects of concentration, temperature profile, and carrier gas on the formation of TiO₂ particles formed in a LFAR. They found that under dilute conditions and slow rates of reaction, smaller particles were produced.

Rao et al. (1998) investigated the formation of borophosphosilicate glass (BPSG) particles in a commercial LPCVD reactor. Here, the authors were concerned with another interesting facet of aerosol dynamics in reactors – the prevention of contaminant particle formation on CVD deposited layers on wafers.

Bilodeau and Proulx (1996) report the development of a 2-dimensional model that simulates particle formation, nucleation, and growth by condensation and Brownian coagulation of ultrafine metal powders in a thermal plasma reactor. They were successful in applying the model to optimization of the system operating parameters.

Reactor Design Methods

All of the above aspects pertinent to the kinetic and transport processes play a role in the successful design and operation of a vapor deposition reactor. In addition to these equations, there are many references in the literature that explore other reactor parameters and design considerations. A brief review of these sources will be presented here.

Dimensionless Parameters

Transport phenomena within a deposition reactor are affected by the flow regime, reactor geometry, inlet nozzle characteristics, exhaust manifold design, reaction kinetics, and species transport properties. The complex nature of these interactions necessitate the use of dimensionless design parameters to gauge the effects measured by experimental data gathering, computer, or flow visualization models.

The dimensionless parameters are based, in theory, on scaling of the applicable transport equations (Jensen, 1993; Bird et al., 1960). Hitchman and Jensen (1993) summarize the various dimensionless parameter groups. This table is reproduced as Table 2-1. The relevant parameters includes the Knudsen (K_n) number, which is a measure of the mean free path relative to the reactor length and is also a function of the reactor pressure. It is an indication of whether the reactor is operating in a high-pressure regime termed as a “continuum” or, a state characterized by predominantly wall collisions referred to as the “free molecular flow” regime (Jensen, 1993). Also, the Peclet number is a valuable tool to gauge the degree of mass and thermal convection relative to diffusion.

Table 2-1: Dimensionless Parameter Groups Characterizing Transport Phenomena in CVD (Source: Hitchman and Jensen, 1993, pp 54-55)

Name	Definition	Physical Interpretation	Typical Order of Magnitude
Knudsen	$Kn = \lambda/L$	<u>Mean free path</u> Characteristic length	$<10^{-2}$
Prandtl	$Pr = \mu/\alpha$	<u>Momentum diffusivity</u> Thermal diffusivity	0.7
Schmidt	$Sc = \mu/D_m$	<u>Momentum diffusivity</u> Mass diffusivity	1 - 10
Reynolds	$Re = \langle v \rangle L/\mu$	<u>Momentum flux by convection</u> Momentum flux by diffusion	$10^{-1} - 10^2$
Peclet (thermal)	$Pe_h = Re Pr$	<u>Thermal flux by convection</u> Thermal flux by diffusion	$10^{-1} - 10^2$
Peclet (mass)	$Pe_m = Re Sc$	<u>Mass flux by convection</u> Mass flux by diffusion	$10^{-1} - 10^3$
Grashof (thermal)	$Gr_t = \frac{g\beta L^3 \Delta T}{\nu^2}$	<u>Buoyancy force</u> Viscous force	1 - 10^5
Grashof (solotal)	$Gr_s = \frac{g\beta L^3 \Delta c}{\nu^2}$	<u>Buoyancy force</u> Viscous force	1 - 10^2
Rayleigh (thermal)	$Ra_t = Gr_t Pr$	<u>Buoyancy force</u> Viscous force	1 - 10^5
Rayleigh (solotal)	$Ra_s = Gr_s Sc$	<u>Buoyancy force</u> Viscous force	1 - 10^2
Damkohler (gas phase)	$Da_g = \frac{R(C,T)_{ref} L}{C_{ref} \langle v \rangle}$	<u>Characteristic time for flow</u> Char. time for gas phase rxn.	$10^{-3} - 10^3$
Damkohler (surface)	$Da_s = \frac{R(C,T)_{ref} L}{C_{ref} D_m}$	Char. time for diffusion to <u>surface</u> Char. time for surface rxns.	$10^{-3} - 10^3$

Predicting the presence of flow conditions conducive to the production of convective “rolls” is also necessary. This is the phenomena that results in the formation of product “wormholes” in the current E-P system that were mentioned briefly in the Introduction. This topic will be discussed in greater detail in the main body of this thesis. This phenomenon can be described in terms of characteristic Rayleigh (R_a) and Reynolds

(Re_c) number relationships (Jensen, 1993). Secondary flow patterns, in the form of rolls, are indicated at flow between infinite plates in excess of critical Re values of 1708 (Jensen, 1993; Jackson and Winters, 1984).

Other Design Calculations

There are many other references available that describe calculations relevant to deposition reactor design. Proper design of inlet nozzles is critical in achieving the desired mixing pattern for the reaction interface. The basic design calculations for nozzles are well presented by Tung (1925) and Abramovich (1963). Zambov et. al. (1998) relates inlet nozzle diameter to Reynolds numbers required to prevent product formation on the inlets. The fundamental design equations for plug flow and other reactors are available in the texts by Levenspiel (1972,1996) and others.

Examples of Reactor Design Methods

Sadakata and Harano (1996) describe a systematic procedure for the design of an industrial scale aerosol reactor based on characteristic mixing times established by desired product characteristics.

Kleijn et al. (1996) contends that the scale-up of a stagnation flow reactor be performed at a constant Peclet number, i.e. – the reactor should be scaled by increasing the gas flow proportionally to the square of the diameter of the reactor. Habuka et al. (1995) provides an examination of the pancake reactor flow patterns by flow visualization techniques. Zambov et al. (1998) describes the design of a LPCVD reactor using horizontal injection. A two-dimensional model was used to optimize the design

and operating parameters with the goal of constant reactant concentrations. Weerts et al. (1997) describe the design of an industrial-scale LPCVD reactor via a one-dimensional, two zone reactor model with equations that neglect the effects of mixing.

Examples of Commercial Reactors and Processes

While there is little information in the literature describing reactors that are similar to the current system at E-P, there are many examples of other high temperature reactors for the production of other metallic and semiconductor compounds that can be used to provide a conceptual framework.

Hlavacek and Puszynski (1996) discuss the design concepts for the production of advanced ceramic materials. Their report describes plasma, flame combustion, Los Alamos, and laser reactors for the production of SiC. Many of the reactors are vertically oriented and though not directly applicable to most semiconductor systems; offer some interesting ideas such as a continuous system that employs a “sweep” gas stream to aid in the migration of product material. Gupta et al. (1996) report a schematic for a concept for a counter-flow jet reactor where the reaction occurs at a cross-flow region of the two streams. Konig (1995) has patented the process of a vertical gas phase reactor that forces the condensation of a finely divided powder product directly from the gas phase without wall reactions.

Other novel features of reactors have been patented. Gebben and Bruce (1995) have developed a system to monitor minute pressure fluctuations within a high temperature reactor to aid in the control of the system. Detering et al. (1998) developed a reactor that quickly quenches the product through use of a convergent-divergent nozzle.

Examples of other patents for novel high temperature reactors exist for the continuous production of silicon nitride (Bachelard et al., 1997), aluminum nitride (Pratsinis et al., 1996) and nanoparticle synthesis (Johnson et al., 1997).

Reactor Models and Simulations

Computational models and/or computer simulations can facilitate successful vapor deposition reactor design. The interaction of the operating parameters with both the mass transport characteristics and the reaction kinetics presents a challenging problem to contend with when designing an optimal reactor. Mathematical models can iteratively solve the differential equations for transport and energy balances, either as stand-alone computations or interfaced with a graphical computer simulation. A solution of the aggregate equations over a set of shell or grid points for the total volume of the reactor is referred to as a finite-element analysis.

Elements of a Reactor Model

Figure 2-3 illustrates the many considerations that must be incorporated into a CVD reactor model.

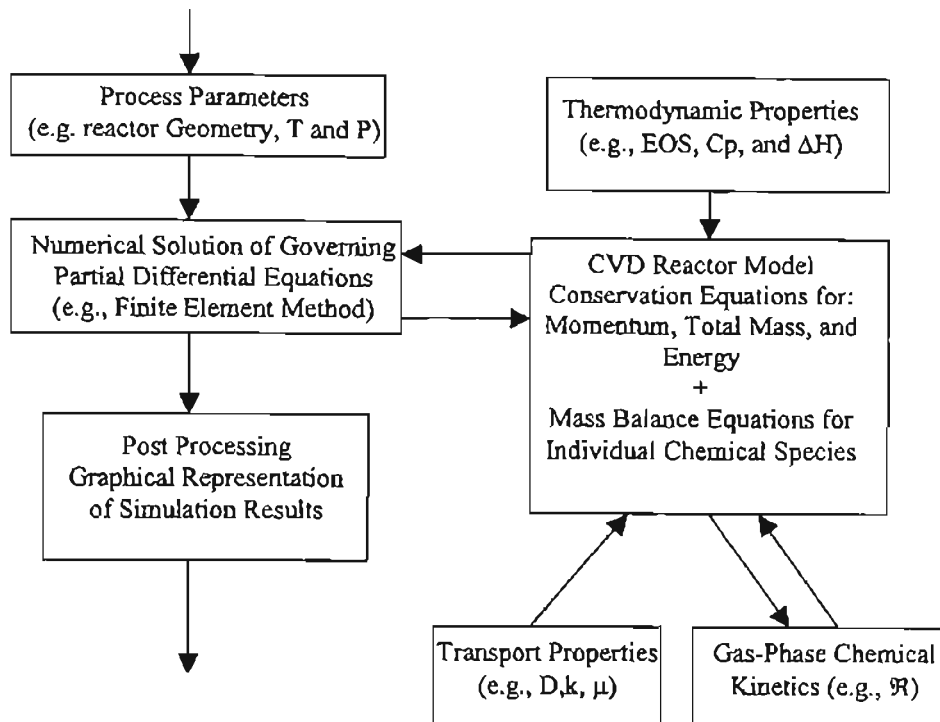


Figure 2-2: Elements of a CVD Reactor Model (Source: Jensen, 1993, p71)

Examples of Numerical Models

Krishnan and Zhou (1995) present a succinct overview of the modeling equations for a deposition process and discuss the methods of reducing the complex kinetics of silicon and tungsten chemistry to a simple Arrhenius format. Moffat and Jensen (1986) report an approach to modeling the complex patterns such as the convective ‘rolls’ discussed earlier. They summarize the modeling equations and their solution via the Galerkin finite element analysis method. The numerical solution to the 3D model

accurately predicted the velocity and temperature profiles as compared with experimental observations of the secondary flow patterns that are driven by buoyancy effects. Further, they note that the buoyancy driven roll formation decreases with decreasing aspect ratio of the reactor and is increased with the use of Ar or N₂ carrier gases as compared with either H₂ or He.

Computational Fluid Dynamic (CFD) Models

Computer simulations that employ finite element analysis of the governing model equations have the added benefit of time savings and graphical depiction of the equation outputs in terms of temperature profiles, velocity vector profiles, concentration of individual species profiles, and dimensionless parametric variables. The commercial packages that have been applied to vapor deposition reactors are FLUENT™, FIDAP™, and PHOENICS™ CFD software. Few examples of the PHOENICS™ and FIDAP™ systems appear in the literature as compared to FLUENT™, which was used in the course of the reactor modeling efforts presented here.

Ranade (1997) offers a good overview of the advantages and disadvantages of CFD models applied to reactors and includes the basic steps involved in the development and validation of the model. The primary impetus behind the use of CFD models for reactors is the ease with which complex transport equations, including turbulent flow, can be solved for mass transfer limited reaction processes.

Hamby et al. (1995) report a FLUENT™ computational model and a reduced control oriented model with an estimation of uncertainty. The authors list the simplifying assumptions made in the development of the control model. The control

model simplifies the partial differential equations to be solved via the assumptions of spatial uniformity, isothermal operation, and reduced kinetics expressions for silane (SiH_4) deposition.

Gobbert et al. (1997) describe a LPCVD FIDAP™ simulator that contains three levels of detail; a large “reactor scale” level, a finer “feature” scale model, followed by a “mesoscopic” scale. The third level of detail allowed the authors to couple mesh scales across a range of sizes to resolve the appropriate detail dependent upon the reactor configuration. Also noteworthy, the authors simplified the diffusion components of the mass transport equations by use of the “multi-component dilute approximation.”

Angermeier et al. (1997) present a full 3-dimensional FLUENT™ model for epitaxial growth with 80,000 cubic finite elements. Their model represents a rigorous solution, but also includes a step whereby the authors transform the set of non-linear conservation equations to a global set of algebraic equations. Their model also relied upon simplified kinetics of Si growth. They note the effects of buoyancy on convective currents and the relationship that the sidewalls impart relative to the reactor aspect ratio.

There are references to CFD models for other systems such as plasma-enhanced CVD (PECVD) that illustrate the ability of the software to handle even complicated reaction schemes if the kinetics are available or can be empirically estimated (Collins et al., 1994).

Optimization of the Reactor and Process Design

Design of Experiments (DOE)

The FLUENT™ model developed by Collins et al. (1994) incorporated the extra step of optimization of the chemical kinetics by tuning the appropriate parameters through the use of experimental design analysis. The techniques collectively referred to as design of experiments (DOE) are commonly relied upon as a process quality control, system and device design, and process optimization tool in the manufacturing industries. The tools are less frequently employed as a means of optimizing computer models, simulators, or computer aided design (CAD) applications.

The methods of Statistical Process Control (SPC) and Design of Experiments (DOE) as pioneered by Deming (1950) and Taguchi (1987) are well studied and applied in the literature. The statistical based methods are presented by Mori (1990) as a set of methods that, “combines engineering and statistical methods to achieve improvements in cost and quality by optimizing product design and manufacturing processes.” Mori (1990) differentiates between the research objectives of analysis and design by stating that the purpose of design is to find the optimum solution of an engineering objective, whereas analysis is concerned with the creation of a model to “express” the system. Since the intent of this research is to effectively combine these two functions via DOE methodology; a brief foray into the literature that provides a basis in these methods will be presented.

Mori (1990) illustrates the four main approaches to determining the optimum solution (or condition) to a design or process problem:

Table 2-2: Comparison of Four Experimental Approaches (Source: Mori, 1990, p23)

	Name of Method	Content of Method	No. of Experiments	Reliability
1	Multi-factor layout	Every combination of Levels tested	Many (81)	High
2	One-factor-at-a-time experiment (Precision Test)	Effect of each factor confirmed (one-at-a-time) by fixing levels of other factors	Several (12)	Low
3	Target method	Only 2 or 3 possible "best" combinations of levels (2 or 3) tested	Few (2-3)	Lowest
4	Experimental design method	Experiment using Orthogonal arrays	Several (9)	Highest

*The number of experiments needed to determine the optimum condition for four factors with three levels (e.g.81).

As shown from the table; a statistical analysis where the experiments are planned via orthogonal arrays (matrices) yields the highest reliability of the conclusions that can be derived from the data. The fundamental advantage of the experimental design approach is the high reliability that is obtained without performing the full array of experiments. Interestingly, Mori (1990) states that often, "engineers use the one-factor-at-a-time method because they know of no other method for optimum condition determination for many variables with many levels."

The mechanics of planning and designing an experimental matrix are well presented by Taguchi (1992, 1993), Mori (1990), Moen et al., (1991), and Barker (1990).

Analysis of Variance (ANOVA)

The optimum condition can be ascertained from an analysis of a plot of the effects that are attributable to each factor studied. As a further degree of confidence in the interpreted results; an analysis of variance (ANOVA) can be conducted. Mori (1990) defines the method as one that, "is a mathematical method that quantifies and verifies the relationship between factors and characteristic values that engineers judge intuitively." Although he states that optimization can be performed without ANOVA analysis, it is required to perform signal-to-noise determinations and applying tolerance design. Further, the method allows the designer to specifically quantify the effect of any given factor within a group of factors studied.

Response Surface Methodology (RSM)

The formal development of response surface methodology (RSM) was initiated within the chemical industry in England by Box and Wilson who sought to relate several input variables that were believed to have an influence on a process yield (Khuri and Cornell, 1996). The authors describe RSM as a method of developing a mathematical model from experimental data that will allow the researcher to establish the optimum levels of the factors explored in the study. This technique is an extension of traditional DOE methods in that the factors are reduced to a set of functions that can be used to establish the appropriate levels even if the experimental ranges are not sufficient. The functions then serve the role of providing a greater understanding of the system outside the bounds of the experiments.

Khuri and Cornell (1996) establish the validity of the assumption that a function describing the effect imparted to a response variable is continuous when measured with a given number of levels. The response is reduced to a polynomial or Taylor expansion function that forms a surface plot called a “hypersurface” which can be used as a predictive tool. This method will allow for subsequent prediction of system performance extrapolated from the available experimental data.

Examples of DOE/RSM Applied to Process Models and Simulators

Boning and Mozumder (1993) report the coupling of DOE and RSM to process and device simulator tuning and process parameter determination. Their system, that incorporates DOE, RSM, and optimization models, can be applied to a variety of manufacturing and design processes. For example, their system can work from a TCAD (Technology CAD) framework and graphically interface with existing simulation tools for wafer fabrication processes.

Similarly, Gaston (1995) presents the integration of DOE for sensitivity analysis to a full 2D TCAD industrial CMOS process problem. Wang et al. (1995) employed a DOE study and RSM functions to optimize the design of a opto-electronic integrated circuit (OEIC) that requires PECVD from the use of both physical experimental data and process simulators.

A three level DOE was used to reveal non-linear response effects in the course of optimizing the operating parameters of inlet nozzles for a vertical polysilicon LPCVD reactor by Balasubramanian et al. (1996). Polynomial equations were then developed to prepare response surface curves to predict wafer uniformity.

Process Prediction and Optimization by Artificial Neural Networks (ANN)

Wang and Mahajan (1995) present the adaptation of DOE and RSM methods to the development of an artificial neural network (ANN) for the modeling and optimization of a CVD barrel reactor for silicon epitaxial growth. The authors establish that RSM optimizations are limited in effectiveness when applied to processes that are affected by many nonlinear variables. This fact is evident in the shortcomings of low-order polynomials that are fit to more complex surfaces. The authors' report that DOE data are used to train an ANN by a "back propagation procedure" and is subsequently tested by another set of DOE data. They present a case example of the predictive performance of an 18th order polynomial as compared to that of an ANN model. Also, Mahajan and Walker (1996) report the on-line prediction of a CVD reactor by a DOE trained ANN that is interfaced with a PC for the control of inlet nozzle flowmeters. A similar feedback controller for PECVD of silicon nitride was developed by Mozumder et al. (1994) that determines a change of state in the process by comparison with a DOE tuned model. The system is then capable of adapting both the process parameters and the model.

CHAPTER III

RESEARCH AND OPTIMIZATION OF THE PRESENT SYSTEM

Introduction

As mentioned in the Introduction, the reactor at Eagle-Picher has been in use for approximately fifty years and requires a high degree of experience to successfully complete a production run. The fact that the system is subject to the experience of the operator indicates that the process is essentially uncontrolled, with relatively few of the variables monitored, controlled, or even apparent. Therefore, research was conducted on the system to gain information to aid in the design of a new reactor. The intent was to provide E-P with short-term improvements in production efficiency through optimization.

The work presented in this chapter was conducted during the summer of 1997 and was limited by both time and resources. Given the limited time to run actual experiments, a statistical Design of Experiments (DOE) approach was relied upon. The DOE approach permitted the maximum gain of information with the fewest runs and the least resources. While not comprehensive; valuable knowledge was gained for the formulation of a new reactor concept. Additionally, the analyzed data were forwarded to E-P and resulted in the improvement of the system that was to remain in use until the new reactor could be phased into operation.

This chapter will cover the set-up and analysis of the experimental matrix in detail. Computer DOE experiments reviewed in Chapter V will assume the basis in DOE

as described here and hence, will refer the reader to an appendix for the specifics related to the those experiments.

Experimental Study

Basis for the Study

In close collaboration with E-P, initial investigations into the chemistry and the physical operation of the current system yielded insight into the important performance parameters. Reynolds number calculations indicate the system to be operating in the laminar flow regime.

Dimensionless Parameter Analysis

The Reynolds number for the reactor tube is given by:

$$N_{Re} = \rho D V / \mu \quad (3-1)$$

As a first approximation, the flow velocity (V) is assumed to be pure argon at 1000° C. For a gas viscosity (μ) of 0.066 cP, density (ρ) of 0.378 kg/m³, and reactor diameter (D) = 90 mm, the Reynolds number is found to be less than 1.0 (Rhodes, 1997). When the actual flow components are included in the stream density, the Reynolds number remains in the range of about 20-25 (Morrison, 1998).

Also, the mass Peclet (Pe_m) number relates the ratio of convective to diffusive transport and is given by $Pe_m = Re \times Sc$ where the Schmidt (Sc) number is given by Jensen (1993) to be the ratio of kinematic viscosity to diffusivity. The Pe_m for our system is < 1.0; indicating highly diffusion controlled conditions. Both dimensionless numbers

appear to be essentially constant regardless of velocity, further affirming the relative importance of diffusive transport in the reactor.

The performance of the present reactor is severely limited by the fast reaction kinetics in conjunction with the laminar flow. Observations, as well as historical analysis of the reactor performance, substantiate these assertions. The product yield is erratic, and often low, with the bulk of product contained within tube-like structures referred to as 'wormholes.' This situation is indicative of poor mass flow of reactants interacting with heat transfer gradients and results in the formation of the wormholes. The structures are more properly referred to as "convective rolls" as described by Jensen (1993).

It is apparent that the process requires a bit of "wizardry" to produce a desirable product output. Thus, the graduate students (T. Morrison, Z. Nikolic, and myself) proceeded to document the process in terms of output variability. Historically, documentation of the process in terms of output, observations, performance characteristics, and evolution of knowledge as to operating conditions was minimal. The students gathered data related to the system operation including: temperature ramp profiles for the furnace and reactant boilers, run time, stoichiometry, yield, carrier gas flow rates, and the heat distribution and temperature control features. As an example, thermocouple measurements were compiled following calibration of new thermocouples for both the reactor furnace and boilers. Additionally, a heat distribution study was conducted of the reactor tube in real time with process runs. This necessitated the design and fabrication of an apparatus for the measurements, which was interfaced with a PC for online data acquisition. A more complete analysis of that data will be available in the thesis of Z. Nikolic (in progress). Historically, temperature measurement and control

were limited to analog readouts logged by hand. Additionally, a high degree of process variability was apparently related to operator judgment and experience.

The product quality can be described in terms of non-subjective analysis such as purity, crystal structure, stoichiometric ratios, and particle size as well as more subjective criteria that include color and consistency. The historical reactor data lacked definition in terms of these product characteristics. The students' activities were consequently aimed at quantifying the product characteristics and investigating the impact of the reactor operating conditions. In close conjunction with E-P analytical staff, approximately 20 products of student produced material were analyzed via Scanning Electron Microscopy (SEM-EDS) and X-Ray Diffraction (XRD) for purity, crystal structure, and particle sizing. This thorough design approach, while certainly more exhaustive as compared to simply designing on the basis of target yield, should further E-P's ability to effectively compete in the increasingly demanding microelectronics industry.

A statistical-based experimental design study was conducted in an attempt to optimize the current process and provide data for the scale-up. While design and analysis of the study was delegated as my primary responsibility; proper credit must be extended to T. Morrison and Z. Nikolic, as well as R. Divis and T. Potts of the E-P staff, for the successful completion of the experiments.

The study's intent was to discern and evaluate the main parameters affecting the synthesis of ZnSe. Seven process factors and their interactions were mathematically analyzed for effects on the response variables. The goal was to perform the first phase of process optimization as well as unveil the critical parameters that must be considered in the new design. The experiments were conducted in conjunction with the temperature

measurements and analytical efforts mentioned above. A summary of the study is presented in outline format in the following section.

Outline of ZnSe Experimental Study

- I. **Objective:** Conduct a factor screening study with the intent of discerning and evaluating the main parameters affecting the PVT synthesis of ZnSe. The effects, relative effects, and interactions of seven parameters on the product quality and yield were studied.
- II. **Background Information:** There is a lengthy history of the process although the variation in yields and number of aborted runs indicates only a low to moderate knowledge of the actual process parameters.

III. **Experimental Variables:**

A. <u>Response Variables:</u>	<u>Evaluation Technique:</u>	
1. Yield	Calculated based on Zn	
2. Product Quality	Appearance, XRD, SEM-EDAX	
B. <u>Factors Under Study:</u>	<u>- Level</u>	<u>+ Level</u>
(Current Level)		
1. (AF) Argon Flow (ml/min, Se/Zn)	225/219	305/305
271/262		
2. (BR) Boiling Rates (BP + deg C, Se/Zn)	33/43	39/49
35/46		
3. (FT) Furnace SS Temp (deg C)	975	1075
1000		

4. (RT) Reactor Tube Dimensions -----	Tube A	Tube B
	(See Table 3-1)	
5. (BRT) Boiler Ramp Time (hrs, Se/Zn)	2:00/2:03	1:00/1:03
		1:45/1:48
6. (XS) Amount of XS Se (moles)	1.00	2.00
		1.21
7. (CD) Cooldown Time	Slow	Fast

C. <u>Background Variables:</u>	<u>Method of Control:</u>
1. Reactant Loading	Maintain 500g Zn loadings in all runs.
2. Fore/Aft Tube Positioning	Measure and maintain consistency.
3. Reactor Tube Centering	Use thermocouple collars to center tube.
4. Welding/Sealing	Pressure checks
5. Starting Material Quality	Use same supplier and specs for each run.
6. Condensation Temp.	Maintain constant with chiller.
7. Furnace Temp. Ramp Rate	Use set profile.
8. Extent of Reaction	Boil off reactants each run.
9. Relative Boiling Rates	Keep Se rate higher.
10. Insulation	Be consistent.
11. Back Pressure	Monitor and minimize each run.

IV. **Replication:** None.

V. **Run Order:** Randomized.

VI. **Design Matrix:** 2^{7-4} fractional factorial (See Table 3-2)

VII. **Data Collection:** Lab notebook form, plots, analytical reports, etc.

VIII. **Statistical Analysis:** Statistical analysis of effects, paired comparison plots, results cube, 3D plots, etc.

IX. **Resource Considerations:**

- A. Time to Complete - Approx. 3 weeks + time for data analysis and any follow-up runs, if necessary.
- B. Schedule - Tentatively, 7/7/97 - 7/28/97 or 7/14/97 - 8/1/97.
- C. Costs - (8 runs x Cost per run) - Value of good product obtained = Costs of experiments.

Table 3-1: Reactor Tube Dimensions

	TUBE A	TUBE B
Total Tube Length (in)	45.75	45.0
Length of Reaction Section (in)	40.0	39.5
Main Tube Diameter (O.D.) (in)	3.75	3.75
Zn Inlet Outside Length (cm)	5.0	3.0
Zn Inlet Diameter (O.D.) (cm)	2.0	2.3
Zn Inlet Inside Length (cm)	18.0	16.0
Se Inlet Outside Length (cm) (end of faceplate to center of down tube)	8.5	7.0
Se Downtube Section Length (cm)	3.0	2.0

Rationale for Establishment of Factor Levels

As described by Moen et al. (1991), the most important consideration when designing an experimental study is the establishment of the levels for the factors under study. If varied improperly, the analyzed data may reflect inaccuracies and lead the researcher to erroneous conclusions. As an example, if the flow rate levels are chosen

too narrowly; they may appear to have less relative effect on a given process parameter than may actually be the case. For this reason, great care was placed on reasonable level establishment. The following outline summarizes the reasoning for each experimental variable that was arrived at after consultation with the other graduate students as well as E-P personnel.

1. **Argon Flow (AF):** Levels set at +/- 15% variation of currently used flows while keeping Se argon flow = Zn to prevent plugging.
2. **Boiling Rates (BR):** Boiler controllers currently set to hold at: Se = 721°C (or BP + 36°C) and Zn = 953°C (or BP + 46°C). Experimental levels are +/- 3°C of these levels. Historical knowledge indicates a significant rate difference with as little as a 3 degree change.
3. **Furnace Temp (FT):** Steady-State furnace temperatures now set at 1000°C, 1000°C, and 925°C (front, center, rear, respectively). Experimental values are for the front and center zones only. History indicates that the rear zone temp needs to be set at 925°C to prevent deposition of Zn on the condenser joint.
4. **Reactor Tube (RT):** There is a relationship between wormhole formation, yield, and reactor tube centering. The new thermocouple collars should give an indication of the delta T across a centered tube, as well. The runs will involve the use of two different reactor tubes (A & B) with the intent of measuring the effects of the dimensions of the tube on product yield and quality.

5. **Boiler Ramp Time (BRT):** Current time to bring boilers to BP are: Se = 1 hr 45 min and Zn = 1 hr 48 min. (Faster Se assures flow of Se prior to flow of Zn to prevent plugging.)
6. **Amount of XS Se (XS):** Richness of Se in the product is desired and current XS loading is 1.21 moles Se.
7. **Cooldown (CD):** The time to cool the reactor after a run has been questioned as a possible source of contamination. Currently, the reactor cools overnight with one fan directed towards the front of the reactor. Experimental plans are to vary the time to cool via the addition of extra fans to channel cool air directly around the reactor.

Experimental Design Matrix

Table 3-2 is a layout of the design matrix used in the experimental study. Note that the column headings are the factor numbers corresponding to the above list. The two digit numbers below the factor number in each column correspond to two-factor interactions where again, each digit signifies the individual factor as given in the above list. The factor and interaction number codes are explained in Tables 3-3 a,b. The plus and minus signs indicate the level setting of the factors as summarized in Tables 3-4 and 3-5.

Table 3-2: Experimental Design Matrix (Source: Moen et al., 1991)

Factors and Interactions							
	1	2	3	4	5	6	7
	24	14	15	12	13	23	34
	35	36	26	56	46	45	25
Test	67	57	47	37	27	17	16
1	-	-	-	+	+	+	-
2	+	-	-	-	-	+	+
3	-	+	-	-	+	-	+
4	+	+	-	+	-	-	-
5	-	-	+	+	-	-	+
6	+	-	+	-	+	-	-
7	-	+	+	-	-	+	-
8	+	+	+	+	+	+	+

Note: All divisor effects = 4

The above design is a 2^{7-4} matrix where 2 is the number of levels of each factor to be studied and the $7-4=3$ exponent is the portion of the full matrix that is to be run. A full factorial study with 2 levels and 7 factors would require 2^7 or 256 runs. Thus, a 2^{7-4} fractional factorial study requires only 2^3 or 8 runs (Mori, 1990). The matrix is one-sixteenth of a 2^7 full-factorial matrix. The nature of fractional factorial statistical design is that the completeness of the data, versus full factorial designs, is compromised in the interest of expediency. This trade-off is advantageous when analyzing processes that are

inherently costly to experiment upon, such as the process that concerns this research. Resolution of data is recovered, to a degree, by statistical manipulation and experience and judgment. The primary advantage of the design is that substantially greater volume of information is gained with a modest expenditure of time and resources.

This particular matrix is commonly used when there is low to moderate process knowledge and the researcher wishes to screen the maximum number of factors with the fewest possible runs. Given our level of knowledge as to the process variables and the time constraints, this appeared to be a prudent choice. Also characteristic of this design, there are numerous two-factor interactions that must be evaluated. Recall that these are given in Table 3-2 as two digit combinations. These interactions must be resolved since the analysis will result in a single weighted value of the importance of each column of the matrix. The value may represent the single factor's importance or one of the two factor interactions that appears below it. These interactions are important and represent the most powerful departure from single variable analytic experimentation. They are resolved by experience and judgment combined with appropriate follow-up experiments which will be reviewed in subsequent sections of this chapter.

Table 3-3 a,b: Factors and Interactions Key

NUMBERS

1	2	3	4	5	6	7
24	14	15	12	13	23	34
35	36	26	56	46	45	25
67	57	47	37	27	17	16

SYMBOLS

AF	BR	FT	RT	BRT	XS	CD
BR/RT	AF/RT	AF/BRT	AF/BR	AF/FT	BR/FT	FT/RT
FT/BRT	FT/XS	BR/XS	BRT/XS	RT/XS	RT/BRT	BR/BRT
XS/CD	BRT/CD	RT/CD	FT/CD	BR/CD	AF/CD	AF/XS

Experimental Design Grid

Table 3-4: 2⁷⁻⁴ Matrix Design Grid

<p>RUN 1</p> <p>AF = - = 225/219</p> <p>BR = - = 718/950</p> <p>FT = - = 975</p> <p>RT = + = tube B</p> <p>BRT = + = fast</p> <p>XS = + = 2.00</p> <p>CD = - = slow</p>	<p>RUN 2</p> <p>AF = + = 305/305</p> <p>BR = - = 718/950</p> <p>FT = - = 975</p> <p>RT = - = tube A</p> <p>BRT = - = slow</p> <p>XS = + = 2.00</p> <p>CD = + = fast</p>	<p>RUN 3</p> <p>AF = - = 225/219</p> <p>BR = + = 724/956</p> <p>FT = - = 975</p> <p>RT = - = tube A</p> <p>BRT = + = fast</p> <p>XS = - = 1.00</p> <p>CD = + = fast</p>	<p>RUN 4</p> <p>AF = + = 305/305</p> <p>BR = + = 724/956</p> <p>FT = - = 975</p> <p>RT = + = tube B</p> <p>BRT = - = slow</p> <p>XS = - = 1.00</p> <p>CD = - = slow</p>
<p>RUN 5</p> <p>AF = - = 225/219</p> <p>BR = - = 718/950</p> <p>FT = + = 1075</p> <p>RT = + = tube B</p> <p>BRT = - = slow</p> <p>XS = - = 1.00</p> <p>CD = + = fast</p>	<p>RUN 6</p> <p>AF = + = 305/305</p> <p>BR = - = 718/950</p> <p>FT = + = 1075</p> <p>RT = - = tube A</p> <p>BRT = + = fast</p> <p>XS = - = 1.00</p> <p>CD = - = slow</p>	<p>RUN 7</p> <p>AF = - = 225/219</p> <p>BR = + = 724/956</p> <p>FT = + = 1075</p> <p>RT = - = tube A</p> <p>BRT = - = slow</p> <p>XS = + = 2.00</p> <p>CD = - = slow</p>	<p>RUN 8</p> <p>AF = + = 305/305</p> <p>BR = + = 724/956</p> <p>FT = + = 1075</p> <p>RT = + = tube B</p> <p>BRT = + = fast</p> <p>XS = + = 2.00</p> <p>CD = + = fast</p>

Note: Units given in Table 3-5

Table 3-5: Summary of Factor Levels

FACTORS	(-) LOW LEVEL	UNITS	(+) HIGH LEVEL
1. AF = Argon Flow	225/219 (12/11)	ml/min Se / ml/min Zn (meter settings)	305 / 305 (16/15)
2. BR = Boiling Rates	718 / 950	deg C Se / deg C Zn (final set points)	724 / 956
3. FT = Furnace Temp (front and center)	975	°C	1075
4. RT = Reactor Tube	Tube A	Tube Dimensions	Tube B
5. BRT = Boiler Ramp Time	2:00 / 2:03 (slow)	hrs:min Se / hrs:min Zn	1:00 / 1:03 (fast)
6. XS = Amount of XS Selenium	1.00 (683.0)	XS moles Se (total g of Se)	2.00 (762.0)
7. CD = Cooldown Time (Rate)	One Fans (slow)	Rate of Cooling	Three Fans (fast)

Tables 3-4 and 3-5 were constructed to summarize the set of run conditions for each experiment and facilitate the run's set-up.

Experimental Design Results

The first stage of the process analysis was to observe and quantify the effects of varying the factors on each response variable. The response variables analyzed include both subjective and non-subjective data. The non-subjective responses include product yield, SEM, EDS, and XRD patterns analyzed qualitatively for impurities.

The results were tabulated and analyzed statistically from the matrix operations discussed below.

Method of Tabulating Results:

The results for each run were summarized following the cool-down and system breakdown using the following criteria as given by Table 3-6:

Table 3-6: Results Criteria and Tabulation Method

Yield (%):
Wt. of Condensate / Mass %:
Wt. of Unreacted Material in Condenser (g):
In Boilers:
In Condenser:
Blowthrough of Product ?:
Quantity (g):
Distribution of Products (approx %):
Front:
Center
Rear:
Wormhole Present ?:
Location:
Length (cm):
Color of Product:
Product Consistency:

The percent yield was calculated on a zinc molar basis:

$$\left[\frac{\text{ActualZnSeMass}(g)}{\text{TheoreticalZnSeMass}} \right] \times 100\% \quad (3-2)$$

Where the theoretical ZnSe mass yield is computed as:

$$\left[\frac{\text{ZnLoading}(g)}{MW_{Zn}} \right] (MW_{ZnSe}) \quad (3-3)$$

Statistical Analysis of Run Data

Data from the eight runs were incorporated into the matrix in the following manner. First, each factor (e.g. – argon flow) for each run is assigned the sign (- or +) from the experimental design matrix grid and is inserted into the analysis table. The magnitude of the response variable (e.g. - % product yield) is then inserted into the table and multiplied by the appropriate sign. The data are then multiplied as follows:

$$AvgLow = \frac{\sum \text{Runs at Low Factor Level}}{\text{Divisor Effect}} \quad (3-4)$$

Where the characteristic divisor effect for the eight run 2^{7-4} matrix is 4 (Moen et al., 1991). Similarly, the average for the high level for each factor is analyzed for each response variable of interest. The delta (Δ) represents the magnitude of the response variable that can be attributed to the particular factor:

$$\Delta = | Avg Low - Avg High | \quad (3-5)$$

The weight (ω) is a normalized value assigned to each factor that represents its relative magnitude of the delta as compared to the factor having the highest delta value for that response variable:

$$\omega = \frac{\Delta_i}{\Delta_{\max i}} \quad (3-6)$$

A weighted factor effect of 0.45 - 0.50 or greater is considered significant. The ranking is a listing of the relative importance of the factors from 1, the most important, to 8, the least important.

The response variables are outlined and classified in the following Tables 3-7a and 3-7b (Morrison, 1998).

Table 3-7 a, b: Response Variables and Classifications for the Experimental Runs

Run	Yield	Wormhole Length	Product Consistency	Product Color	Condensate	Distribution	Sectional Distribution			Wormhole Yield
							Front Zone	Center Zone	Back Zone	
1	51.1	0.80	1.5	3	42.2	1	3	1	2	70.0
2	41.4	0.67	1.5	8	44.4	2	1	3	2	80.0
3	45.5	0.67	4	4	53.9	3	1	2	3	45.0
4	67.7	0.75	3.5	2	23.5	2	2	3	1	55.0
5	61.8	0.67	2	7	44.0	2	2	3	1	75.0
6	58.0	0.67	2.5	6	42.4	2	2	3	1	75.0
7	35.1	0.33	3	1	48.1	1	3	1	1	90.0
8	26.8	1.00	2	5	48.1	3	2	1	3	40.0
midpoint	44.9	0.67	1	9	58.1					

Response Variable Classifications

Yield	Yield is percent yield calculated on a molar basis with zinc as the limiting reagent.
Wormhole Length	The fraction of total tube length (not including the rear connector section) is displayed.
Color	The powders were assigned a number 1-9 with 9 being the brightest.
Consistency	The powders were assigned a number 1, 2, 3, or 4 corresponding to fluffy, fine, grainy, or coarse.
Condensate	Condensate is percent yield of total mass of reactants.
Distribution	1 designates front zone with most product, 2 center, and 3 back.
Distribution: Front Zone	3 = greatest amount of product contained in this zone.
Distribution: Center Zone	2 = second greatest amount of product.
Distribution: Back Zone	1 = least amount of product contained in this zone.
Wormhole Position	None (0) - Bottom (1) - Top (2) - Complex (3)
Wormhole Yield	Yield is percent of total yield.

Analysis of Non-Subjective Response Variables

The primary criterion that the experimental run analysis was based, is the product yield. The non-subjective response variables were product yield, as well as the wormhole length as measured from the front to the rear of the reactor tube. The results are tabulated in Table 3-8.

Table 3-8: Results for Yield Response Variable

FACTORS

RUN NO.	1 = AF	2 = BR	3 = FT	4 = RT	5 = BRT	6 = XS	7 = CD
1	-51.1	-51.1	-51.1	51.1	51.1	51.1	-51.1
2	41.4	-41.4	-41.4	-41.4	-41.4	41.4	41.4
3	-45.5	45.5	-45.5	-45.5	45.5	-45.5	45.5
4	67.7	67.7	-67.7	67.7	-67.7	-67.7	-67.7
5	-61.8	-61.8	61.8	61.8	-61.8	-61.8	61.8
6	58.0	-58.0	58.0	-58.0	58.0	-58.0	-58.0
7	-35.1	35.1	35.1	-35.1	-35.1	35.1	-35.1
8	26.8	26.8	26.8	26.8	26.8	26.8	26.8
AVG " - "	-48.38	-53.08	-51.43	-45.00	-51.50	-58.25	-52.98
AVG " + "	48.48	43.78	45.43	51.85	45.35	38.60	43.88
Δ	0.10	9.30	6.00	6.85	6.15	19.65	9.10
ω	0.01	0.47	0.305	0.35	0.313	1.00	0.46
RANKING	7	2	6	4	5	1	3

Note that the inconsistent use of significant figures is due to the need to carry the weight ω , to the one-hundredths decimal place.

Factors 6 and 2 columns have the greatest impact on the yield. Note that the cooldown time (CD) is the third factor weighted higher than 0.40, but is assumed to be inconsequential in terms of yield. It was included in the study to explore the impact that the factors have on product quality. It is, however, a relative gauge of background noise with respect to yield.

Recall from the design matrix (See Table 3-2), that the factors must be resolved from the interactions. For example, factor 2 is the boiling rate but must be resolved from the interactions of: 1-4 (AF-RT), 3-6 (FT-XS), 5-7 (BRT-CD). As stated above, CD is of no effect; thus the 5-7 interaction can be neglected. The remaining factors and interactions are then: factor 2, interactions 1-4 and 3-6. Similarly, column 6 of the design matrix was analyzed. These interactions are best resolved graphically by response plots where a departure from parallel is an indication of significant interaction. These plots with respect to yield and column 2 and 6 are shown in Figures 3-1 through 3-5.

Interactions for Yield

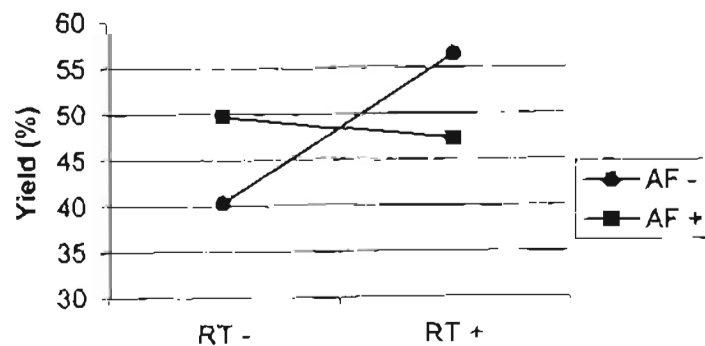


Figure 3-1: RT/AF Interaction Check

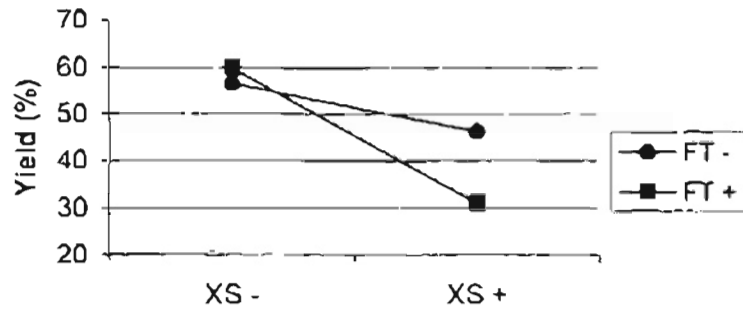


Figure 3-2: FT/XS Interaction Check

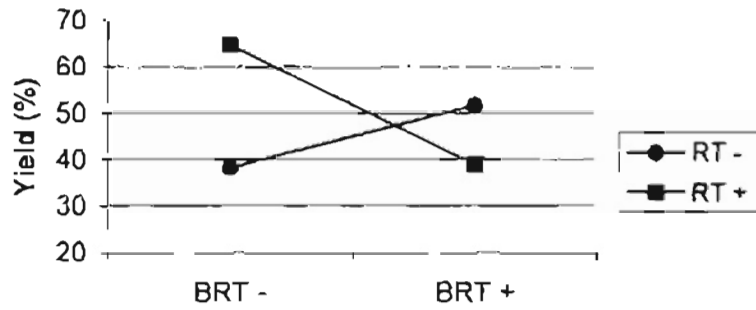


Figure 3-3: BRT/RT Interaction Check

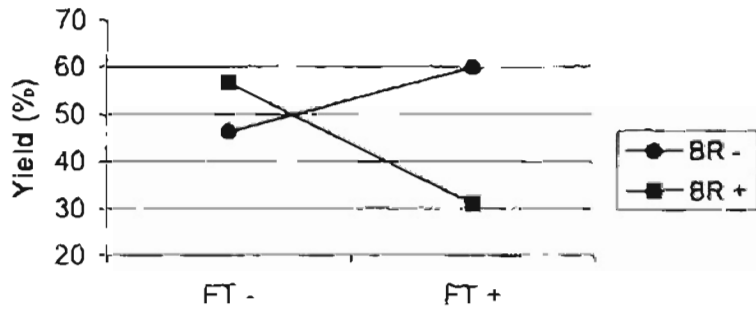


Figure 3-4: FT/BR Interaction Check

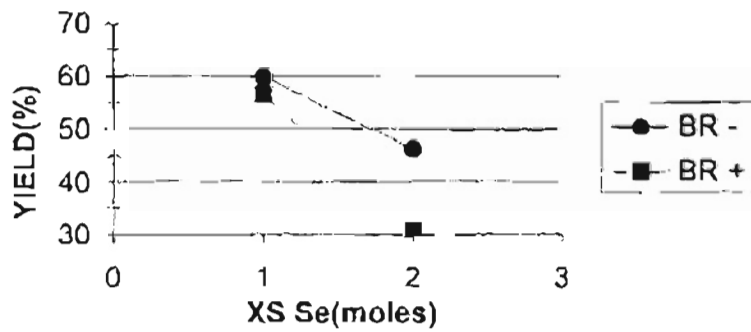


Figure 3-5: XS/BR Interaction Check

The plots indicate a slight interaction between the amount of excess selenium (XS) and the rate at which the reactants are vaporized (BR), which corresponds to the two most important individual factors. The effect of these two parameters on the product yield is illustrated in a 3-dimensional surface plot as shown by the Figure 3-6. It is apparent that a high amount of excess selenium is not required as previously believed.

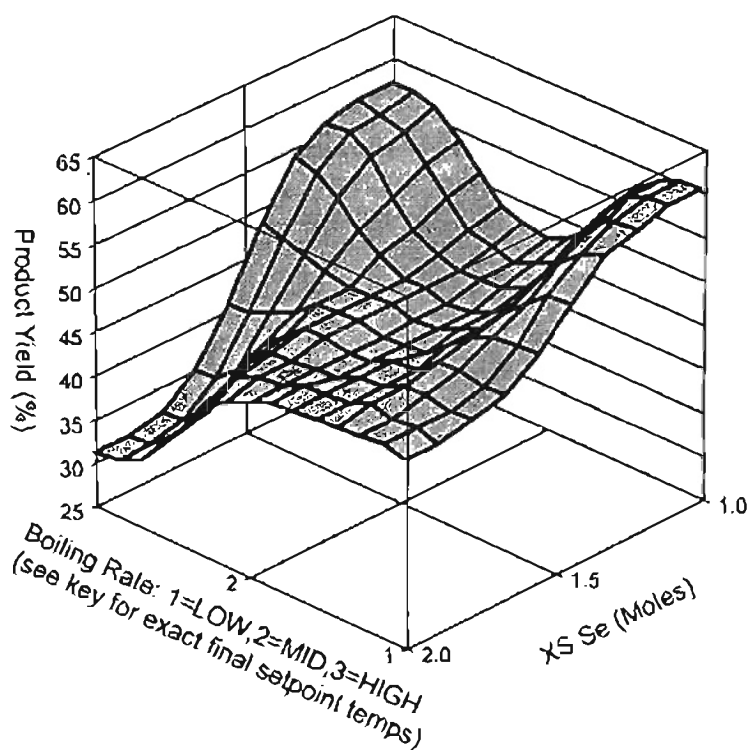


Figure 3-6: Interaction of Boiling Rate (BR) and XS Se on the Product Yield

Similarly, the other important interaction is the choice of reactor tube and the amount of time that is allowed for the boilers to ramp to their respective final setpoints. Although less understood due to the vagaries of the different tubes, the RT effect on yield

does emphasize the importance of the manufacturing specifications. This effect is a result of the added radial dimension of 2 cm to tube B, which allows for slightly more residence time and radial mixing. It is also displayed as a 3D plot in Figure 3-7. All other possible interactions were deemed negligible from similar examination of their 3 dimensional shapes.

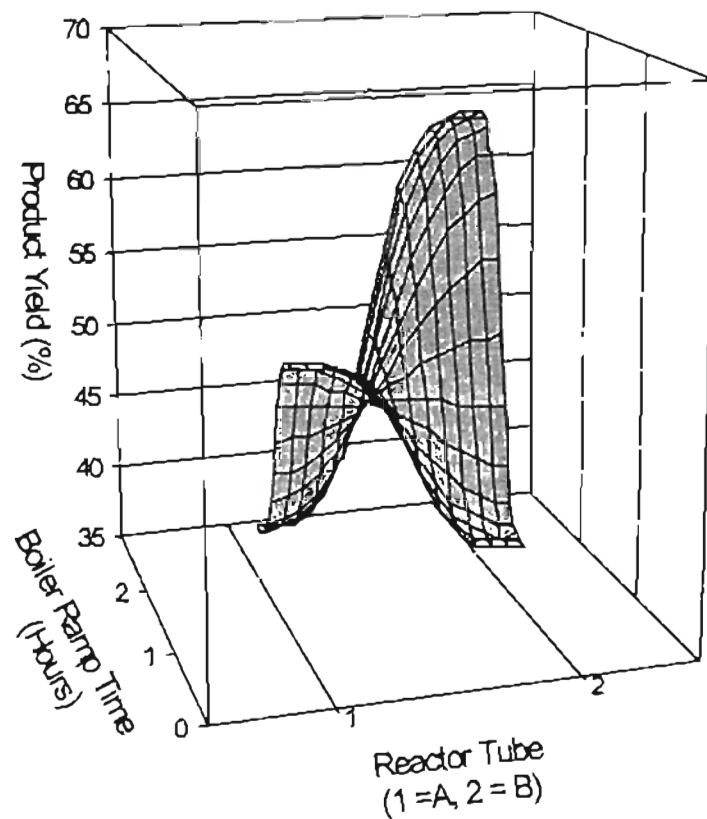


Figure 3-7: Interaction of Reactor Tube (RT) and Boiler Ramp Time (BRT) on the Product Yield

Table 3-9: Results for Wormhole Length Response Variable

FACTORS							
RUN NO.	1 = AF	2 = BR	3 = FT	4 = RT	5 = BRT	6 = XS	7 = CD
1	-0.80	-0.80	-0.80	0.80	0.80	0.80	-0.80
2	0.67	-0.67	-0.67	-0.67	-0.67	0.67	0.67
3	-0.67	0.67	-0.67	-0.67	0.67	-0.67	0.67
4	0.75	0.75	-0.75	0.75	-0.75	-0.75	-0.75
5	-0.67	-0.67	0.67	0.67	-0.67	-0.67	0.67
6	0.67	-0.67	0.67	-0.67	0.67	-0.67	-0.67
7	-0.33	0.33	0.33	-0.33	-0.33	0.33	-0.33
8	1.00	1.00	1.00	1.00	1.00	1.00	1.00
AVG " - "	-0.62	-0.70	-0.72	-0.59	-0.61	-0.69	-0.64
AVG " + "	0.77	0.69	0.67	0.81	0.79	0.70	0.75
Δ	0.16	0.02	0.06	0.22	0.18	0.01	0.12
ω	0.70	0.07	0.25	1.00	0.82	0.05	0.52
RANKING	3	6	5	1	2	7	4

KEY : Fraction of total tube length is displayed.

As shown in Table 3-9, the important factors (or columns) are AF, RT, and BRT. The possible interactions for wormhole length were examined similarly as for yield. The only apparent significant interaction is AF/BR as illustrated in the next section.

Interactions for Wormhole Length

Figure 3-8 indicates that high boiling rate, high carrier gas flows, and again, the dimensions of the reactor tube exacerbate lengthening of the wormhole structure.

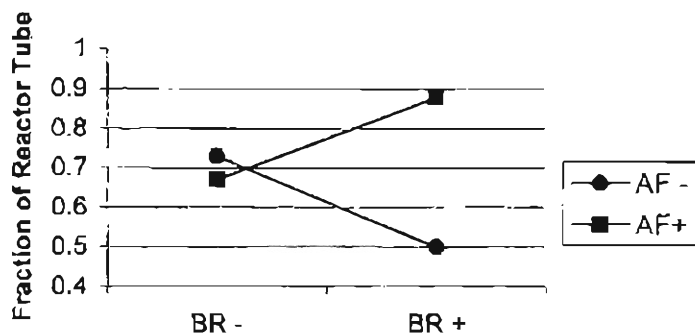


Figure 3-8: Interactions Check for AF/BR on Wormhole Length

Other Non-Subjective Response Variables

Attempts were made to analyze the system in terms of condensate quantity, distribution of product within the tube, position of the wormhole within the reactor tube, and the yield contained within the wormhole. These results were inconclusive due to the inaccuracy of the data collection methods, e.g. – the mass of product deposited within various zones was estimated visually as opposed to taking actual measurements.

Analysis of Subjective Response Variables

As described in the Introduction, the process output has historically been described by ambiguous terminology. Typically, a run would be characterized as good when the product was, “nice and bright,” or “loose and fine,” etc. It was necessary to attach a degree of reproducibility and consistency to the product descriptions. The data were analyzed for the effects of the factors on semi-standardized descriptors of the

product appearance. The results and keys for the quantification of the response variables are given in Tables 3-10 through 3-12.

Table 3-10: Subjective Response Variables Results and Key

Experiment No.	Run No.	Product Color*	Product Consistency**
5	1	3	1.5
9	2	8	1.5
8	3	4	4
7	4	2	3.5
4	5	7	2
3	6	6	2.5
6	7	1	3
2	8	5	2
10	midpoint	9	1

Key: * 9 = Brightest

** Fuffy = 1, Fine = 2, Grainy = 3, Coarse = 4

Table 3-11: Product Color Response Variable Results

RUN NO.	FACTORS						
	1 = AF	2 = BR	3 = FT	4 = RT	5 = BRT	6 = XS	7 = CD
1	-3	-3	-3	3	3	3	-3
2	8	-8	-8	-8	-8	8	8
3	-4	4	-4	-4	4	-4	4
4	2	2	-2	2	-2	-2	-2
5	-7	-7	7	7	-7	-7	7
6	6	-6	6	-6	6	-6	-6
7	-1	1	1	-1	-1	1	-1
8	5	5	5	5	5	5	5
AVG " - "	-3.75	-6.00	-4.25	-4.75	-4.50	-4.75	-3.00
AVG " + "	5.25	3.00	4.75	4.25	4.50	4.25	6.00
DELTA	1.50	3.00	0.50	0.50	0.00	0.50	3.00
WEIGHT	0.50	1.00	0.17	0.17	0.00	0.17	1.00
RANKING	2	1	3	3	4	3	1

Table 3-12: Product Consistency Response Variable Results

RUN NO.	FACTORS						
	1 = AF	2 = BR	3 = FT	4 = RT	5 = BRT	6 = XS	7 = CD
1	-1.5	-1.5	-1.5	1.5	1.5	1.5	-1.5
2	1.5	-1.5	-1.5	-1.5	-1.5	1.5	1.5
3	-4.0	4.0	-4.0	-4.0	4.0	-4.0	4.0
4	3.5	3.5	-3.5	3.5	-3.5	-3.5	-3.5
5	-2.0	-2.0	2.0	2.0	-2.0	-2.0	2.0
6	2.5	-2.5	2.5	-2.5	2.5	-2.5	-2.5
7	-3.0	3.0	3.0	-3.0	-3.0	3.0	-3.0
8	2.0	2.0	2.0	2.0	2.0	2.0	2.0
AVG " - "	-2.63	-1.88	-2.63	-2.75	-2.50	-3.00	-2.63
AVG " + "	2.38	3.13	2.38	2.25	2.50	2.00	2.38
DELTA	0.25	1.25	0.25	0.50	0.00	1.00	0.25
WEIGHT	0.20	1.00	0.20	0.40	0.00	0.80	0.20
RANKING	4	1	4	3	5	2	4

The product color is a sharper, brighter yellow if the system is given a longer (an additional 6 hours or more) time to cool down and lower boiling rates and Ar flows. It may be that rapid cooling entails removing the reactor tube containing the product while it is still quite hot which exposes the product to the air at a higher temperature which promotes oxidation and thus dulling.

High amounts of excess selenium appear to decrease the coarseness of the final product. Again, lower boiling rates are preferred with respect to the consistency, as well.

Experimental Design Follow-up Runs

Response Variable Linearity

The linearity of the factors effects on the response variables was evaluated graphically following insertion of a midpoint data point. If a factor is not linear within

the range tested; the effect could be erroneously reported. Figure 3-9 illustrates the technique with respect to the effect of excess Se on the product yield.

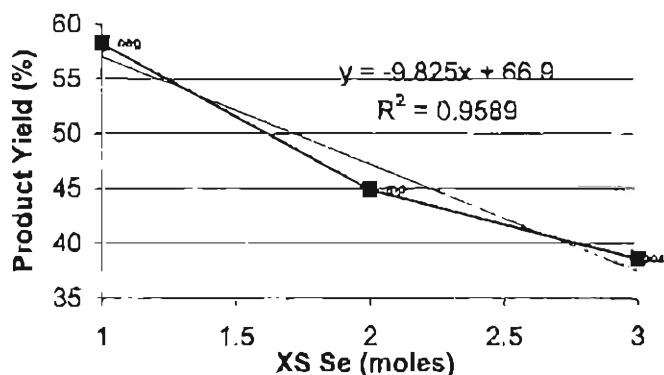


Figure 3-9:
Linearity Check for XS Se Effects

In addition to the midpoint run, an attempt at confirming the preliminary conclusions was made. The conditions for these two runs are listed in Table 3-13.

Table 3-13: Follow-up Run Conditions

<u>FACTOR</u>	<u>SYMBOL</u>	<u>MIDPOINT CONDITIONS</u> (EXP 10 / RUN MP)	<u>CONFIRMATION</u> (EXP 11 / RUN CC)
1	AF	245/262 ml/min (Se/Zn)	305 ml/min (both Se/Zn)
2	BR	721/953 (final setpoints: Se/Zn)	718/950
3	FT	1025 C	975 C
4	RT	Tube B	Tube B
5	BRT	1.5 hrs	2.0 hrs
6	XS	1.5 moles (723g total)	0.50 moles (644g total)
7	CD	Semi-Fast (two fans)	Fast (three fans)

Experimental Design Conclusions and Discussion

Summary of Results

For the response variables studied, the design matrix reduces from a 2^{7-4} to a 2^3 or 2^2 thus eliminating confounding effects and simplifying analysis of the data.

The dominant factor affecting yield is the quantity of excess selenium in the reactor with a lower loading of XS Se preferred. We conjecture that the reactor has typically been run while 'flooded' with Se. This condition produces a favorable environment for the formation of wormholes. The wormholes reduce the yield by limiting the quantity and efficiency of the Se/Zn contacting pattern. A preferred design would allow the two reactants to flow together with turbulence thus limiting wormhole formation and improving yields. All other factors had effects that were less than 50% of the XS Se loading's effect on yield. It should be noted that the other factors exhibited little or no effect on yield in the range studied - i.e. any given factor may not exhibit an appreciable effect on a response at the levels that were studied.

The second most important factor that affects the yield is the boiling rate. A lower BR is preferred and has a weight of 0.47 relative to the XS Se factor. Additionally, these two factors for this response variable exhibit a slight interaction with one another (see 3D plot Fig. 3-5). Optimized conditions for highest yields should be: low XS Se (XS = 0.5moles), low boiling rate (BR = final boiling setpoints 718/950° C Se/Zn), high Ar flow (AF = 600 total ml/min), low furnace temp (FT= 975°C), reactor tube B (RT), and slow boiler ramp times (BRT = 2.0 hrs).

Following the above analysis, it was decided to gauge the yield as a function of the wormhole length. There are three factors and one interaction that affect this response variable. The dominant factor is the reactor tube that is used (see Table 3-1 for the dimensions of the two tubes) with tube A preferred. The reactor tube used results in a 20% difference in the length of the wormhole formed. However, the preferred tube in terms of yield is tube B that can account for a 7% greater yield. The second most important factor with a weight of 0.82 relative to the reactor tube is the boiler ramp time with slower BRT preferred. Of third highest importance is the flow of argon, with lower preferred, and a weight relative to the reactor tube of 0.70. There is a slight interaction between the flow of Ar and the boiling rate on the length of the wormhole as shown in Figure 3-6. According to this analysis, the length of the wormhole can be minimized by operation with low Ar flow and low boiling rate or; due to the interaction, at high Ar flow and high boiling rates. This makes intuitive sense given that plugs are more likely to develop due to the migration of one reactant to the opposite inlet under low flow and high boiling rates. By similar reasoning, the converse should be equally likely.

The preferred settings for less wormhole formation can be coordinated with those for yield. There is a conflict, of sorts, with respect to the tube preferred by the two response variables, however. It was decided to choose the appropriate reactor tube for the confirmation run on the basis of the less subjective analysis of the yield.

As opposed to the examination of its length, an analysis of the quantity of material that is contained within the wormhole would be preferable. This approach should prove to be more reliable, but again it was difficult to objectively analyze the data in these terms after the fact. The analysis of “wormhole yield” is therefore not included

in this report, as it does not lend itself to accurate analysis or definitive conclusions. Likewise, it was attempted to break the data down in terms of wormhole position and the distribution of product, both by individual zone and general location of deposition within the reactor. However, linking the yield with location or distribution of products within the reactor did not prove to be reliable.

The two remaining subjective response variables of product color and consistency were analyzed as follows. Each of the runs were characterized on a comparative basis relative to the other eight products.

Color is impacted only by the boiling rate with a lower rate producing a brighter yellow product. Similarly, the product's consistency is affected by the boiling rate with the lower rate giving a "fluffier" product, while a lower excess Se loading results in a coarser product. Neither of these response variables is affected by a significant interaction.

The midpoint run did not reveal a non-linearity of the important factors with respect to yield. The more subjective response variable factors exhibited poor linearity which gives a rough indication of the degree of subjectivity and, hence, the reliability of the analysis.

Results of Initial Confirmation Run

It was essential that a confirmation run be completed in the time remaining to validate the conclusions drawn from the data with respect to the yield. The conditions were derived from a listing of the net effects of each factor taking into account the relevant interactions. The levels for the confirmation run were chosen from ranges

within the study's experimental values, with the exception of the loading of Se. Perhaps if low XS Se was advantageous; it assumed that the effect would be linear if the experimental range were extended. Thus the run was made at an excess Se loading that was one-half of the level previously attempted.

The confirmation run completed at the end of the summer 1997 resulted in a ZnSe yield of only 35% with a large wormhole. Probable explanations for the confirmation producing a yield less than expected are as follows:

- 1) The experimental runs contain one or more anomalies leading to incorrect factor analysis. One example may be a run that plugged midway through the experiment. The solution is to replicate one or more of the runs and check for repeatability.
- 2) A lack of repeatability could indicate a special cause of variation within a run.
- 3) A lack of repeatability could also indicate that there is a parameter that is not identified within the process. Any unknown factor would then have introduced uncontrolled variation within one or more of the experimental runs thus skewing the analysis of factors.
- 5) A strong interaction was overlooked in the analysis.
- 6) The excess selenium level was set at a level outside the linear range that was previously studied.

Follow-up Analysis and Confirmation

The above data were further analyzed during the Fall of 1997 to determine a cause for the low yield of the confirmation run. The most likely (and simplest to test)

hypothesis is that of number six listed above. An opportunity was available in the first week of January 1998 to conduct an experiment on-site at E-P.

The conditions for the new run are identical to the confirmation run (EXP11) as listed above in Table 3-13 with the exception of increasing the amount of excess selenium (XS) to 1.0 mole (644g). This quantity brings the parameter within the linear range previously tested.

Additionally, it was conjectured that the front-end heat loss through the Fiberfrax insulation material was substantial. The first run conducted during the week entailed the collection of additional temperature data via thermocouples placed at various locations at the front-end of the inlet tubes. The temperature readings indicated temperature drops of 200°C from the boiler settings. It was also discovered that the time for the front-end temperatures to reach steady state was approximately 15-30 minutes more than anticipated. The subsequent confirmation run, in addition to adjusting the XS level, incorporated a two-stage ramp of the boiler temperatures prior to reaching boiling points of the two reactants. Also, the front-end insulation was increased to prevent heat loss.

The second confirmation run resulted in a yield of 69.8% with an evenly distributed bed of brightly colored product. The run represented perhaps the best result in terms of yield and product distribution to date.

Based on this and the previous summer's results, the following report was submitted to Eagle-Picher outlining the recommendations for process improvement and optimization of the current system. The initial feedback was positive with respect to improvement and reproducibility of process.

Recommendations and Conclusions

I. Recommended Operating Parameters for ZnSe Synthesis:

- A. Carrier Gas (Ar) Flow : 305 ml/min (both boilers)
- B. Current Calibrated Flowmeter Settings : 15 Zn / 16 Se
- C. Furnace Temperature Settings : 975°C (front and center), 912°C (rear)
- D. Tube Size : Small (Tube 'B' preferred)
- E. Boiler Ramp Time : approx. 2.0 hrs (see also Section III)
- F. Final Boiler Ramp Temperatures : 950°C (Zn), 718°C (Se)
- G. Reactant Loading : 500.0 grams (Zn), 685.0 grams (Se)

II. Heat Transfer Considerations

Run success and reproducibility can be greatly enhanced with attention to three areas of operation within the present system that relate directly to the transfer of heat to the reactor.

A. Front- End Temperature Control:

It is highly desirable that the temperature profile of the front (boiler) end of the apparatus be allowed to reach a steady-state prior to boiling of the reactants. Our recommendation is to monitor the temperatures of the boiler inlet tubes that transfer reactants to the reactor. This is easily accomplished by the addition of two or three thermocouples in this area.

B. Front-End Heat Loss:

To aid in the minimization of reactant reflux in the bottom boiler, as well as providing a measure of steady state temperature control, it is recommended that additional insulating material be heavily layered around the front end. Preferably, a modular two-zone heater that encompasses the exposed areas of the front of the apparatus should be used.

C. Furnace Temperatures:

The analysis of the experimental data indicates a decreased tendency towards “wormhole” formation at the slightly lower furnace temperature setting of 975°C. Secondary velocity profiles due to convective heat transfer are decreased when the interaction of the temperature and carrier gas flow is considered.

III. Mass Transfer Considerations

There are several areas in which the current system procedures can be slightly modified to allow for greater control of both the rate of transfer of material into the reactor and the reacting interface. Here, the goal is to improve the run yield by avoiding the blowthrough of reactants and the formation of wormholes.

A. Carrier Gas Flow:

The semi-optimized flowrates for the ZnSe synthesis represent a 10 percent increase in the current procedure. This raises the reactor tube inlet velocities to minimize plugging. These conditions allow the system to increase reactant residence time slightly and should result in higher yields.

B. Boiler Ramp Procedure:

As stated above, it is advantageous to allow the system to arrive at a steady state temperature before allowing the reactants to come to a boil. This is best achieved by setting the programmable boiler controllers at temperatures that are 10 degrees below the respective boiling points of the reactants (approx. 675°C for Se and 897°C for Zn). The second step of the ramp then includes the final set points. This method of assuring constant temperature at the front end assists in the establishment of constant mass transfer rates at the critical early stage of the run that is otherwise prone to plugging. This procedure also prevents overshooting the final setpoints, which can disturb the balance of the two mass transfer rates.

C. Final Boiler Setpoints:

The new final setpoints represent a three-degree decrease in the current settings. This should result in a slightly more dilute reactant gas phase concentration in the tube to assist in the prevention of plug formation. Also note that the recommendation does not include setting the Se to boil first. This serves the purpose of producing an optimum contacting pattern within the reactor and reducing the amount of Se waste.

Summary

The above recommendations should provide a degree of optimization to the production of ZnSe in the present system. This is accomplished by establishment of procedures and operating parameter setpoints that result in the following: 1) Reduction in the number of sources of uncontrolled variation within the process, 2) operation of the

reactor at as near steady state as possible, and 3) transport of reactants into the reactor at nearly the same initial point in time and at the same rate. These procedures and operating parameters should result in improved run yield and reproducibility with minimal outlay of expense and effort.

CHAPTER IV

PROPOSED NEW REACTOR DESIGN AND MODELING

Introduction

The information that was gained as a result of the experimentation with the current system was used to establish the basis for the new reactor design. Also, close collaboration with Eagle-Picher staff provided the research group the opportunity to learn, in greater detail, the sponsor's corporate objectives.

This chapter will outline the new reactor design basis and the objectives that were interfaced with E-P goals. Presentation of the new reactor design will cover the theory and the methods related to the chemical, kinetic, thermodynamic, and transport phenomena associated with the process.

We will proceed from the theoretical foundation to a review of the computational fluid dynamics (CFD) modeling used in the course of finalizing the reactor's design. The model's background theory, approach, assumptions, and limitations will be discussed in detail.

Basis for the Design

The following list of design criteria and rationale outlines the constraints considered in the development of the various design concepts. Table 4-1 summarizes the design basis for the new reactor.

Product Specifications:

Obviously, E-P's product purity specification was a primary consideration. The current acceptable assay is 5-9's (99.999% pure) ZnSe. Although there is no empirical evidence requiring a particular crystal morphology or particle size distribution; the objective is to produce a hexagonal particle with a fineness of approximately 20 microns or less.

Product Yield and Throughput:

The target yield is 80% averaged across runs and based on moles of zinc. This can be compared to the historical yield of approximately 35-40% which may be lower if the aborted runs with zero yields were included (Morrison, 1998).

The product output per batch run is targeted to be 2 kgs; as compared to an approximate output of 0.60 kg with the present system.

Process Performance:

As discussed earlier; the historical performance of the process is erratic. The goal is to address all of the probable process variables intrinsic to the new design. Next, we will establish reasonable ranges for operation with the objective of reducing the number of wasteful aborted runs.

Process Familiarity and Ease of Operation

Implementation of a new reactor would be facilitated by a design that does not represent a great departure from the present system. This translates to mean that a

Table 4-1: Summary of the Design Basis

Design Criteria	Target
Reactor Orientation	Horizontal
Capacity	2.0 kg/run
Operation Mode	Batch
Product Purity	99.999+ %
Product Morphology	Hexagonal
Failed Run Rate	< 5.0 % of runs
Yield	80+ %

Alternative Design Concepts Considered

Several concepts were considered in the course of arriving at a final design. First, those concepts involving continuous operation and/or vertical orientation of the reactor tube were eliminated as possible routes.

The more radical schemes that were also discarded included wet methods, insertion of a rotating extruder to aid in product removal during the run, and a cyclone reactor.

As presented in a design review meeting with E-P personnel early in 1998, various horizontal batch systems were originally proposed and rejected. The other physical modifications to the reactor tube that were considered include: 1) injection of an inert stream at various points within the reactor to alleviate plugging, 2) insertion of

various items including baffles, obstacles, etc. into the reactor tube to either segregate reactant flows for a period of time or to aid in mixing, and 3) counter-current and crosscurrent orientation of injection nozzles. All of the above physical modifications were rejected on the basis that the added complexity in the fabrication, system breakdown, or clean-out procedures would be prohibitive. From an engineering design perspective, the schemes would unnecessarily complicate the modeling efforts. Additionally, all the advantages offered by the various concepts could be attained by an even simpler approach.

Overview of the New Reactor Design

Design Concepts

The new reactor design is based on the following features: 1) horizontal, concentric reactor tubes, 2) optimized nozzle orientation, and 3) vertically oriented boilers with back pressure monitoring and control. The new design features are best explained by discussion of the inherent design and operational problems associated with the present system. The new design's resolution of each problem is summarized in Table 4-2.

Table 4-2: Characteristics of the Proposed New Design

Old System Problem	New Design Solution
Frequent aborted runs due to plugging, low yields as a result of poor flow characteristics, wormhole formation, etc. :	Optimized design and orientation of inlet nozzles via CFD modeling.
Time and labor intensive system turnaround, hazardous cleanup, frequent welding, quartz breakage, inconsistencies of reactor dimensions, process variation due to run-to-run set-up methods, etc.:	Reactor system designed to be essentially static. Tube-in-a-tube reactor where main outer tube remains in place with boilers welded semi-permanently. The inner tube is withdrawn from the rear of the apparatus following each run, the product is dumped, and the main tube is “reloaded” with the same or other inner tube for the next run.
Poor heat transfer control at front end of system:	Redesign front-end heaters to include full enclosure of boilers and inlet tubes, add thermocouple system for monitoring.
Poor mass flow control of reactants, uncertain run times:	Reorient both boilers vertically, add argon carrier feed tube positioned at bottom of boiler to measure back pressure. From head pressure correlation, calculate height of molten reactants and thus mass flow. Set boiling rates via feedback loop from pressure readings.

New Design Features and Advantages

1. Horizontal reactor technology and experience can be readily transferred and implemented to the new system.

2. Improved turnaround time and fewer aborted runs via reduction in plugging, welding, and breakage frequency. Simplified cleanup procedures whereby the inner tube that contains the product is inverted, scraped, and re-inserted for the next run. Acid washing is required infrequently and each new run setup is not limited by quartz-ware since inner tubes are readily available.
3. Greater process control. Static system eliminates many sources of variation in the process. Back-pressure controlled boilers allow for “dialed” in mass flow rates and run times.
4. Overall improved/increased capacity, yield, efficiency, and safety.

Illustration of New Reactor System

Depicted below in Figure 4-1 is the new reactor system. Detailed Autocad drawings are available in the thesis of Morrison (1998).

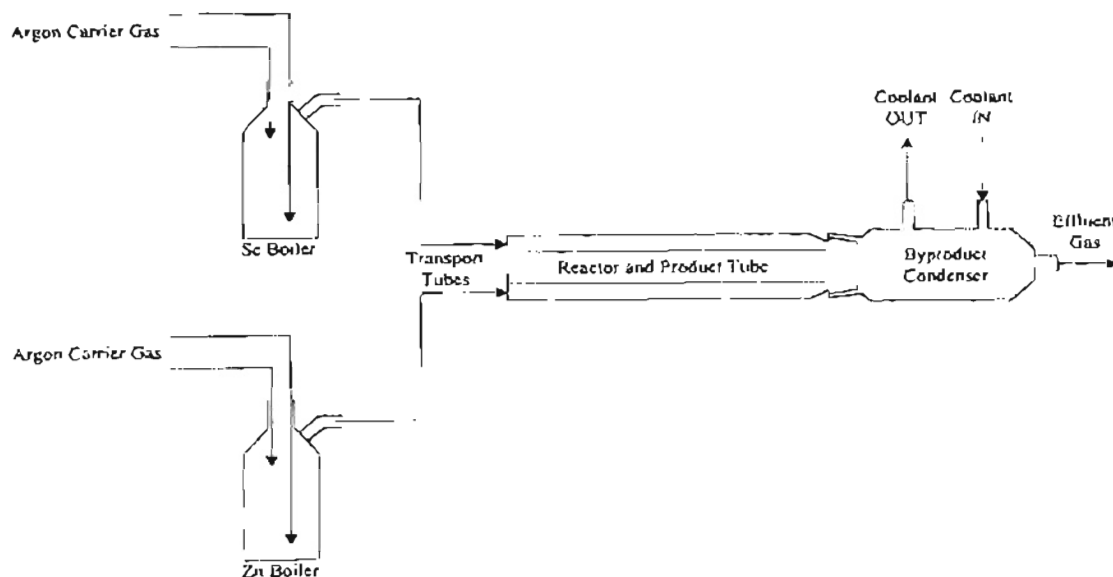


Figure 4-1: New Reactor System Drawing

New Design Research Objectives

Several engineering aspects of the new design required research to achieve the aforementioned performance characteristics. The areas emphasized in this work include nozzle design, system component sizing, reactor modeling, and process optimization.

CFD Modeling of Proposed Design

The complex nature of the flow phenomena necessitated the use of computer simulations in the course of designing the new reactor. This section will give a brief overview of the modeling theory, equations, assumptions, software basics, and the development steps. The model was developed in collaboration with Morrison (1998) whose thesis may be relied upon for additional information as well as an alternative modeling approach.

Modeling Theory and Steps

Summarized below are the steps given by Himmelblau and Bischoff (1968) that outline the theory behind computer and mathematical modeling of chemical processes. The steps provided a conceptual guide used in the course of the development of the model. (See also: Figure 2-2 of Literature Review.)

1. Formulation of the problem and establishment of criteria and requirements.
2. Classification of the process and establishment of subsystems.
3. Determination of relationships between subsystems.
4. Analysis of variables.

5. Mathematical modeling of process variables.
6. Evaluation of how well the model represents reality.
7. Interpretation of results and application of the model.

Purpose and Classification of the Model

A phenomenological model that can accurately describe the transport phenomena was required to gauge the effects that the complex flow phenomena have on the performance of the reactor. The model can only then be applied to the formulation of the new system. Finally, the model should then facilitate the optimization of the new design through the use of parametric variation of the model inputs.

Computational Fluid Dynamic (CFD) models are ideally suited for application to the above goals. Specifically, the approach in this work is classified as a multiple-gradient, deterministic transport model. The model incorporates reacting flow and also accounts for heat transfer effects. FLUENT (version 4.0) was chosen as the modeling software.

FLUENT CFD Basics

FLUENT is a commercially available CFD package that incorporates many subsystems such as fluid flow, heat and mass transfer, and chemical reactions that can be applied to a myriad of physical models. The subsystems are integrated and solved via numerical finite volume difference equations. The resulting profiles depicting species, velocity, temperature, or other phenomena can be observed as outputs.

The package has many readily applied “structured” models, however, our unique application is an “unstructured” problem that requires the user to input a geometry.

FLUENT geometries can be two or three dimensional, depending on the application needs. For simplicity’s sake, the model developed in this work was based on a 2-D axi-symmetric geometry. Subsequent work by Nikolic (In progress) should improve upon this approach by the development of a full, 3-D geometry.

The physical geometry is divided into finite volumes in the form of a mesh over which the applicable differential equations are iteratively solved. A greater mesh density produces a higher resolution of results. The user then designates the faces that comprise the physical model, which includes walls, inputs, outputs, and zones.

The physical model is then combined with user-inputs for the reacting mixture subsystem that includes kinetics, physical and chemical properties, and other necessary parameters that will be discussed in detail later.

Basic Steps for Creation of a Physical Model

A chart outlining the essential steps used to develop a physical model within FLUENT/UNS is given as Figure 4-2. The chart is by no means comprehensive, but is intended to provide a broad overview of the many steps that FLUENT/UNS modeling requires.

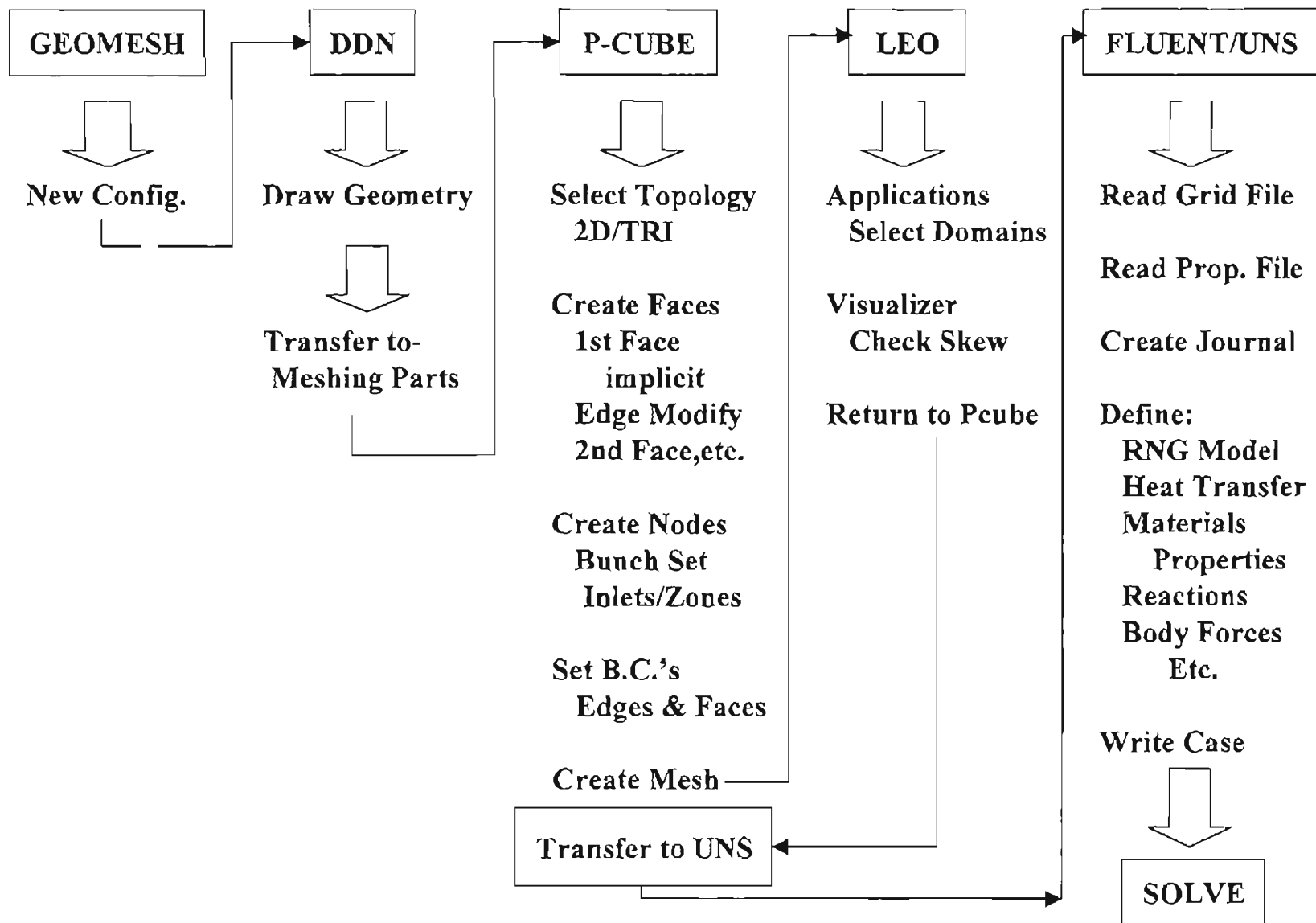


Figure 4-2: Steps to Development of FLUENT Physical Model

Summary of Governing Equations

FLUENT V4.0 (1996) lists the following equations that apply to our model of interest. FLUENT solves the Navier-Stokes equations for conservation of mass and momentum for laminar flows.

Mass Conservation (Continuity) Equation

$$\frac{\partial \rho}{\partial t} + \frac{\partial}{\partial x}(\rho u) + \frac{\partial}{\partial r}(\rho v) + \frac{\partial v}{r} = S_m \quad (4-1)$$

Where, x and u are the axial coordinate and velocity, respectively and r, v are the radial coordinate and velocity, respectively for 2D axi-symmetric geometries. The S_m term is for accumulation (used in some FLUENT structured models, but is equal to zero here.)

Mass Conservation (Continuity) Equation for Multicomponent Systems

$$\frac{\partial c_A}{\partial t} + \left(u_x \frac{\partial c_A}{\partial x} + v_r \frac{\partial c_A}{\partial r} \right) = \Psi_{AB} \left(\frac{\partial^2 c_A}{\partial x^2} + \frac{\partial^2 c_A}{\partial r^2} \right) + R_A \quad (4-2)$$

Where, ψ is the binary diffusivity coefficients for the components and products.

Momentum Conservation Equations

$$\begin{aligned} \frac{\partial}{\partial t}(\rho u) + \frac{1}{r} \frac{\partial}{\partial x}(r \rho u u) + \frac{1}{r} \frac{\partial}{\partial r}(r \rho v u) = -\frac{\partial p}{\partial x} + \frac{1}{r} \frac{\partial}{\partial x} \left[r \mu \left(2 \frac{\partial u}{\partial x} - \frac{2}{3} (\nabla \cdot \vec{v}) \right) \right] \\ + \frac{1}{r} \frac{\partial}{\partial r} \left[r \mu \left(\frac{\partial u}{\partial r} + \frac{\partial v}{\partial x} \right) \right] + F, \end{aligned} \quad (4-3)$$

$$\begin{aligned} \frac{\partial}{\partial t}(\rho v) + \frac{1}{r} \frac{\partial}{\partial x}(r \rho u v) + \frac{1}{r} \frac{\partial}{\partial r}(r \rho v v) = -\frac{\partial p}{\partial r} + \frac{1}{r} \frac{\partial}{\partial x} \left[r \mu \left(\frac{\partial}{\partial x} + \frac{\partial}{\partial r} \right) \right] \\ + \frac{1}{r} \frac{\partial}{\partial r} \left[r \mu \left(2 \frac{\partial v}{\partial r} - \frac{2}{3} (\nabla \cdot \vec{v}) \right) \right] - 2 \mu \frac{v}{r^2} + \frac{2}{3} \frac{\mu}{r} (\nabla \cdot \vec{v}) + \rho \frac{w^2}{r} + F. \end{aligned} \quad (4-4)$$

$$\nabla \cdot \vec{v} = \frac{\partial u}{\partial x} + \frac{\partial v}{\partial r} + \frac{v}{r} \quad (4-5)$$

Where, w is the swirl velocity and F_i denotes force terms that may be used by FLUENT to include other phenomena such as coriolis, centrifugal, or user defined, etc.

Turbulence Equations

For turbulent or transitional flows, FLUENT/UNS offers the choice of a “Standard $k-\epsilon$ Model” as well as a “Renormalization Group (RNG) Model.” The RNG model is particularly applicable to models that may involve swirling flows and hence, was the choice to describe localized areas of turbulence such as the convective roll formations that may occur in our reactor. It is assumed that regions of low Reynolds number default to the conventional Navier-Stokes equations for laminar flows. More detailed explanations of the turbulent models are detailed in the FLUENT V4.0 Volume 2 manuals (1996). The RNG equations for momentum are given as:

$$\frac{\partial}{\partial t}(\rho u_i) + \frac{\partial}{\partial x_j}(\rho u_i u_j) = \frac{\partial}{\partial x_j} \left[\mu_{\text{eff}} \left(\frac{\partial u_i}{\partial x_j} + \frac{\partial u_j}{\partial x_i} \right) \right] - \frac{\partial p}{\partial x_i} \quad (4-6)$$

where, μ_{eff} is the effective viscosity given by:

$$\mu_{\text{eff}} = \mu_{\text{mol}} \left[1 + \sqrt{\frac{C_\mu}{\mu_{\text{mol}}}} \frac{k}{\sqrt{\epsilon}} \right]^2 \quad (4-7)$$

k and ϵ are the turbulent kinetic energy and rate of dissipation, respectively and are given by:

$$\frac{\partial}{\partial t}(\rho k) + \frac{\partial}{\partial x_i}(\rho k) = \frac{\partial}{\partial x_i} \left(\alpha_s \mu_{eff} \frac{\partial k}{\partial x_i} \right) + \mu S^2 - \rho \epsilon \quad (4-8)$$

and,
$$\frac{\partial}{\partial t}(\rho \epsilon) + \frac{\partial}{\partial x_i}(\rho u_i \epsilon) = \frac{\partial}{\partial x_i} \left(\alpha_\epsilon \mu_{eff} \frac{\partial \epsilon}{\partial x_i} \right) + C_{1\epsilon} \frac{\epsilon}{k} \mu S^2 - C_{2\epsilon} \rho \frac{\epsilon^2}{k} - R \quad (4-9)$$

Where, the α terms are effective Prandtl numbers, S is the modulus of the mean rate-of-strain tensor , C terms are 1.42 and 1.68, and the R term is given by:

$$R = \frac{C_{\mu} \rho \eta^3 (1 - \eta / \eta_0) \epsilon^2}{1 + \beta \eta^3} \frac{\epsilon^2}{k} \quad (4-10)$$

Energy Equations for Flow

$$\frac{\partial}{\partial t}(\rho h) + \frac{\partial}{\partial x_i}(\rho u_i h) = \frac{\partial}{\partial x_i} (k + k_t) \frac{\partial}{\partial x_i} - \frac{\partial}{\partial x_i} \sum_j h_j J_j + \frac{Dp}{Dt} + (\tau_{ik})_{eff} \frac{\partial u_i}{\partial x_k} + S_h \quad (4-11)$$

Where, k is the molecular conductivity, k_t is the conductivity due to turbulent transport, J_j is the diffusion of the j^{th} species and the S_h term accounts for the heat of chemical reaction given by:

$$S_{h, reaction} = \sum_j \frac{h_j^0}{M_j} + \left[\int_{T_{ref}}^{T} c_{p, j} dT \right] R_j \quad (4-12)$$

Energy Equation for Solids

In conducting solids,
$$\frac{\partial}{\partial t} \rho h = \frac{\partial}{\partial x_i} \left(k \frac{\partial T}{\partial x_i} \right) + \dot{q}''' \quad (4-13)$$

Where, h is the sensible heat from the integral of $C_p dT$ and q'' is the volumetric heat source.

Rate Equations

The Arrhenius reaction rate equation solved by FLUENT is:

$$R_{r,k} = \Gamma \left(v'_{i,k} M_i T^{\beta_k} A_k \prod_{j' \text{ reactants-and-products}} C_j^{v_{j,k}} \exp(-A_E / RT) \right) \quad (4-14)$$

Where, $v_{i,k}$ is the stoichiometric coefficient for species i in reaction k , M is the molecular weight of the i th species, β is the temperature exponent, A_k is the pre-exponential factor, C_j^i is the molar concentration of species j , $v_{j,k}$ is the exponent on the concentration of species j (order), and A_E is the activation energy for the reaction. The Γ term incorporates species third body efficiencies and is usually omitted in FLUENT/UNS.

Modeling Methods and Approach

While FLUENT solves the governing equations; the user is required to enter the kinetics rate forms for the reactions, as well as other terms and parameters. This section will outline the methods used to develop the necessary inputs for the model as well as the related assumptions.

Reactions and Kinetic Rate Forms

The solid ZnSe product is formed in the reactor from the gas phase in two steps:





The literature provides no kinetic data or exact mechanism for the gas phase reaction. For modeling purposes, a simple second order overall Arrhenius rate form is assumed:

$$R_{\text{ZnSe}} = k_{\text{oe}} e^{(-A_E/RT)} C_{\text{Zn}}^1 C_{\text{Se}_2}^1 \quad (4-17)$$

The first step of Eqn. (4-15) is slightly exothermic and the second (Eqn. 4-16) condensation step is appreciably more exothermic for a total heat of reaction of -176 KJ/mol. The thesis of Morrison (1998) contains a more complete approach to the system's thermodynamic considerations. A rate constant was idealized via calculation from the plug flow reactor (PFR) design equation. The assumptions when applying this approach are related to the nature of the controlling mechanism of the process. The process is not kinetic controlled. The equilibrium of Eqn. (4-15) lies far to the right with a k value of the order of 10^5 or higher and can be assumed to be irreversible. It is not necessary to derive a rate constant from kinetic theory when the process is predominately controlled by other phenomena. As discussed in Chapter III, the actual Reynolds number is approximately 20. Species transport in regimes of creeping flow are characteristically diffusion controlled (Nauman, 1983 and Jensen, 1993). Hence, the CFD model was based on an idealized rate constant that was 'backed out' of the PFR design equation given by Levenspiel (1972):

$$F_{A0} dX_A = (-R_A) dV \quad (4-18)$$

Solution of this mass balance PFR design equation in an integrated form for a 2nd order irreversible reaction yields a rate constant.

$$k = \left[2\varepsilon_A(1 + \varepsilon_A) \ln(1 - X_A) + \varepsilon_A^2 X_A + (\varepsilon_A + 1)^2 \frac{X_A}{1 - X_A} \right] / \tau C_{A0} \quad (4-19)$$

A detailed solution of this equation is contained in Appendix A. The basic steps involved estimating residence times and reactant volumetric flow rates based on experimental data and operating conditions of the present reactor. The resulting idealized k value of 6.89×10^5 L/mol-sec is most likely a low estimate and can be compared to the value calculated from kinetic theory by Morrison (1998) of 3.0×10^6 L/mol-sec.

The activation energy was estimated from experimental data and solution of the following equation (Levenspiel, 1996).

$$\ln \frac{\text{rate}_1}{\text{rate}_2} = \ln \frac{k_1}{k_2} = \frac{A_E}{R} \left(\frac{1}{T_2} - \frac{1}{T_1} \right) \quad (4-20)$$

The equation was solved with estimated reaction rates from experimental data and rate constant k values from Eqn. (4-18) taken at two different temperatures from the present system. The resulting activation energy of 8.1×10^7 J/Kmol is admittedly dubious, given the nature of the experimental data with respect to the uncertainty in the run time estimates (see Design Basis section). This calculation is also detailed in Appendix A. The value can be compared to that derived from transition state theory by Morrison (1998) of 1.9×10^8 J/Kmol. Again, the kinetics parameters are not controlling, but the values derived via experimental data here compare reasonably well with those from molecular theory calculations.

The reactions of Equations (4-15) and (4-16) were modeled on the assumption that all of the gas phase ZnSe product results in deposited solid material. FLUENT can solve multiple reactions, but development of a model that can simulate the growth of a deposited bed presents many problems. The model can simulate condensation, but it has difficulty displaying non-steady state processes. Thus, the process was simplified for modeling purposes to a steady state process where the gas phase product represents a

'pseudo' solid product. The validation of this approach is presented in subsequent sections.

Transport Properties

FLUENT has the capability of calculating most properties including viscosity, density, conductivity and diffusivity simply from tabulated Lennard-Jones parameters for each of the reactants and products. However, these properties were entered individually as temperature dependent piece-wise functions since certain properties were used as fitted empirical coefficients. The Lennard-Jones calculations within FLUENT are an "all-or-nothing" approach that must be applied to all parameters and, therefore, would not have allowed the fitting of certain parameters. Tabulation of the temperature functions for the transport properties as well as the thermodynamic quantities of heat capacities and heats of formation are available in an appendix of Morrison's thesis (1998).

Empirical Parameter Fitting

As mentioned above, the process is strongly controlled by diffusive mass transport. Hence, the diffusivity parameter was the focal point of this phase of research. The following diffusivity pairs need to be entered into the model.

Group I (reactants): Zn/Se₂, Zn/Ar, Se₂/Ar

Group II (products): ZnSe/Zn, ZnSe/Se, ZnSe/Ar

The reactant combinations were available in the literature (Wahlbeck, 1992) or entered as polynomial functions derived from Chapman-Enskog parameters (Morrison, 1998). The product pairs involving ZnSe were used as coefficients in the CFD model to empirically

fit the yield results to experimental data. An optimized run that was completed during the first week of January 1998 as discussed in the preceding chapter was used as the basis for comparison. The diffusivities of the Group II pairs were adjusted iteratively to arrive at a yield as exhibited by concentration profile output of the model equal to 70%. The theoretical basis for this approach is that the controlling mechanism (diffusivity of ZnSe product) is the obvious choice to adjust in order to simulate the condensation reaction (Eqn. 4-16). The CFD profiles were analyzed for distribution of product within the reactor and the backflow of reactants, in addition to the product yield. The target was to adjust the diffusivity parameter until the target product yield was achieved with an even distribution and no backflow of reactants into the boilers as observed in the experimental test case. The diffusivity of ZnSe in Ar was established to be 1.0×10^{-6} (m²/sec) via this method.

Summary of Assumptions

- 1- The reactor dimensions are well represented as a 2D axisymmetric geometry.
- 2- Diffusivity rather than convective mixing determine the reaction's rate.
- 3- The kinetics are not controlling and can be derived from idealized conditions.
- 4- The overall reaction is depicted as a second order Arrhenius rate form.
- 5- The overall reaction is exothermic.
- 6- For modeling purposes, the reactor walls are assumed to operate isothermally.
(i.e. – Eqn. 4-13 equals zero.)
- 7- The deposition of solid product can be simulated from gas phase concentrations by the fitting of empirical parameters.

- 8- The process is assumed to be a pseudo-steady-state.
- 9- Radiation effects are negligible.
- 10- The RNG model for turbulent flow is applicable and defaults to Navier-Stokes in the laminar region.

Summary of Key Kinetic and Transport Model Parameters

Table 4-3: Key Kinetic and Transport Variables

Rate Constant	6.89×10^5 L/mol-s
Reaction Order	2nd
Activation Energy	8.0×10^7 J/Kmol
Diffusivities	Group I (See above): 1.0×10^{-4} m ² /sec Group II (See above): 1.0×10^{-6} m ² /sec

Boundary Conditions

The model requires that the following conditions be entered: 1) The inlet initial concentration of each reactant in terms of mass fraction, 2) Initial velocity of each inlet, 3) Inlet stream temperatures, 4) Wall temperatures or heat fluxes.

Modeling Results and Discussion

The following strategies were employed in the course of fitting the kinetic/transport model described above to reproduce the experimental results obtained from the system in use at E-P.

Flow Regime and Product Rate Determining Phenomena

A test of the critical modeling assumption related to the controlling mechanism was made by inducing a higher degree of convective mixing within the model. Modeling experiments that ramped the inlet velocities as high as fifteen times the operating conditions (approx. 5.0 liters/min) were entered into the FLUENT model of the current system. The maximum Re number at the front of the reactor was approximately 50. This confirms that the reactor operation will remain within the laminar to creeping regime, regardless of the operating flow. Further, the reaction interface is heavily dependent upon diffusion of the reactants.

Elimination of Backflow within the Model

During the course of fitting the diffusivity of ZnSe to the experimental runs, the FLUENT output was also monitored for presence of backflow of product into the reactant boilers. It was observed that as an additional measure of 'fit'; the backflow of product material would become apparent with increasing diffusivity of ZnSe. Conversely, the backflow would retreat at lower diffusivities. Since no backflow of product material occurred within the experimental reactor regardless of operating conditions, the empirical fit then became a matter of adjusting the product diffusivity to produce the optimized

experimental yield with no backflow. A small sampling of the parameter fitting runs is shown in Table 4-4 (note that the target yield is 69.7 %.):

Table 4-4: Sample of Empirical Parameter Fitting Regimen

Group II Diffusivity (m²/sec)	Product Yield (%)	Backflow Present?
0.25 x 10 ⁻⁵	68.8	YES
1.0 x 10 ⁻⁵	34.0	NO
1.0 x 10 ⁻⁶	75.9	NO
1.0 x 10 ⁻⁷	48.3%	YES

Follow-up Test with Experimental Data

The model was further tested against an additional experimental run that was believed to have a good estimate of mass flow rates. Recall that the experimental mass flows are based on estimates of run times. The run times are derived from observation of the boiler analog power output readings where a marked decrease in power occurs when the boilers are emptied of reactant material. The experimental run chosen resulted in a yield of 87.6%. The estimated mass flow rates, velocities, and inlet mass fractions of reactants were calculated via spreadsheet (Appendix C) and entered into the model. The model produced a simulated yield of 78.1%. This value is within the error associated with the uncertainty of the mass flow rates estimates.

Conclusions and Recommendations

There are a limited number of experimental runs that were available to correlate with the CFD model. The model represents the experimental data within error as provided by mass flow rate uncertainty. Measurements of simulated yields, backflows, and velocity profiles appear reasonable when compared to experimental observations and theoretical background.

The modeling work that is ongoing by other students should build upon the foundation presented here. The efforts at 3D modeling and resolution of the flows on a non-reacting basis will add a higher degree of confidence to the results. Further, the boiler design should be implemented to provide exact measures of reactant mass flow rates. The improved quality of experimental data would then enhance the accuracy of the parameter correlations within the model.

CHAPTER V

NEW DESIGN OPTIMIZATION

Introduction

With the development of a representative CFD model of the new reactor complete; efforts were then directed towards optimizing the reactor's design within the model. The original intent had been to construct an experimental prototype to perform final testing and development work. However, changes in the business climate obviated the availability of funds for such a prototype. It then became necessary to conduct all experiments within the computer model. The objective was to optimize the product yield as well as the flow characteristics to avoid the formation of plugs. The computer experiments entailed the variation of the process operating and physical parameters. Examples of operating parameters are reactant flow rates and the reactor temperature. The physical parameters include the size and configuration of the nozzles, and the dimensions of the reactor tube.

The Literature Review chapter contains examples of device design optimization within CFD models. Collins et al. (1994) and Gaston (1995) successfully incorporated DOE and RSM techniques to the optimization of computer models for the design of semiconductor devices. The purpose of this chapter is to detail the experimental design approach applied to the FLUENT model as a substitute for prototype testing.

FLUENT Model Experimental Designs

Chapter II outlines a theoretical foundation for DOE methodology that will not be reiterated here except to note that the advantages are especially applicable to computer models. High-performance computer simulations allow for almost unlimited experimental freedom given the speed with which individual experiments can be completed. The matrix chosen for the initial battery of FLUENT experiments involved 64 runs, which would have been a prohibitively large number if performed on an actual physical apparatus. There were two phases to the experimental optimization to be referred to as Study I and Study II.

Design Optimization: Study I

Given the experience gained with both the present reactor process and the computer model; the following factors were deemed most important and are given in Table 5-1. The rationale for the experimental levels is shown in Table 5-2.

Table 5-1: Design Optimization Study I Factors and Levels

PHYSICAL	FACTOR	SYMBOL		EXPERIMENTAL LEVELS		
				LOW	units	HIGH
1	NOZZLE ANGLE	NA		0	degrees	45
2	NOZZLE DIAM.	ND		2.5	mm	6
3	NOZZLE POSITION	NP		1	cm	3
4	REACTOR LENGTH	RL		750	mm	900
OPERATING						
5	REACTANT FLOW RATE	FR	Se =	3.10×10^{-2}	mol/sec	1.67×10^{-3}
			Zn =	6.20×10^{-2}	mol/sec	3.30×10^{-3}
6	REACTOR TEMP.	ZT		1223	K	1323

Table 5-2: Rationale for Experimental Levels (Morrison, 1998)

Species	Parameter	Level	Value	Rationale for Levels
Zinc	mol flow	+	3.3×10^{-3} mol/sec	Stoichiometrically equal flow for Selenium (+) mole flow
		-	6.2×10^{-4} mol/sec	This was the max mol flow rate estimated from the 3 wormhole runs
	nozzle dia	+	6 mm	Same as Selenium (-) nozzle diameter
		-	2.5 mm	Set not to exceed 85% speed of sound in pure Se ₂
	nozzle angle	+	45°	Set at 50% of "best mixing case"
		-	0°	Set at pure cocurrent mixing, 100% diffusion controlled
	nozzle position	+	10 mm	arbitrary, 1 nozzle diam.
		-	30 mm	arbitrary, 5 nozzle diam.
Selenium	mol flow	+	1.67×10^{-3} mol/sec	Estimated from bubble transport through molten metal.
		-	3.1×10^{-4} mol/sec	Stoichiometrically equal flow for Zinc (-) mole flow
	nozzle dia	+	6 mm	Set to exceed 1.5 m/sec exit velocity
		-	2.5 mm	Same as Zinc (-) nozzle diameter
	nozzle angle	+	45°	Set at 50% of "best mixing case"
		-	0°	Set at pure cocurrent mixing, 100% diffusion controlled
	nozzle position	+	10 mm	arbitrary, 1 nozzle diam.
		-	30 mm	arbitrary, 5 nozzle diam.
Argon	mole flow	constant	2.0×10^{-4} mol/sec	Corresponds to 300 ml/min at 300K

*See Morrison 1998, Nozzle design for CFD

Background Variables

Table 5-3: Background Variables: Study I

VARIABLE	SETTING	Notes/Units
OPERATING		
Carrier Gas (Ar) Flow Rate	2.0×10^{-4} mol/sec	=300ml/min @300K
KINETIC/THERMO PARAMETERS		
Rate Constant	3.00×10^{16}	
Overall Order	2nd	
Activation Energy	8.10×10^{17}	
TRANSPORT PROPERTIES		
Thermal Conductivity Ar	Piecewise Linear Functions	
Thermal Conductivity Zn	Piecewise Linear Functions	
Thermal Conductivity Se	Piecewise Linear Functions	
Viscosity Zn	Piecewise Linear Functions	
Viscosity Se	Piecewise Linear Functions	
Viscosity ZnSe	Piecewise Linear Functions	
Diffusivity Zn/Ar	1.00E-04	Wahlbeck
Diffusivity Zn/Se	Piecewise Linear Functions	Chapman-Enskog
Diffusivity Se/Ar	1.00E-04	Wahlbeck
Diffusivity ZnSe/Ar	1.00E-06	Expr. Data
Diffusivity ZnSe/Se	1.00E-06	Expr. Data
Diffusivity ZnSe/Zn	1.00E-06	Expr. Data

Design Matrix

The computer model DOE studies allowed for the completion of a 2^6 full factorial design that eliminated confounding interactions. Documentation of the design is left to the reader to explore further in Appendix C. The design matrix, FLUENT DDN reactor dimension coordinates, spreadsheet calculations for the model operating parameters, run data, and spreadsheet analysis of the data, are all contained in the appendix.

Study I Results and Analysis

As shown in Appendix C, the data for the 64 runs were reduced by spreadsheet calculation to quantify the variation that is attributable to each factor and interaction.

Single Factor Results

Table 5-4: Study I Factor Results (Yield)

	PHYSICAL PARAMETERS				OPERATING	
	1 = NA	2 = ND	3 = NP	4 = RL	5 = FR	6 = ZT
AVG -	51.5	50.2	59.1	51.9	65.3	53.9
AVG+	61.5	62.8	53.9	58.6	47.7	59.2
Δ	10.0	12.6	5.2	6.7	17.6	5.3
ω	0.57	0.72	0.30	0.38	1.00	0.30
RANK	3	2	5	4	1	5
SIG?	YES	YES	NO	NO	YES	NO

Table 5-1 can be referred to as a guide to the symbols used in the Table 5-4. Note that the response variable is product yield. The yield is based on zinc as described by Equations (3-2) and (3-3). The component concentrations were analyzed from FLUENT profiles, after convergence to a steady state solution, by integration of the component mole fractions within the reactor volume. Also, recall from Chapter III that the averages, Δ , and ω values are calculated from Equations (3-4) to (3-6) in the results tables.

From the above analysis; the dominant factors are the nozzle angle (NA), the nozzle diameter (ND), and the flow rates of reactants (FR). The nozzle position (NP) and the temperature of the reactor (RT) have little effect on yield relative to the other factors within the range studied. As will be discussed later, the reactor length will be analyzed further in an attempt to elucidate its effect.

The two factors of reactant flow rate and nozzle diameter are plotted with a midpoint run in Figures 5-1 and 5-2.

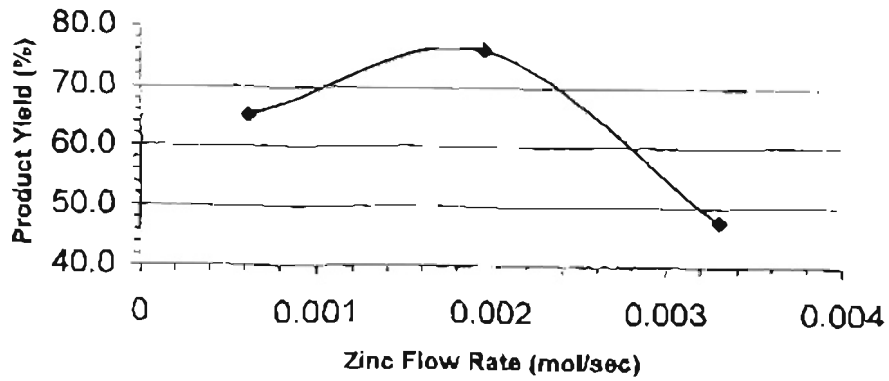


Figure 5-1: Effect of Zinc Flow Rate on Product Yield

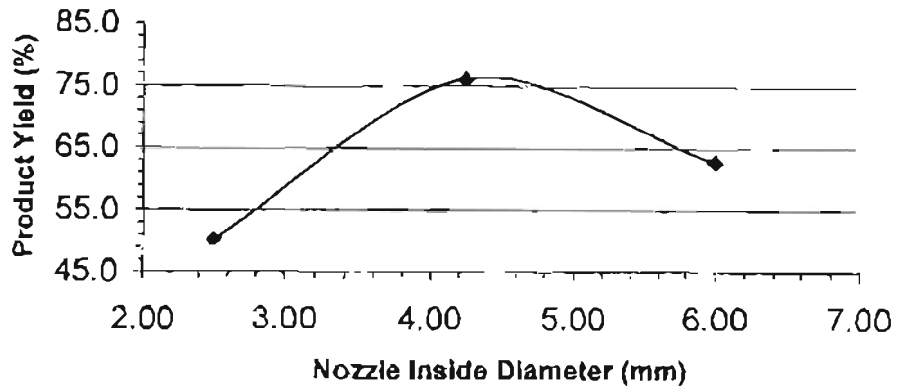


Figure 5-2: Effect of Nozzle Diameter on Product Yield

The plots indicate a non-linearity of the factor's relative effects, however the effects of the other factors are not normalized. In other words, a single midpoint run can not account for the variation introduced by the other four factors. It is, however, a relative gauge of the "reasonable-ness" of the chosen levels. The levels are typically

chosen to encompass the optimum conditions as narrowly as possible. The higher yield at the midpoint confirms that the levels are centered near the optimum conditions.

Reactor Sizing and Conversion

To confirm that the reactor length has a minimal impact on product yield, a separate run was made following the midpoint run. The run was executed at the midpoint conditions with the exception of lengthening the reactor by 25% from 1000mm to 1250mm. The result was a product yield of 74.8% as compared to the midpoint run of 76.2%. The lack of gain in yield that may have been expected is explained from residence time considerations. There is a reactor length at which the diffusive forces are in effect balanced by the convective mixing forces. Therefore, given a constant flow rate; increasing the length of the reactor serves no purpose i.e.- maximum conversion is found at a finite reactor volume for a specified molar flow rate and batch size. This is the converse of a turbulent flow regime system where conversions can approach 100% with infinite residence times and when the equilibrium is highly favorable to products (Levenspiel, 1972).

Two-Factor Interactions

Table 5-5: Study I Interactions Results (Yield)

	Factor Combinations														
	1-2	1-3	1-4	1-5	1-6	2-3	2-4	2-5	2-6	3-4	3-5	3-6	4-5	4-6	5-6
avg-	53.8	55.4	56.0	56.4	56.8	58.1	55.3	54.1	57.0	55.5	55.8	56.1	56.2	56.6	55.8
avg+	57.4	57.7	57.1	56.7	56.2	54.9	57.8	56.8	56.1	57.5	57.2	57.0	56.9	56.4	57.3
Δ	3.5	2.3	1.1	0.3	0.6	3.2	2.5	2.7	0.9	2.0	1.3	0.9	0.7	0.3	1.5
ω	1.00	0.66	0.32	0.08	0.17	0.91	0.71	0.78	0.24	0.57	0.38	0.27	0.21	0.07	0.43
rank	1	5	9	14	13	2	4	3	11	6	8	10	12	15	7
sig	NO	NO	NO	NO	NO	NO	NO	NO	NO	NO	NO	NO	NO	NO	NO

The analysis does not reveal any significant interactions between the factors. Also characteristic of this matrix; there are no three factor interactions, or confounding effects (Moen et al., 1991).

Study I Preliminary Conclusions

As discussed above, the experiments show that the optimum set of operating and physical parameters should maximize the product yield with a minimum reactor volume. The experiments in this study screened the factors and directed our attention to the flow rates and nozzle diameters. Interactions within this set of factors are negligible. A second study was needed to arrive at the final optimum design.

Design Optimization: Study II

The objective of the second study was to gather results from a new experimental matrix that centered on the important factors of flow rate and nozzle diameter as established in Study I. Study II's purpose was to vary the nozzle diameters and flow rates of reactants independently from one another.

Design Matrix and Factor Levels

The two nozzles and the two flow rates constitute four factors of a 3^{4-1} fractional factorial matrix. The matrix includes a third level that will allow for development of prediction functions. The new background variables that are held constant include the angle of the nozzles (perpendicular to face plate), the nozzle positions (1.0 cm from the centerline), the reactor length (900mm), and the reactor temperature (950° C). The

background variables listed in Table 5-3 are still held constant in Study II, as well. The new factor levels are summarized in Table 5-6:

Table 5-6: Study II Factors and Levels

Factor Symbol	Previous Range	Low Level (-)	Mid Level (o)	High Level (+)
NDZ	2.5 – 6.0 mm	5.0 mm	8.5 mm	12.0 mm
NDS	2.5 – 6.0 mm	5.0 mm	8.5 mm	12.0 mm
FRZ	0.000620 - 0.0033 mol/s	0.000728 mol/s	0.00201 mol/s	0.00330 mol/s
FRS	0.00031- 0.00167 mol/s	0.000364 mol/s	0.00102 mol/s	0.00167 mol/s

Prediction of Plugging Within the Steady State Model

Trends that were observed in Study I indicated improved yields at lower flows and larger nozzle diameters. Study II incorporated a criterion to estimate plugging from the model output. The simulations conducted under unoptimized conditions revealed that the velocity profiles of the reactants near the nozzle inlets into the reactor occasionally turn into the radial direction. Further, there are run conditions that will produce higher quantities of ZnSe near the nozzle orifices.

The secondary flow patterns occur as a result of thermally driven natural convective forces and buoyancy effects that result in radially oriented flow vectors. This phenomenon contributes to the formation of the convective rolls or “wormholes” (Jensen, 1993; Jackson and Winters, 1984). The model is a steady state solution that otherwise will not reveal the presence of such a plug or wormhole structure. However, it was necessary to attach a quantifiable value to this phenomenon that can be analyzed within the matrix for the prediction of plugging. This was accomplished by quantifying the

product at the inlets by taking an average surface integral of the ZnSe mole fraction present at that location. The data was then compiled within the matrix as a “plugging factor.” The criteria for plugging was established by inspection of representative runs at conditions that were known to be conducive to plugging as observed in low yield experimental data. The criteria for plugging was set at a plugging factor greater than 0.01. Consequently, there are two response variables in this second study - the product yield and the plugging factor.

Study II: Results and Analysis

Again, the compendium of run data, results, analysis spreadsheets, etc. pertinent to Study II is available in Appendix C. The calculated results are summarized in Tables 5-7 and 5-8:

Table 5-7: Study II Results (Yield)

	FACTOR			
	NDZ	NDS	FRZ	FRS
AVG LOW	50.9	66.4	78.3	44.2
AVG MID	59.7	59.5	54.4	65.5
AVG HIGH	68.5	53.2	46.5	69.5
RANGE (H-L)	17.6	-13.3	-31.8	25.3
Total Avg Yield (%)	59.72			
σ	21.74			

Table 5-8: Study II Results (Plugging Factor (PF))

	FACTOR			
	NDZ	NDS	FRZ	FRS
AVG LOW	0.01045	0.00399	0.00516	0.00918
AVG MID	0.00629	0.00564	0.00863	0.00880
AVG HIGH	0.00535	0.01246	0.00831	0.00411
RANGE (H-L)	-0.0051	0.00847	0.00315	-0.00507
Total Avg. PF	0.007364			
σ	0.008319			

Where, σ is the standard deviation of the entire population across the 27 runs and is given by the positive square root of the variance (Bethea and Rhinehart, 1991):

$$\sigma = \left(\frac{1}{n} \sum_{i=1}^n (X_i - \mu)^2 \right)^{1/2} \quad (5-1)$$

Several trends are apparent from the Tables 5-7 and 5-8. With respect to yield; the two nozzles have an inverse relationship, where a small Se but a larger Zn nozzle are preferred to produce higher yields. Likewise, a high mole flow of Zn with a low flow of Se will increase the product yield. Comparison of the actual inlet velocities is necessary. This combination of physical and operating parameters produces inlet velocity ratios of 10 Se to 1 Zn. These phenomena are best investigated graphically. The following 3-D figures relate the effects of flow rate and nozzle diameter on the product yield and the plugging factor. Figure 5-3 shows the effect of the zinc nozzle diameter and flow rate versus the product yield.

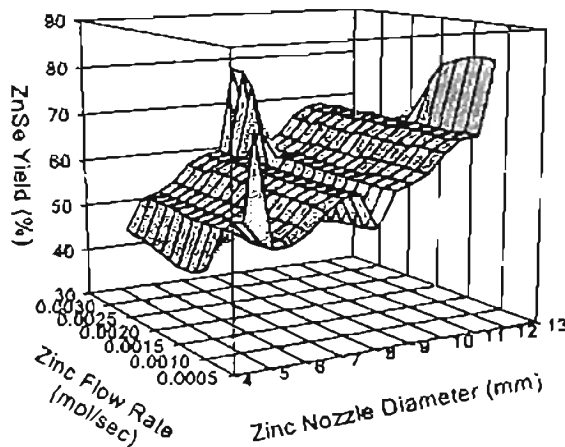


Figure 5-3: Effect of Zinc Nozzle Diameter and Flow Rate on ZnSe Product Yield

Figure 5-4 also illustrates the fact that lower flows (velocities) and smaller diameters favor higher yields:

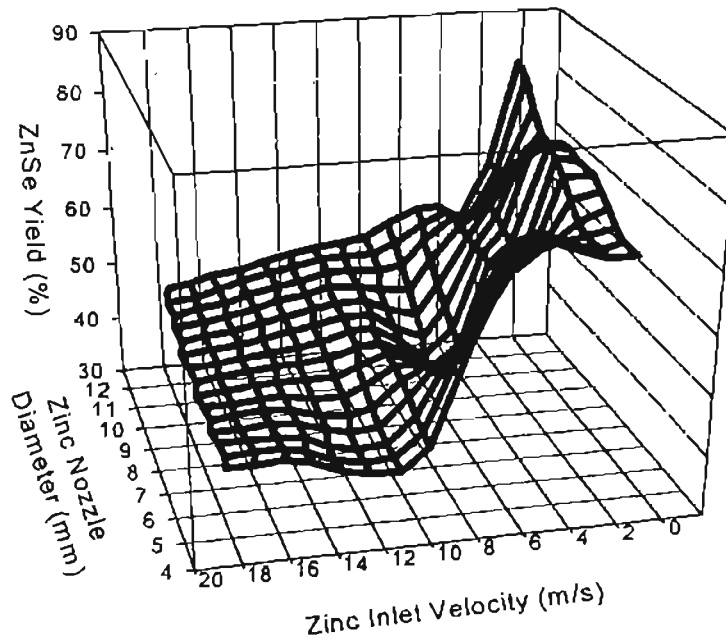


Figure 5-4: Effect of Zinc Nozzle Diameter and Velocity on ZnSe Product Yield

Figure 5-5 shows the same relationship for Se flow and nozzle diameter, but it also reveals that high yields can be attained with higher flows and larger nozzles.

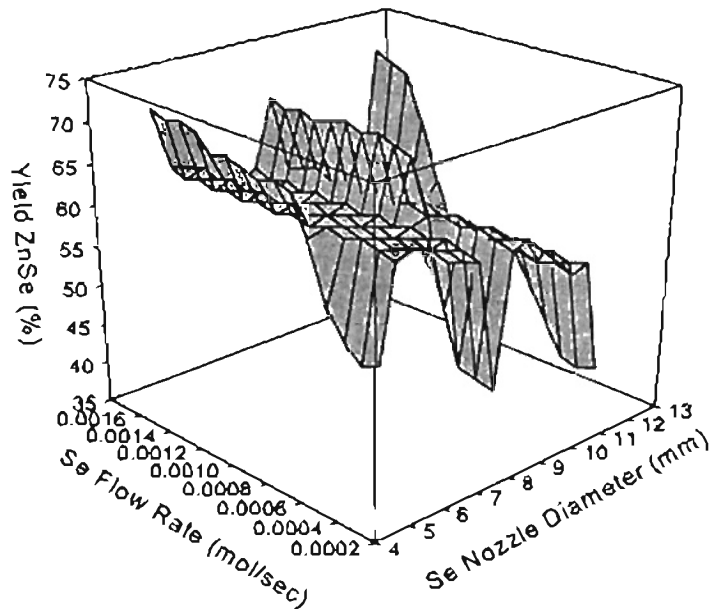


Figure 5-5: Effect of Selenium Nozzle Diameter and Flow Rate on ZnSe Product Yield

As discussed above, higher yields can be attained with a given combination of nozzles and flow only if they do not produce plugs at the nozzles. With the plugging factor set by a line drawn on the plot at 0.010, Figure 5-6 shows that the smaller zinc diameters are permissible if the flows are at least 0.0010 mol/sec for nozzle diameters less than 6.0mm. The figure notes this area with an arrow that indicates the “sweet spot.” This area corresponds to an operating region where small (5.0-6.0mm) nozzles may actually utilize low flow rates while maintaining an acceptable plugging factor.

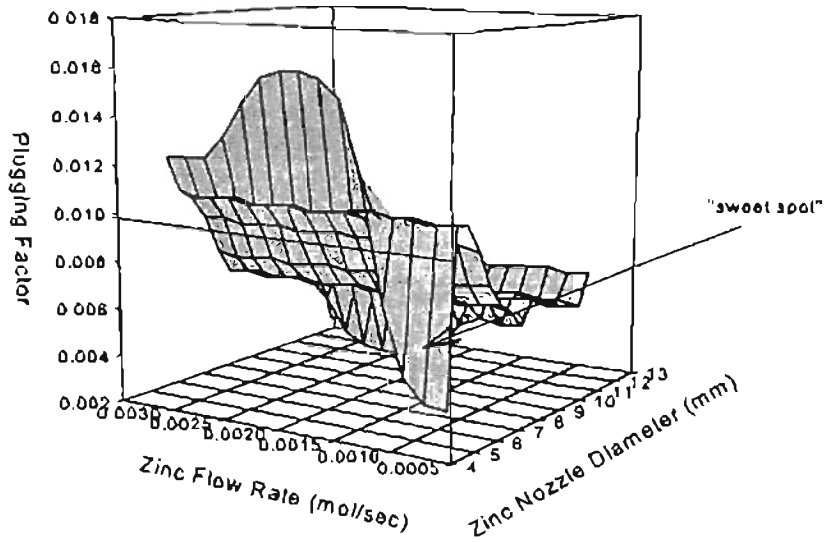


Figure 5-6: Effect of Zinc Nozzle Diameter and Flow Rate on the Plugging Factor

Similarly, Figure 5-7 shows, that for any flow rate, the maximum diameter is approximately 9.0 – 10.0 mm.

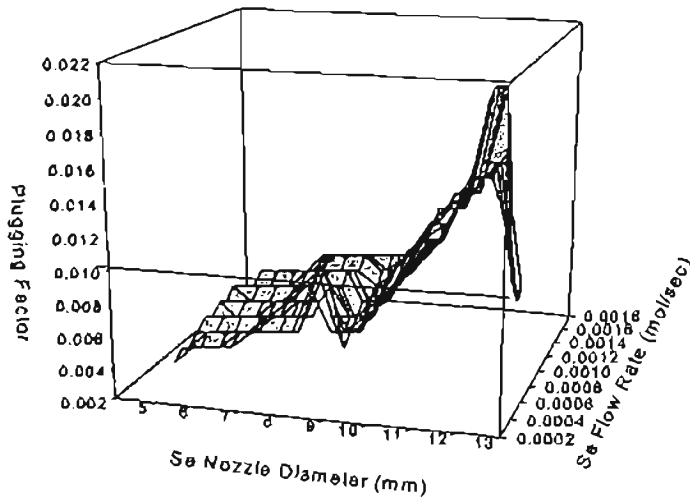


Figure 5-7: Effect of Selenium Nozzle Diameter and Flow Rate on the Plugging Factor

Confirmation Runs

Several confirmation runs were conducted to further “tune” the parameters. The nozzle diameters were established to be 8.5 mm and the appropriate flows calculated from the spreadsheet in Table C-4. The exact data points are located in the table and listed as “confirm” runs. Attempts were made to maximize the yield while maintaining a plugging factor of < 0.010 . All runs resulted in plug factors < 0.010 , but the flows that were < 0.001 mol/sec were in the range of 0.007. The optimum was chosen to be at flow rates of 0.000728 mol/sec and 0.00364 mol/sec Zn and Se, respectively. These flows were near the minimum allowable to achieve the desired product batch size and reasonable run time. Appendix B contains the calculations for actual yields and run times for the design basis batch size. The runs are shown in Figure 5-8.

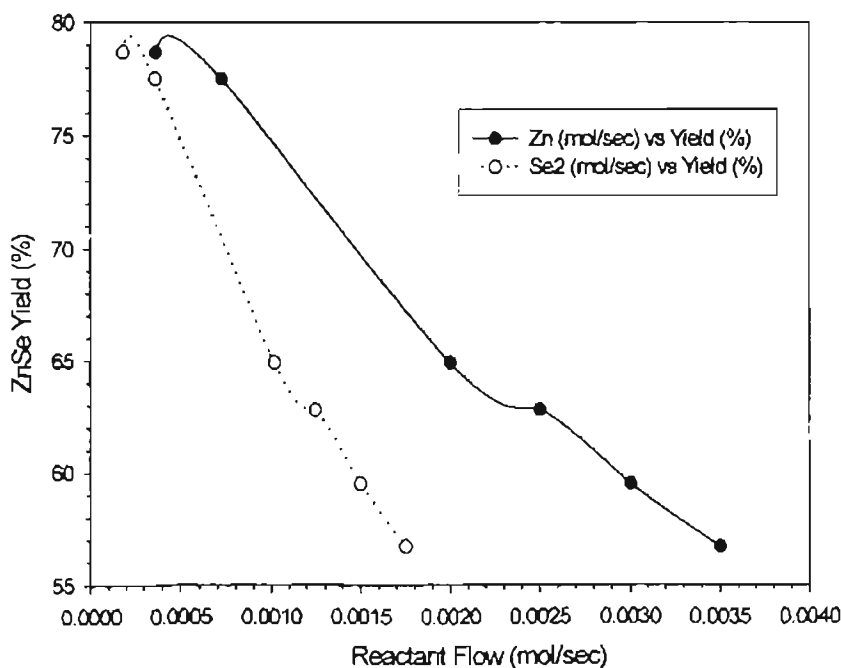


Figure 5-8: Reactant Flow Rates Effect on ZnSe Product Yield

(from confirmation runs 1-6)

Summary of New Design

Table 5-9: Optimal Reactor Dimensions and Conditions

Parameter	Setting
Reactor: Tube Length (mm)	1000
Inside Diameter (mm)	90
Nozzles: Inside Diameters (mm)	8.50
Lengths (mm)	20.0
Angles (degrees)	0
Positions from Centerline (mm)	20.0
Temperature (deg. C)	950
Flow Rates: Selenium (mol/sec)	3.64×10^{-4}
Zinc (mol/sec)	7.28×10^{-4}
Ar Carrier (total ml/min)	600

FLUENT/UNS Profiles of the System

Figures 5-9 through 5-15 are output contour plots of the FLUENT/UNS model configured and operated as shown in Table 5-9. Figures 5-9 and 5-10 profile the compositions of the reactor tube in terms of mole fractions of Zn and Se₂, respectively. The profiles of the ZnSe product are shown in Figure 5-11. It should be noticed in this figure that the product is evenly distributed with an increasing concentration of product going down the reactor length. Also, there is an absence of appreciable amounts of ZnSe near the inlet nozzles. The product profile of Figure 5-11 should be compared to that of Figure 5-12. Figure 5-12 is an experimental run from the Study II matrix and corresponds to a set of poor operating conditions. The product distribution, in this run, was obviously poorly distributed with the largest concentrations located at the end and the very front of the reactor tube. There is also a large amount of material at the nozzle

inlets, which would likely produce a plug. Note also that the run corresponds to a plugging factor of approximately 0.0150, well in excess of the 0.010 criteria. The validity of the PFC methodology is apparent from the graphical output of this run.

Similar to the concentration profile comparisons, the velocity vectors appear to substantiate the optimum conditions as given in Table 5-9. Figure 5-13 shows the optimum condition velocity, where there is an absence of radially-oriented vectors characteristic of secondary flow patterns. Recall that these structures were minimized in the experimental designs by the analysis of the plugging factor. This run can be compared to the unoptimized run depicted in Figure 5-14, where the Se_2 inlet vectors are perpendicularly oriented towards the Zn inlet. Recall that this run produced a PFC of greater than 0.0150.

Figure 5-15 depicts the interior temperature profiles of the reactor. Recall that although the model was developed as an isothermal wall, the system certainly does not operate isothermally due to the exothermic reaction. Forthcoming work by Foster and Nikolic (in progress) will address this issue.

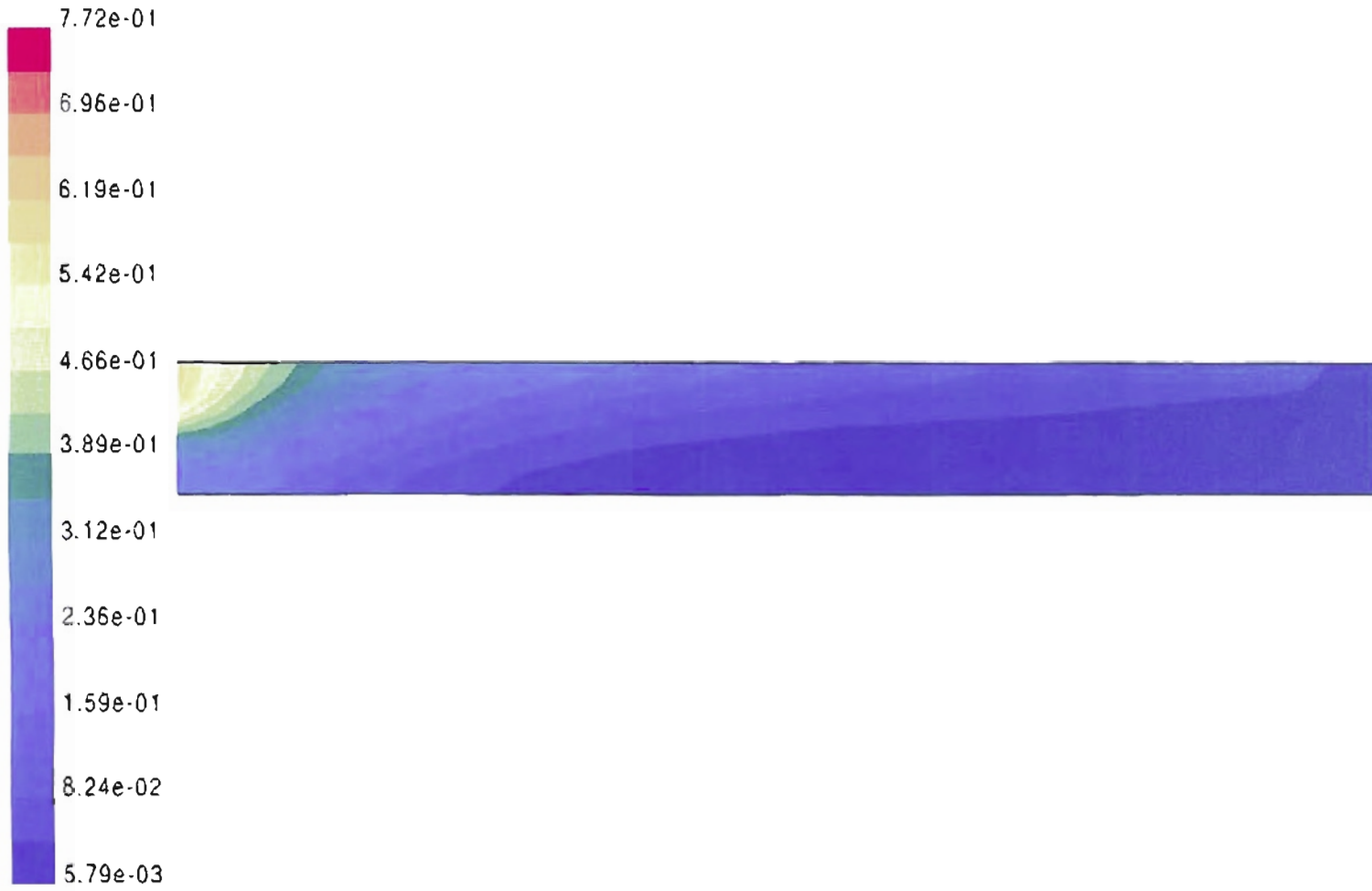


Figure 5-9:
FLUENT Profiles of Mole Fraction of Zn-g
(Optimized Conditions)

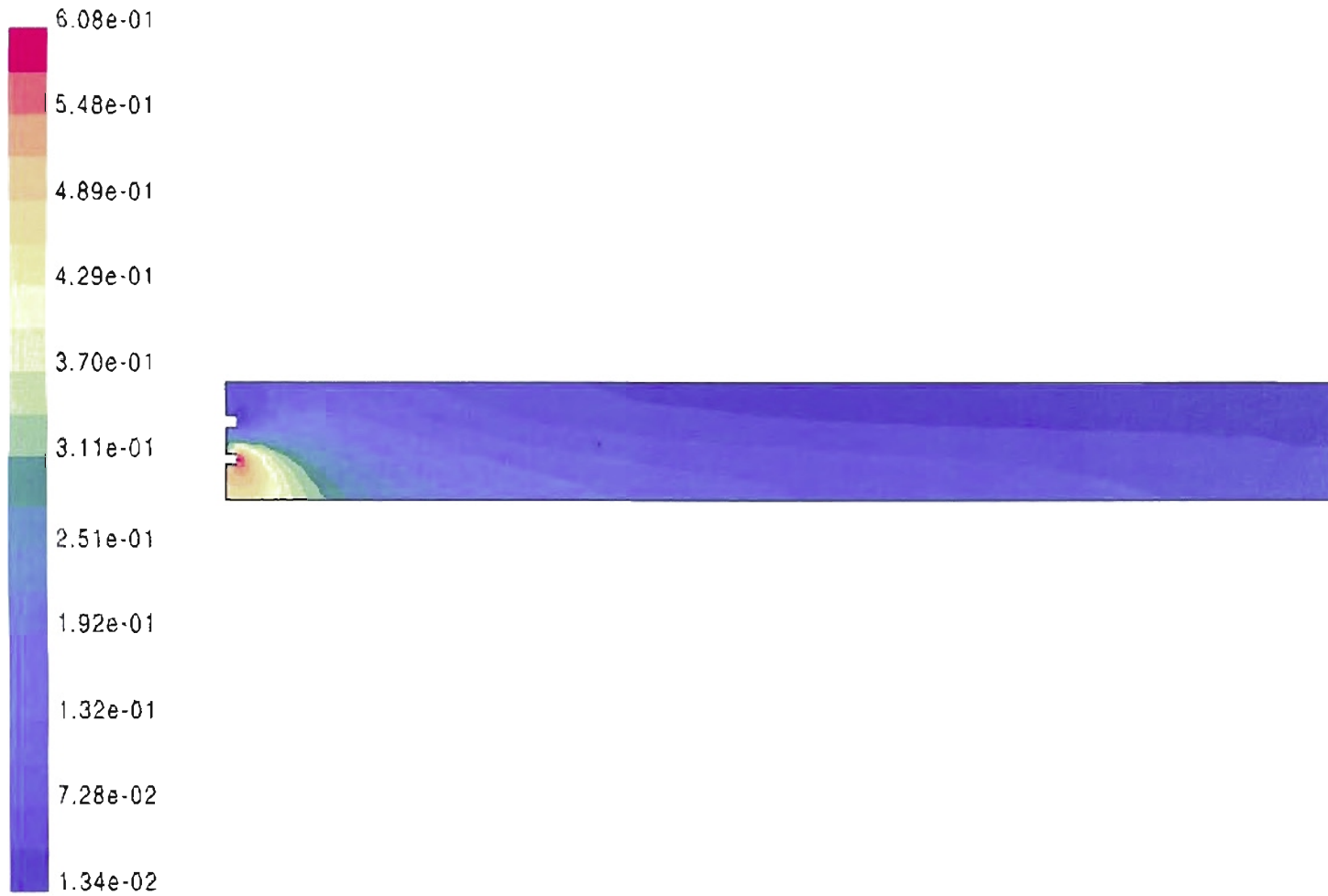


Figure 5-10:
FLUENT Profiles of Mole Fraction of Se2-g
(Optimized Conditions)

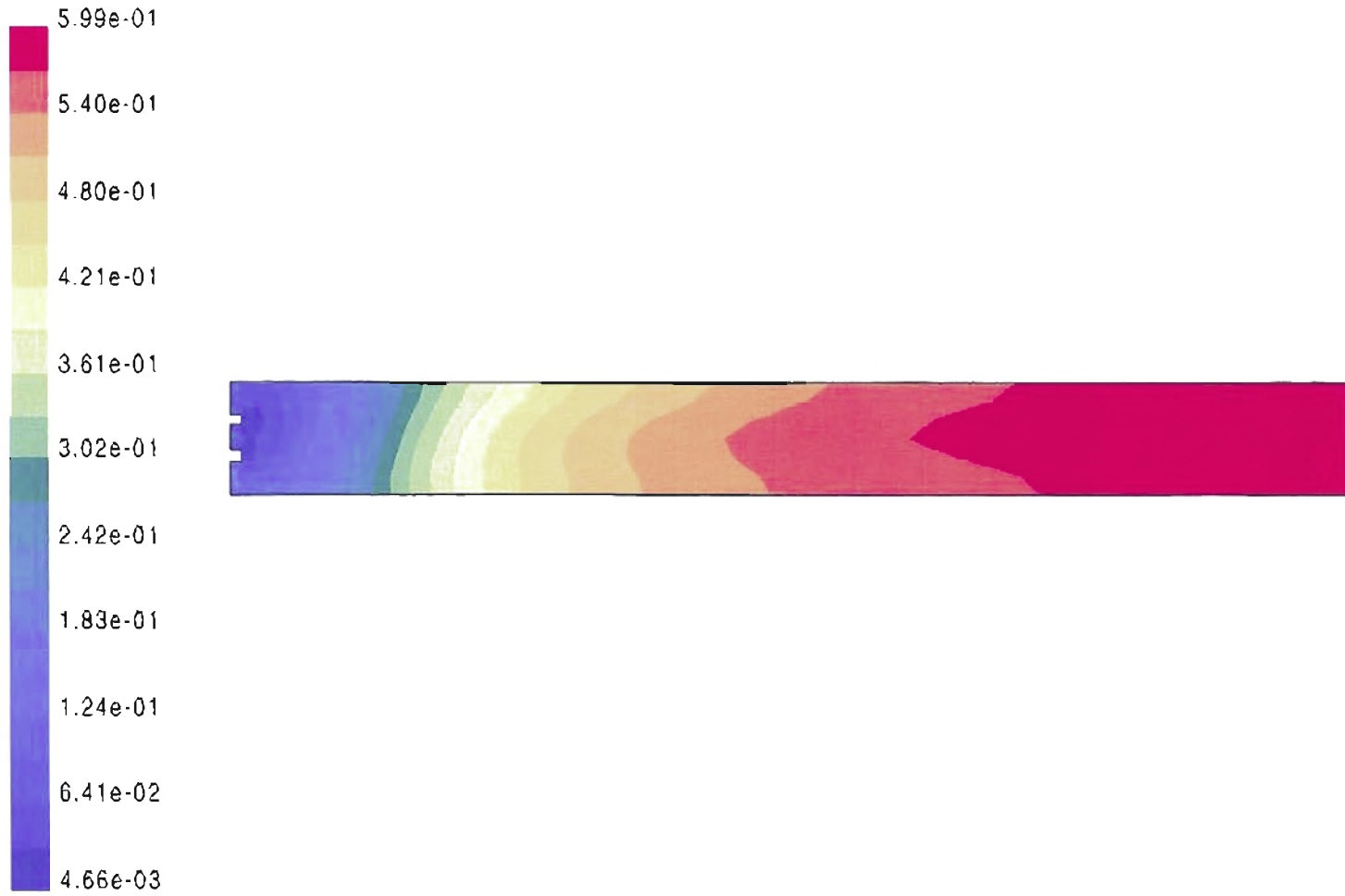


Figure 5-11:
FLUENT Profiles of Mole Fraction of ZnSe-g
(Optimized Conditions)

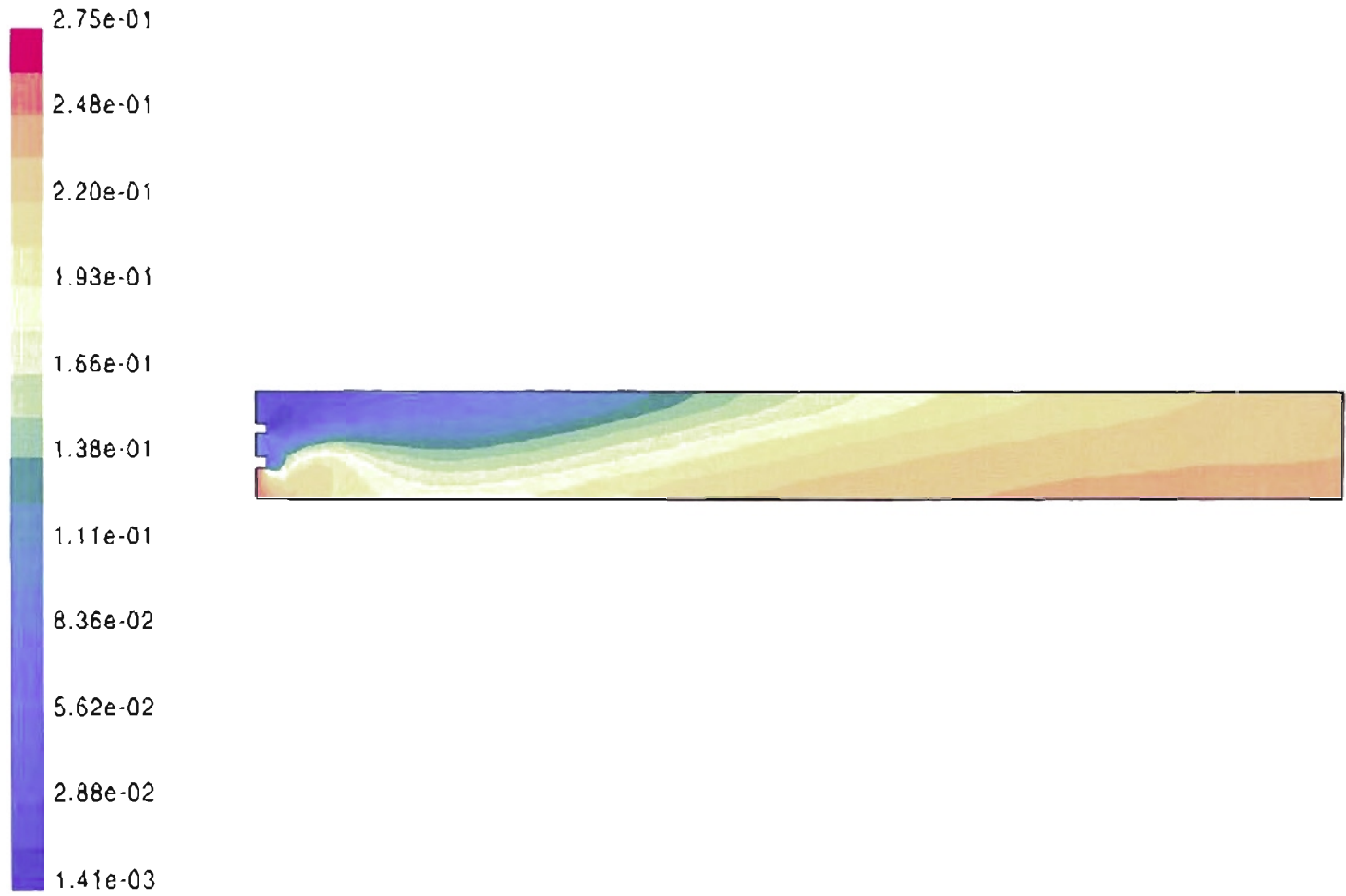


Figure 5-12:
FLUENT Profiles of Mole Fraction of ZnSe-g
(Unoptimized Conditions)

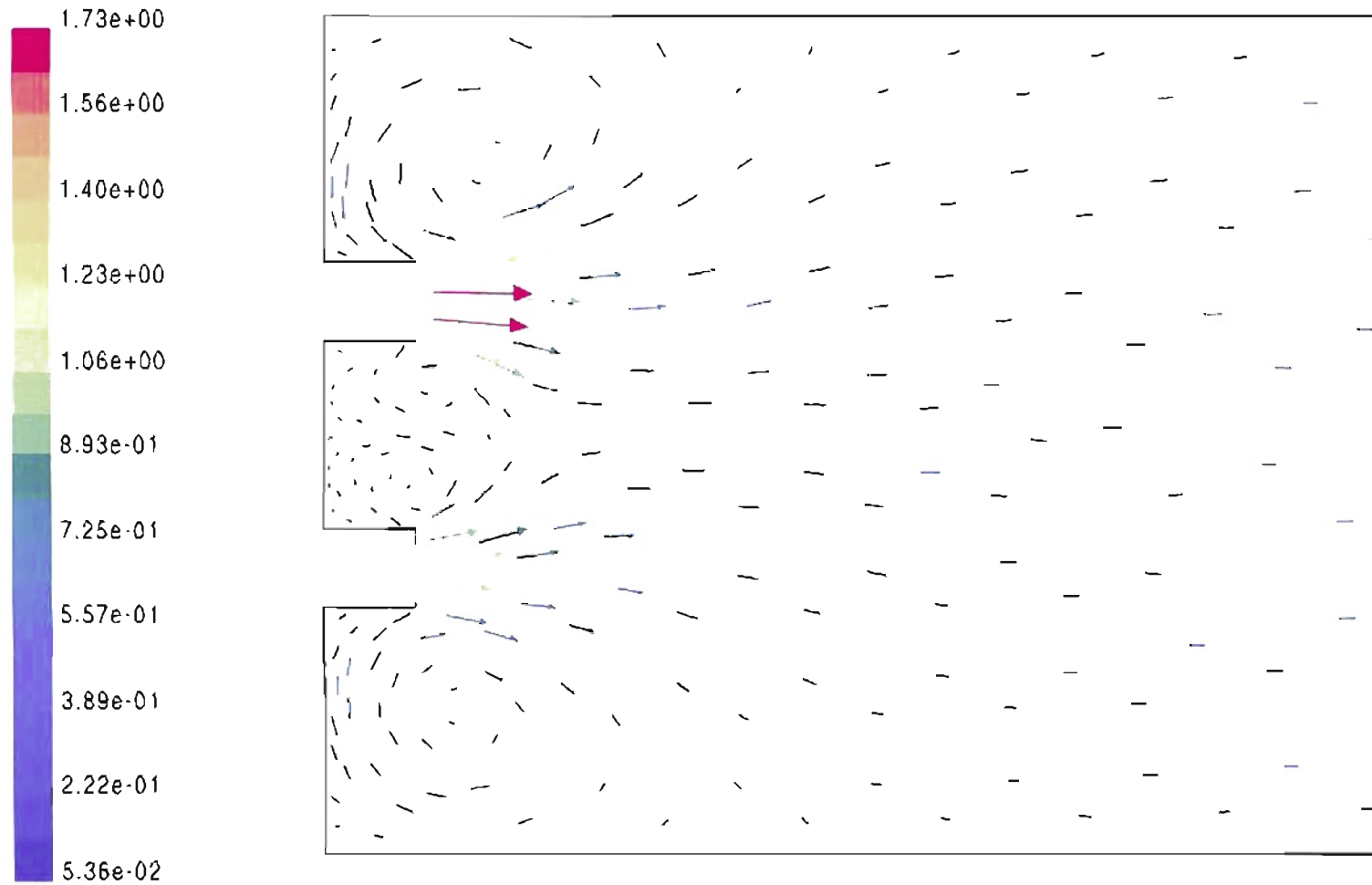


Figure 5-13:
FLUENT Velocity Vectors Colored By Velocity Magnitude (m/s)
(Optimized Conditions)

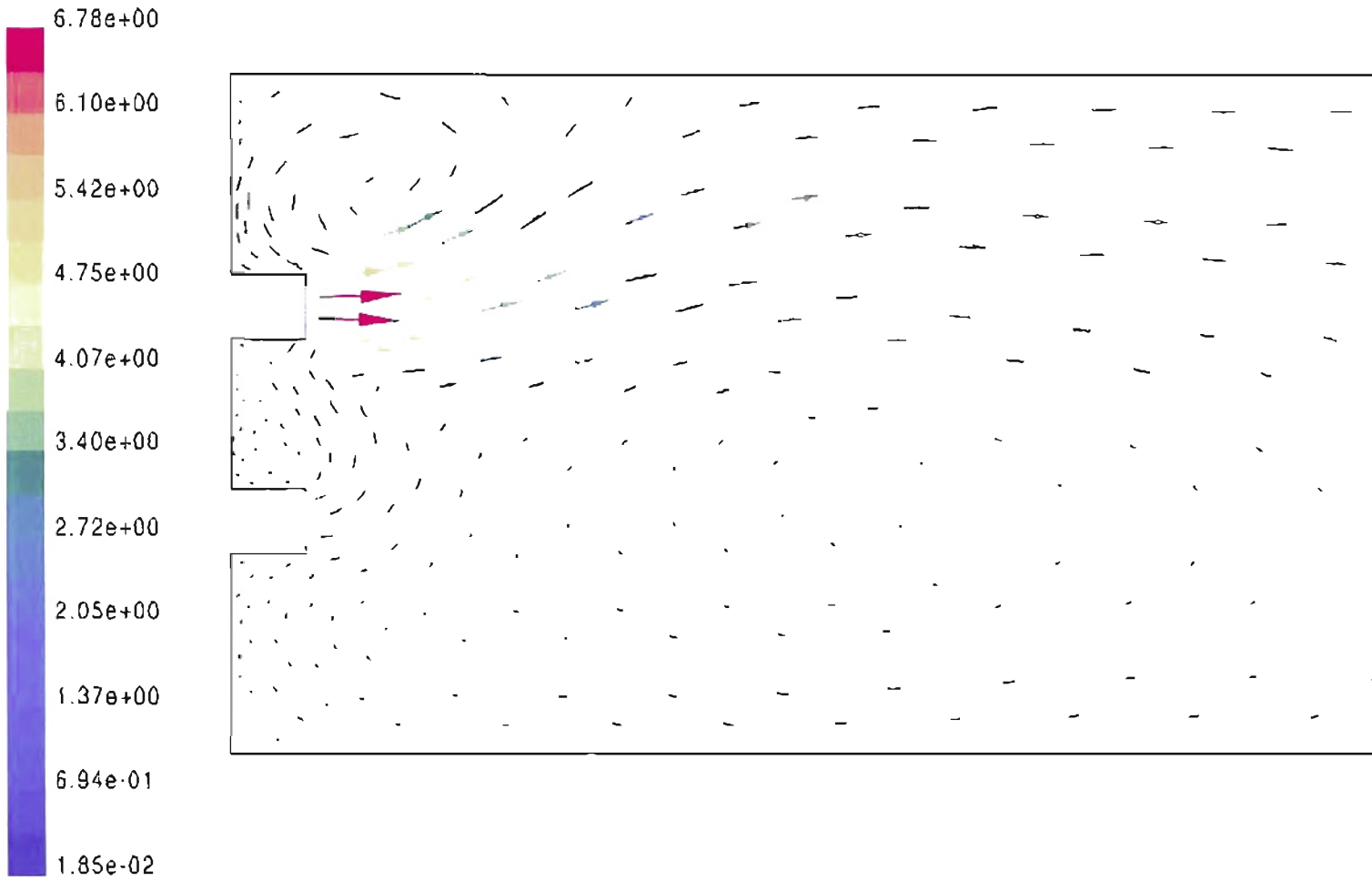


Figure 5-14:
FLUENT Velocity Vectors Colored By Velocity Magnitude (m/s)
(Unoptimized Conditions)

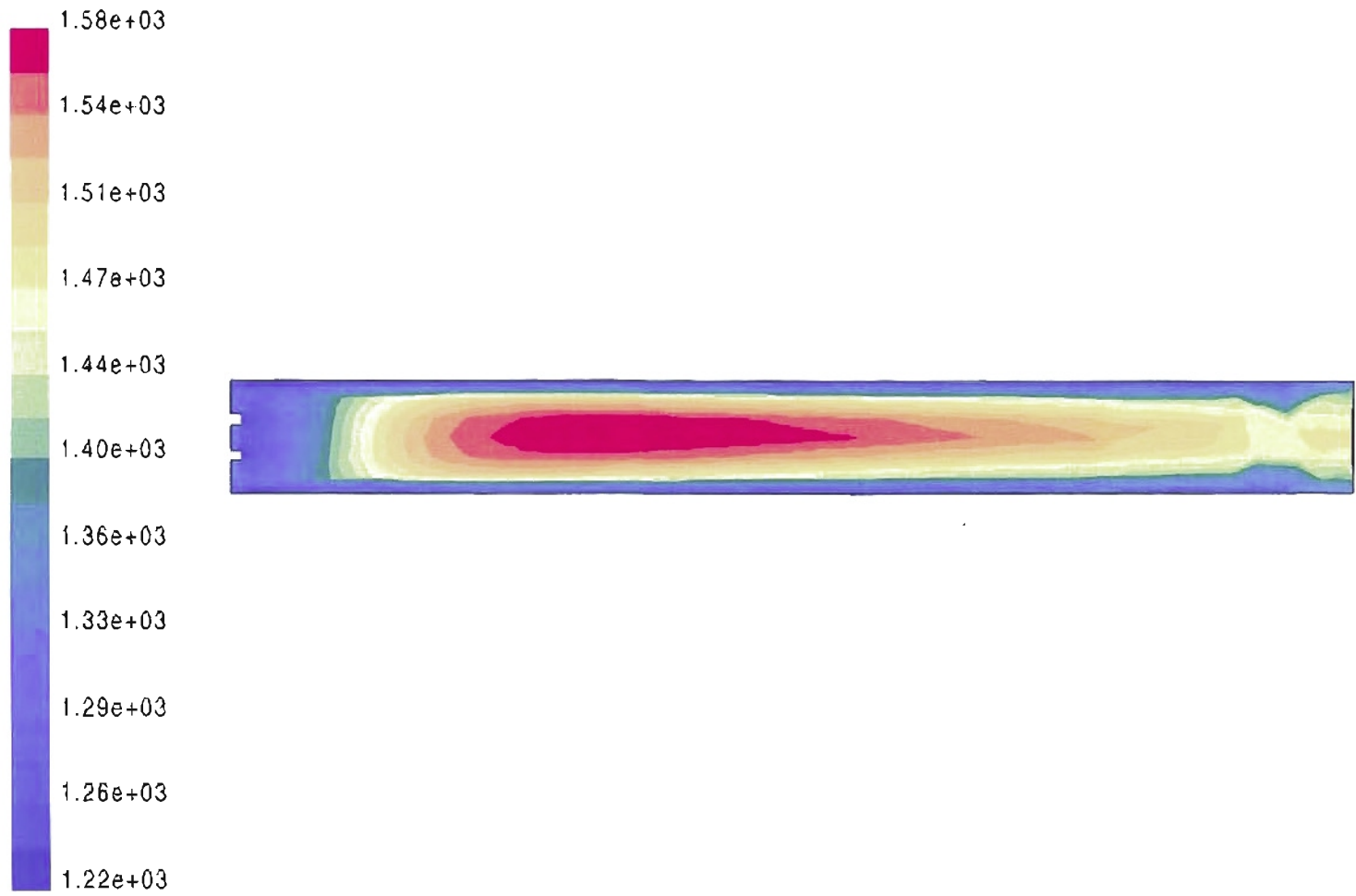


Figure 5-15:
FLUENT Profiles of Static Temperature (K)

Discussion of Design Results

The following points related to the model and the resulting design need to be considered. The diameter was kept the same while adjusting the reactor length to maintain constant Peclet numbers. As recommended by Kleijn et al. (1996), this approach to stagnation flow reactors is advantageous rather than fixing the height to length aspect ratio.

The optimum nozzle design was limited by plugging phenomena and represents a compromise between the run time that is dictated by the desired batch size, and the residence time required for sufficient diffusive mixing, i.e.- yield. Zambov et al. (1998) gives an explanation of the above compromise through analysis of the governing equations that dictate radial and axial mixing and plugging.

Inert Carrier Gas Effects

The modeling experiments did not include variation of the carrier gas flow rate. It was discerned in the experiments with the present system discussed in Chapter III, that the system prefers lower Ar flow rates. The interactions are such that the higher flows may aid in the prevention of plugging but also have the deleterious effect of decreasing the residence time, thus limiting diffusive mixing. The chosen Ar flow rates were based on those earlier studies and are further substantiated by calculations made by Morrison (1998).

Another conceptual approach to the effect of carrier gas flow rates in diffusion controlled systems is offered by Gebhart (1971). By analogy to heat transfer systems, the noncondensable, inert carrier has the effect of increasing the resistance to mass transfer in

product yield that a given set of reactant flows will produce with both nozzle diameters set at 8.5mm.

Notice that Figure 5-17 reaffirms the optimum nozzle diameter sizing for flows within this range. At approximately 8 – 9 mm diameters, there is a maximum plug factor that approaches (but remains less than) 0.010.

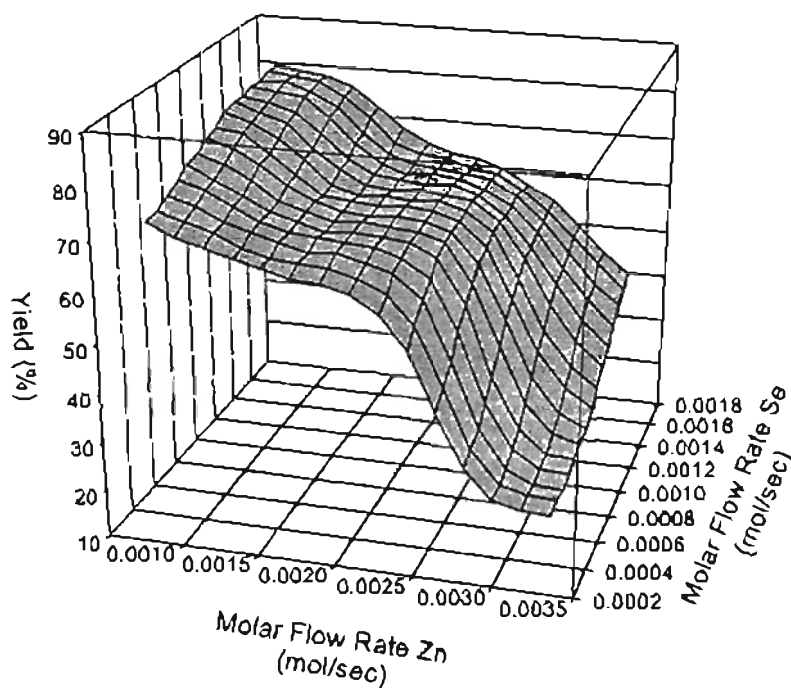


Figure 5-16:
Response Surface for the Effect of Reactant Flow Rates
at Constant Inlet Diameters on the Product Yield

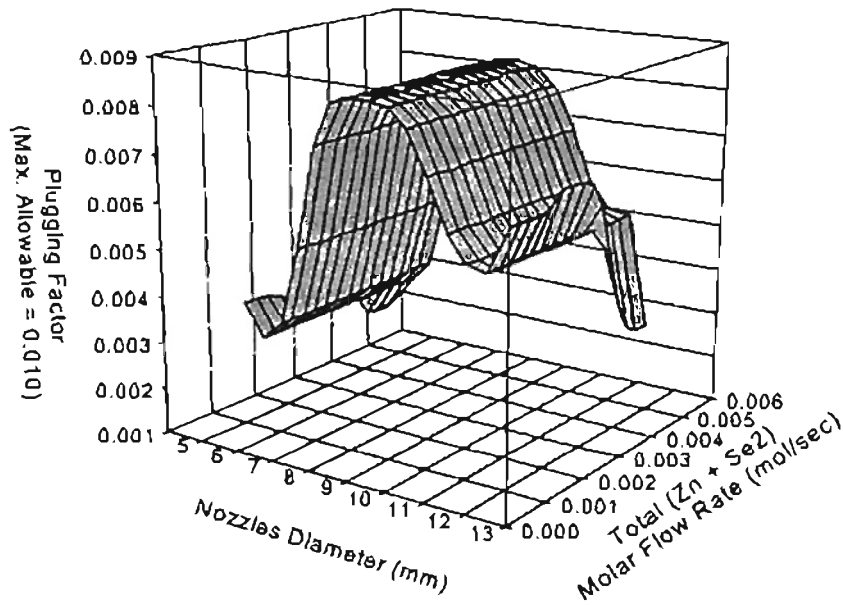


Figure 5-17:
Response Surface for the Effect of Nozzle Diameter
and Total Flow Rate on the Plugging Factor

Equations for the Surfaces

Although the 3D plots can be read directly, it would be of greater use if the functions could be solved numerically for the two response variables. This would allow for more accurate value determination as well as possible computer coding, if desired. Therefore, an attempt was made to fit the two surfaces to appropriate and dependable functions. A background in the theory and procedure is outlined by Khuri and Cornell (1996). Examination of the statistics of the function fits was based on a review of Bethea and Rhinehart (1991).

The surface for yield is assumed to be approximately planar and fit to the following equation by regression analysis via SigmaPlot 4.0 software.

$$f_1 = 83.61 + -18128.87x + 11432.79y \quad (5-2)$$

Where, the dependent variable f_1 is the yield, x is the diameter, and y is the total mole flow. The standard error of estimate is given to be 6.02 % with a regression coefficient (R) of 0.93. It should be noted that the function only applies to diameters within a few tenths of 8.5 mm.

The surface for the plugging factor closely resembles a Gaussian distribution of the factor about a mean value. The equation fit to this surface is:

$$f_2 = 0084e^{-0.50 \left[\left(\frac{x-8.8769}{2.5583} \right)^2 + \left(\frac{y+0.0299}{4.7836} \right)^2 \right]} \quad (5-3)$$

Where, f_2 is the dependent plug factor, x is the diameter, and y is the total mole flow rate with a standard estimate error of 0.0008 and an R coefficient of 0.91. This equation can apply across a range of diameters and total flow rates and should be used as a check for the conditions established by the first function (f_1). Again, f_2 should have a value of less than 0.010 for successful operation.

Summary of Steps to Establishing New Operating Conditions

Figure 5-18 gives one permutation that will allow the application of the above functions to develop operating conditions different from those given in Table 5-9. There are, of course, many other possibilities, but each approach would require development of new response surfaces. The data contained in Appendix C can be readily adapted to yield many other surfaces such as temperature, reactor length, etc. These can then be applied in a similar fashion to the procedure given below in terms of flows and diameters:

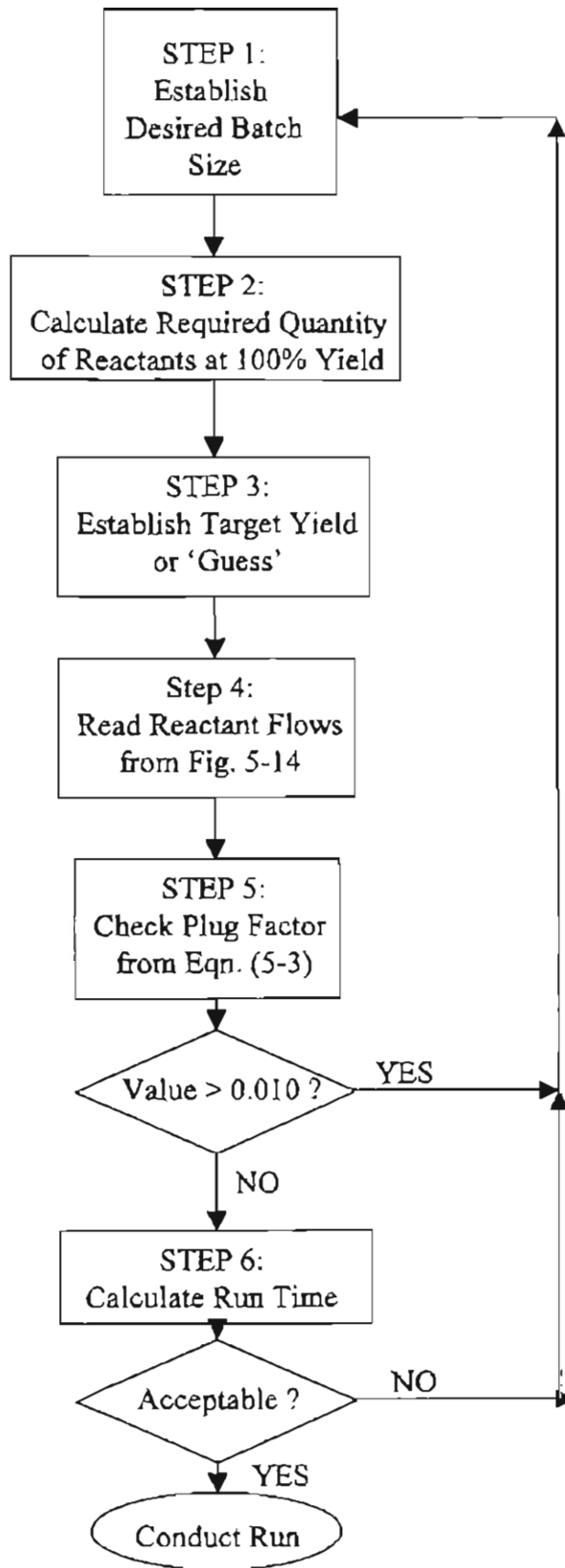


Figure 5-18: Steps to Establishing New Operating Conditions

CHAPTER VI

CONCLUSIONS AND RECOMMENDATIONS

Conclusions

The present and the newly designed reactor systems are both strongly influenced by diffusion controlled operating conditions. The diffusive transport of reactants exceeds that of convective transport at the reaction interface. The process produces the desired hexagonal crystals with particle size distributions of less than approximately 20 microns. However, the mass transfer limited nature of the process complicates the physical operation of the system. There is a propensity for the reactor inlets to plug as a result of the development of secondary flow characteristics within the reactor tube. The proposed new reactor was designed to address these technical issues. The following conclusions relevant to the new design are noted.

Overall New Design

The system, as proposed, accomplishes the design basis targets with respect to batch size, run time, product yield, and elimination of plugged runs. Additionally, the new system offers substantial improvements in the areas of; ease of operation, process controllability and predictability, simplification of operating procedure, and safety.

Consequently, the system should provide enhanced economic competitiveness to the overall process.

Computer Modeling

The computer model is well correlated to the experimental data within the bounds of uncertainty in the present system data. A 2-dimensional, pseudo-steady-state, finite volume CFD model can reasonably represent the new reactor design. Insertion of idealized kinetic expressions and empirically fit diffusion coefficients into the model allows for the simulation of an actual 3-dimensional system.

Optimization of Parameters

The inlet velocities and flow rates of reactants primarily dictate the new reactor performance. Optimal operating conditions and physical dimensions of the reactor can be established from an experimental matrix executed within the computer model. The 2D model can be adapted to adequately predict the 3D phenomena associated with secondary flow characteristics. The likelihood that plugging conditions may develop can be accounted for in the determination of the ideal operating conditions. Various combinations of RSM functions can be used as predictors of reactor performance or as a means of establishing new operating conditions.

Recommendations

Implementation

The new reactor design should be implemented in tandem with follow-up modeling efforts. The system performance, once built, can be tuned using the model as

developed in the course of this work and by others. The model accuracy can be enhanced with improved mass flow rates provided by the new system. This would allow for iterative improvement in both the accuracy of the model and performance of the new reactor.

Other Group II-VI compounds could be synthesized in the proposed reactor with additional modeling (that includes new kinetics and properties) to establish separate operating conditions. Experimental yield and mass flow data will need to be collected prior to the modeling work for each new product.

Modeling Follow-up Efforts

The model reliability can be further improved with the development a 3-dimensional representation of the reactor for better resolution of the secondary flow patterns. Additionally, effort should be focused on development of a non steady-state model that can predict the deposition of the product layer. This would entail significant work devoted to the determination of appropriate kinetic expressions for the reaction mechanism that are presently unknown. There are other researchers currently working on the heat transfer aspects of the reactor model, which can be incorporated at a later date. However, the effects of radiation need to be addressed, as well. As noted in a preceding chapter, the data gathered in the course of this work can be analyzed further to yield additional predictive functions. The run results presented here could be augmented with new data that becomes available from improvements in the computer model.

The analytical data related to particle size distributions of the product powder provided by the sponsor were incomplete at the time of conclusion of this manuscript, but

could eventually be included in the experimental matrix to provide size distributions of the product from the model output.

As outlined in the literature review, it is possible to incorporate the DOE data into a computer model that can be used to develop an artificial neural network. The DOE data can “train” a network that can take in back pressure measurements from the new boilers and adjust the mass flow of reactants, temperatures, etc. to yield an optimal product yield and deposition pattern. Now that my thesis is complete, it is safe to recommend this and other interesting projects for further work.

BIBLIOGRAPHY

- Abramovich, G.N. (1963). The Theory of Turbulent Jets, M.I.T. Press, Cambridge, MA.
- Angermeier, D., Monna, R., Slaouui, A. and Muller, J.C. (1997). "Modeling and Analysis of the Silicon Epitaxial Growth with SiHCl_3 in a Horizontal Rapid Thermal Chemical Vapor Deposition Reactor," J. Electrochem. Soc. 144 (9), 3256-3260.
- Balasubramanian, N., Kong, C.W., Jang, C. and Kovelamudi, R.B. (1996). "Optimized Polysilicon Deposition Using Response Surface Methodology," Semiconductor International 19 (8), 247-254.
- Bachelard, R., Disson, J.P. and Morlhon, B. (1997). "Continuous Process for the Preparation of Silicon Nitride by Carbonitriding and Silicon Nitride Thereby Obtained,' U.S. Patent 5,662,875.
- Barker, T.B. (1990). Engineering Quality by Design: Interpreting the Taguchi Approach, Marcel Dekker, Inc., New York and Basel.
- Battat, D., Faktor, M., and Garrett, I. (1976). "Preparation and Properties of Solid State Materials," Wilcox, W.R., Ed., Dekker, New York, 2, 43-128.
- Bethea, R.M. and Rhinehart, R.R. (1991). Applied Engineering Statistics, Marcel Dekker, Inc., New York.
- Bilodeau, J.F. and Proulx, P. (1996). "A Mathematical Model for Ultrafine Iron Powder Growth in a Thermal Plasma,' Aerosol Science and Technology 24, 175-189.
- Bird, R.B., Stewart, W.E. and Lightfoot, E.N. (1960). Transport Phenomena, John Wiley and Sons, New York.
- Boning, D.S. and Mozumder, P.K. (1993). "DOE/Opt: A System for Design of Experiments, Response Surface Modeling, and Optimization Using Process and Device Simulation," [Http://www.mtl.mit.edu/~boning/doe/doe.html](http://www.mtl.mit.edu/~boning/doe/doe.html).
- Bredol, M., Merikhi, J., and Ronda, C. (1996). "Method of Manufacturing ZnS Particles," U.S. Patent 5,498,369.
- Brown, L.W. (1964). "Experimental Vertical Synthesis Run," Eagle-Picher Research Book 81, 20-28.

- 2D TCAD Simulations, Colloquium, (Inst. Of Electrical Engineers), IEEE, No. 33, 17/1-17/6.
- Gavrishchuk, E.M. and Dadanov, A.Y. (1990). "Preparation of High-Purity Zinc Selenide for Powerful IR Optics," *Materials Science Forum* 62-64, 321-322.
- Gebben, V.D. and Bruce, W.D. (1995). "Method for Enhancing Production of Titanium Dioxide," U.S. Patent 5,573,744.
- Gebhart, B. (1971). Heat Transfer – 2nd Ed., McGraw-Hill, Inc., New York.
- Geissler, U., Hartmann, E., Krause, E., and Siche, D. (1996). "Investigation of the Transition Range in Seeded Vapour Grown ZnSe Crystals," *J. of Crystal Growth* 159, 175-180.
- Gobbert, M.K., Merchant, T.P., Borucki, L.J. and Cale, T.S. (1997). "A Multiscale Simulator for Low Pressure Chemical Vapor Deposition," *J. Electrochem. Soc.* 144 (11), 3945-3951.
- Greene, J.E. and Eltoukhy, A.H. (1981). "Semiconductor Crystal Growth by Sputter Deposition," *Surface and Interface Analysis* 3 (1), 34-54.
- Gupta, V., Safri, S.A. and Mountziaris, T.J. (1996). 'Gas-Phase Decomposition Kinetics in a Wall-Less Environment Using a Counter-Flow Jet Reactor: Design and Feasibility Studies,' *Ind. Eng. Chem. Res.* 35 (9), 3248-3255.
- Habuka, H., Mayusumi, M., Tate, N. and Katayama, M. (1995). "Gas Flow and Heat Transfer in a Pancake Chemical Vapor Deposition Reactor," *J. of Crystal Growth* 151, 375-383.
- Ham, D., Mishra, K. and Rajeshwar, K. (1991). "Anodic Electrosynthesis of Cadmium Selenide Thin Films," *J. Electrochem. Soc.* 138 (1), 100-108.
- Hamby, E.S., Demos, A.T., Kabamba, P.T. and Khargonekar, P.P. (1995). "A Control Oriented Modeling Methodology for Plasma Enhanced Chemical Vapor Deposition Processes," *Proceedings of the American Control Conference*, Seattle, WA., 220-224.
- Himmelblau, D.M. and Bischoff, K.B. (1968). Process Analysis and Simulation: Deterministic Systems, Wiley, New York.
- Hintermann, H.E., and Laeng, P. (1983). "Specialty Steels and Hard Materials," (Comings, N.R., ed.), Oxford, 407-414.
- Hitchman, M.L., and Jensen, K.F., eds. (1993). Chemical Vapor Deposition Principles and Applications, The Academic Press, San Diego, CA.

- Hitchman, M.L., and Jensen, K.F., (1993). Chemical Vapor Deposition – An Overview,” Chapter 1: Chemical Vapor Deposition Principles and Applications, The Academic Press, San Diego, CA.
- Hitchman, M.L., and Jensen, K.F., (1993). Chemical Vapor Deposition at Low Pressures,” Chapter 4: Chemical Vapor Deposition Principles and Applications, The Academic Press, San Diego, CA.
- Hlavacek, V. and Puszynski, J.A. (1996). “Chemical Engineering Aspects of Advanced Ceramic Materials,” *Ind. Eng. Chem. Res.* 35 (2), 349-377.
- Hornbeck, R.W. (1975). Numerical Methods, Quantum Publishers, Inc., New York.
- Jackson, C.P. and Winters, K.H. (1984). “Finite-Element Study of the Benard Problem Using Parameter Stepping and Bifurcation,” *Int. J. Num. Methods Fluids* 4, 127-145.
- Jackson, S.C., Baron, B.N., Rocheleau, R.E. and Russel, T.W.F. (1987). “A Chemical Reaction Model for Physical Vapor Deposition of Compound Semiconductor Films,” *AIChE Journal* 33 (5), 711-720.
- Jackson, W.B. (1993). “Electronic and Optical Characterization of Chemical Vapor Deposition Films for Device Applications,” Chapter 9: Chemical Vapor Deposition, Principles and Applications, Hitchman, M.L., and Jensen, K.F., eds., Academic Press, San Diego, 515-586.
- Jasinski, J.M., Meyerson, B.S. and Scott, B.A. (1987). “Mechanistic Studies of Chemical Vapor Deposition,” *Ann. Rev. Phys. Chem.* 38, 109-140.
- Jensen, F.F. (1993). “Fundamentals of Chemical Vapor Deposition,” Chapter 2: CVD Principles and Applications, Hitchman, H.L and Jensen, K.F., eds., Academic Press, San Diego, 32-85.
- Johnson, D.L., Dravid, V.P., Teng, M.H., Host, J.J., Hwang, J. and Elliott, B.R. (1997). “Nanoparticle Synthesis Apparatus and Method,” U.S. Patent 5,665,277.
- Kimura, H., and Komiya, H. (1973). ‘Melt Compositions of II-VI Compounds During Crystal Growth in a High-Pressure Furnace,” *J. of Crystal Growth* 20, 283-291.
- Khuri, A.I. and Cornell, J.A. (1996). Response Surfaces: Designs and Analyses, 2nd Ed., Marcel Dekker, Inc, New York.
- Kleijn, C.R., van der Meer, Th.H. and Hoogendoorn, C.J. (1989). “ A Mathematical Model for LPCVD in a Single Wafer Reactor,” *J. Electrochem. Soc.* 136 (11), 3423-3433.

- Kleijn, C.R., Kuijlaars, K.J. and Van Der Akker, H.E.A. (1996). "Design and Scale-up of Chemical Vapor Deposition Reactors for Semiconductor Processing," *Chem. Eng. Science* 51 (10), 2119-2128.
- Kodos, T.T., Friedlander, S.K. and Pratsinis, S.E. (1987). "Effect of Reactant Mixing on Fine Particle Production in a Tubular Flow Reactor," *Ind. Eng. Chem. Res.* 26, 1999-2007.
- Konig, T. (1995). "Process for the Preparation of Finely Divided Metal and Ceramic Powders," U.S. Patent 5,472,477.
- Korostelin, Y.V., Kozlovsky, V.I., Nasibov, A.S., and Shapkin, P.V. (1996). "Vapour Growth of II-VI Solid Solution Single Crystals," *J. of Crystal Growth* 159, 181-185.
- Korostelin, Y.V., Kozlovsky, V.I., Nasibov, A.S., and Shapkin, P.V. (1996). "Vapour Growth and Characterization of Bulk ZnSe Single Crystals," *J. of Crystal Growth* 161, 51-59.
- Krishnan, A. and Zhou, N. (1995). "Analysis of Chemical Vapor Deposition in Industrial Reactors," *Proceedings of the ASME/JSME Thermal Engineering Joint Conference* 4, ASME, 113-120.
- Kucharczyk, M. and Zabłudowska, K. (1986). "Review of Methods for Preparation of Zinc and Cadmium Sulfide, Selenide and Telluride Single Crystals," NASA Technical Memorandum, NASA TM-88426. A translation of "Przegląd metod otrzymywania monokryształów siarczków selenków i tellurków cynku i kadmu," *Zeszyty Naukowe Politechniki Białostockiej. (Ser) matematyka fizyka, Chemia*, Poland, No. 1, pp. 3-21, 1976.
- Kuijlaars, K.J., Kleijn, C.R. and van der Akker, H.E.A. (1996). "Modeling of Selective Tungsten Low-Pressure Chemical Vapor Deposition," *Thin Solid films* 290-291, 406-410.
- Lerner, E.J. (1998). "Race is on to develop blue-green diode lasers," *Laser Focus World*, April, 91-99.
- Levenspiel, O. (1972). *Chemical Reaction Engineering* – 2nd Ed., John Wiley and Sons, New York.
- Levenspiel, O. (1996). *Chemical Reactor Omnibook*, (ISBN: 0-88246-170-2), Distributed by Oregon State University Book Stores Inc., Corvallis, OR.
- Mahajan, R.L. and Walker, K.J. (1996). "On-Line Prediction and Optimization of a CVD Barrel Reactor: An Experimental Study," *Proceedings of the ASME Fluids Engineering Division* 242, 69-80.

- Marfaing, Y. (1991). "Optoelectronics with II-VI and IV-VI," *Materials Science and Engineering B9*, 169-177.
- Mattox, D.M. (1979). "Coatings for Fusion Reactor Environments," *Thin Solid Films 63*, 213-216.
- Misiewicz, J., Huber, C., and Heiman, D. (1994). "Zn-MnSe Epitaxial Layers and ZnSe/MnSe Heterostructures Grown by Pulsed-Layer Deposition," *Proceedings of the 9th International Conference on Ternary and Multinary Compounds, 1993, Japan J. of Appl. Phys., Part 1(32)*, 372-374.
- Moen, R.D., Nolan, T.W. and Provost, L.P. (1991). Improving Quality Through Planned Experimentation, McGraw-Hill, New York.
- Moffat, H., and Jensen, K.F. (1986). "Complex Flow Phenomena in MOCVD Reactors," *J. of Crystal Growth 77*, 108-119.
- Moon, R.L. and Huong, Y.M. (1993) "Organometallic Vapor Phase Epitaxy of III-V Materials," Chapter 6: CVD Principles and Applications, Hitchman, H.L. and Jensen, K.F., eds., Academic Press, San Diego, 245-384.
- Mori, T. (1990). The New Experimental Design: Taguchi's Approach to Quality Engineering, ASI Press, Tokyo, Japan.
- Morrison, D. (1998). "Analysis and Design of a Laminar Flow Aerosol Reactor for the Production of ZnSe Powders," M.S. thesis, Department of Chemical Engineering, The Oklahoma State University, Stillwater, Okla.
- Morton Advanced Materials, (1998). "CVD Zinc Selenide Product Information," www.mortoncvd.com/morton.html, Woburn, MA.
- Mountziaris, T.J. and Jensen, K.F. (1991). "Gas Phase and Surface Reaction Mechanisms in MOCVD of GaAs with Trimethyl-Gallium and Arsine," *J. Electrochem. Soc. 138* (8), 2426-2439.
- Mozumder, P.K., Saxena, S. and Collins, D.J. (1994). "A Monitor Based Controller for Semiconductor Processes," *IEEE Transactions on Semiconductor Manufacturing 7* (3), 400-411.
- Nauman, E.B. and Buffham, B.A. (1983). Mixing in Continuous Flow Systems, John Wiley and Sons, New York.
- Nikolic, Z. (In Progress). M.S. thesis, Department of Mechanical and Aerospace Engineering, The Oklahoma State University, Stillwater, Okla.

- Nouhi, A. and Stirn, R.J. (1986). "Highly Conducting Zinc Selenide Films by Reactive Magnetron Sputtering," *J. Vac. Sci Technol.* 3(1), 403-407.
- Okuyama, K., Ushiro, R., Kousaka, Y., Seinfeld, J.H. and Flagan, R.C. (1992). "Evaluation of Fine Particle Formation by CVD in a Laminar-Flow Aerosol Reactor," *Intl. Chem. Eng.* 32(4), 750-758.
- Pierson, H.O., ed., (1981). Chemical Vapor Deposited Coatings, American Chemical Society, Columbus, OH., 27-45.
- Pratsinis, S.E. (1988). "Simultaneous Nucleation, Condensation, and Coagulation in Aerosol Reactors," *Journal of Colloid and Interface Science* 124 (2), 416-427.
- Pratsinis, S.E., Akhtar, M.K., Wang, G. and Panda, S. (1996). "Process for Aluminum Nitride Powder Production," U.S. Patent 5,525,320.
- Pratsinis, S.E. and Vemury, S. (1996). "Particle Formation in Gases: A Review," *Powder Technology* 88, 267-273.
- Pruppacher, H.R. and Klett, J.D. (1978). Microphysics of Clouds and Precipitation, D. Reidel Pub. Co., Boston, MA.
- Ranade, V.V. (1997). "Improve Reactors via CFD," *Chemical Engineering*, May, 96-102.
- Rao, N.P., Nijhawan, S., Kim, T., Wu, Z., Campbell, S., Kittelson, D. McMurry, P., Cheng, C.C. and Mastromatteo, E. (1998). "Investigation of Particle Generation During the Low-Pressure Chemical Vapor Deposition of Borophosphosilicate Glass Films," *J. of Electrochem., Soc.* 145 (6), 2051-2057.
- Reist, P.C. (1993). Aerosol Science and Technology – 2nd Ed., McGraw-Hill, New York.
- Rhodes, G. (1997). Personal communication, Oklahoma State University, Stillwater, Ok.
- Sadakata, M., Xu, Y.B. and Harano, A. (1996). "A Systematic Approach for the Design of Aerosol Reactors," *Powder Technology* 88, 261-266.
- Schonherr, E., Freiberg, M., and Hartmann, H. (1997). "In-situ Observed Twin Formation on ZnSe Crystals Growing by Sublimation," *Cryst. Res. Technology* 32 (8), 1041-1047.
- Sigmaplot V.4.0,(1997). SPSS, Inc., San Rafael, CA.
- Spirin, G.G., Vinogradov, Y.K., and Belyaev, O.V. (1996). "Experimental Study of Molecular Thermal Conductivity of Quartz," *High Temperature* 34, 25-30. Translated from *Teplofizika Vysokikh Temperatur* 34, 29-34, (1996).

- Su, S.H., Yokoyama, M. and Su, Y.K. (1997). "9 Inch Diagonal ZnS and ZnS:Mn Films Fabricated by Metallorganic Chemical Vapor Deposition," *J. Electrochem. Soc.* 144 (12), 4310-4313.
- Taguchi, G. (1987). *System of Experimental Design*, Unipub/Krause International Publications, White Plains, N.Y.
- Taguchi, G. (1992). *Taguchi Methods: Research and Development, Quality Engineering Series 1*, Konishi, S. ed., ASI Press, Tokyo, Japan.
- Taguchi, G. (1993). *Taguchi on Robust Technology Development*, ASME Press, New York.
- Thiandourne, C., Angermeier, D. and Gorochoy, O. (1998). "Modeling and Process Optimization of ZnSe and ZnS Epitaxial Growth in a Vertical Metallorganic Vapor-Phase Epitaxy Reactor," *J. Electrochem. Soc.* 145 (8), 2887-2891.
- Tung, H.C. (1955). "Nozzle Design," M.S. Thesis, Department of Mechanical Engineering, Oklahoma State University, Stillwater, Okla.
- Wahl, G. (1993). "Protective Coatings," Chapter 10: CVD Principles and Applications, Hitchman, H.L. and Jensen, K.F., eds., Academic Press, San Diego, 591-660.
- Wahlbeck, P.G., Myers, D.L., and Truong, V.V. (1985). "Validity of the Ruff-MKW Boiling Point Method: Vapor Pressures, Diffusion Coefficients in Argon and Helium, and Viscosity Coefficients for Gaseous Cadmium and Zinc," *J. of Chem. Phys.* 83 (5), 2447-2456.
- Wang, J.S., Teng, C.C., Middleton, J.R. and Feng, M. (1995). "Process Integration and Optimization of GaAs MESFET and MSM Based Opto-Electronics Integrated Circuit (OEIC) Using Statistical Experimental Design Techniques," Proceedings of the IEEE/CPMT Int'l Electronics Manufacturing Technology Symposium, 471-479.
- Wang, Y. and Pollard, R. (1995). "An Approach for Modeling Surface Reaction Kinetics in Chemical Vapor Deposition Processes," *J. Electrochem. Soc.* 142 (5), 1712-1724.
- Wang, X.A. and Mahajan, R.L. (1995). "CVD Epitaxial Deposition in a Vertical Barrel Reactor: Process Modeling and Optimization Using Neural Network Models," *J. Electrochem. Soc.* 142 (9), 3123-3127.
- Weerts, W.L.M., de Croon, M.H.J. and Marin, G.B. (1997). "Low Pressure Chemical Vapor Deposition of Polycrystalline Silicon: Analysis of Nonuniform Growth in an Industrial-Scale Reactor," *J. of Electrochem. Soc.* 144 (9), 3213-3221.

- Wen, C.S. (1996). The Fundamentals of Aerosol Dynamics, World Scientific, Singapore.
- White, R.T., Espino-Rios, R.L., Rogers, D.S., Ring, M.A. and O'Neal, H.E. (1985). "Mechanism of the Silane Decomposition: I. Silane Loss Kinetic and Rate Inhibition by Hydrogen, II. Modeling of the Silane Decomposition (All Stages of Reaction)," *Int. J. Chem. Kinet.* 17 (10), 1029.
- Xu, C., Hampden-Smith, M.J., Kudas, T.T., Duesler, E.N., Rheingold, A.L. and Yap, G. (1995). "Synthesis and Structure Determination of (hfac)Ag(SET₂), Pd(hfac-C)(hfac-O,O)(SET₂), and ((hfac)Ag)₄(SET₂): Ligand Exchange Reactions Relevant to Aerosol-Assisted Chemical Vapor Deposition (AACVD) of Ag_{1-x}Pd_x Films," *Inorganic Chemistry* 34 (Sept. 95), 4767-4773.
- Zambov, L., Popov, C. and Ivanov, B. (1998). "Design of Injection Feed Multiwafer Low-Pressure Vapor Deposition Reactors," *J. Electrochem. Soc.* 145 (7), 2494-2498.

APPENDIX A

DERIVED KINETIC AND THERMODYNAMIC PARAMETERS

Derivation of Idealized Rate Constant

The following is a calculation of an idealized rate constant for a reaction of overall second order. Units typically used in the relationships are given in the Nomenclature section. Also, specific assumptions relative to the calculations are discussed in the body of Chapter IV.

For an ideal plug flow reactor, a material balance written in terms of the disappearance of component A results in the PFR design equation (Levenspiel, 1996):

$$F_{A0}dX_A = (-R_A)dV \quad (\text{A-1})$$

The equation applies for any expansion coefficient, ϵ_A , for an ideal gas at constant pressure and temperature with changing number of moles in the gas phase:

$$\epsilon_A = \frac{(V_{X_A=1}) - (V_{X_A=0})}{V_{X_A=0}} \quad (\text{A-2})$$

Where, V is the component gas phase volume or volumetric flow rate, and X_A is the conversion of reactant A:

$$X_A = 1 - \frac{C_A}{C_{A0}} \quad (\text{A-3})$$

Where, C_A and C_{A0} refer to the concentrations of A at the inlet and any time t , respectively.

For a general second order, irreversible reaction, the rate equation is given by:

$$-R_A = k C_A^1 C_B^1 \quad (A-4)$$

The integration of the design equation (A-1) results in the following for $\epsilon_A \neq 0$:

$$k = [(2 \epsilon_A (1 + \epsilon_A) (\ln(1-X_A)) + \epsilon_A^2 X_A + (\epsilon_A^2 X_A + (\epsilon_A + 1)^2 X_A / (1-X_A))] / \tau C_{A0} \quad (A-5)$$

Where, τ is the reactor residence time given by the ratio of the reactor volume and the volumetric flow V_0 :

$$\tau = V/V_0 \quad (A-6)$$

The volumetric flow rates and inlet concentrations are calculated by equations given in Appendix B and incorporated into an Excell spreadsheet given by Tables C-4 (a & b). Assuming that the conversion of A (Zn) approaches 100 %, Eqn. (A-5) is solved for $k \approx 6.89 \times 10^6$ L/mol-s.

Activation Energy Estimates From Experimental Data

The activation energy (A_E) was estimated by the following methods from experimental data gathered from the system in operation at Eagle-Picher.

Method I

The first method is based on the Arrhenius temperature dependence of the rate constant given by:

$$k = k_0 e^{-A_E/RT} \quad (A-7)$$

Table A-1 was developed from two experiments conducted at different temperatures that have reliable run time estimates based on the boiler power readings:

Table A-1: Experimental Rate Data (Method I):

Run ID	Temp. (K)	Est. Run Time (s)	Product (grams)	Product (moles)	Rate (mol/m ³ -s)	X _{A=Zn} (%)	ln (Rate)
E3R6	1348	165	641	4.40	0.0776	58.0	-2.556
E9R2	1248	190	614	4.26	0.0648	55.6	-2.764

With only two reliable runs, we assume linearity, and take a slope of the points and take the slope given by Levenspiel (1996) as:

$$\text{Slope (ln(rate) vs. } T^{-1}) = -A_E/R \quad (\text{A-8})$$

Where, R is the universal gas constant with the value of 8.314 J/mol-K and the activation energy, A_E, is found to be 2.93 x 10⁷ J/ Kmol.

Method II

The second method evolves from the following relationship given by Levenspiel (1972,1996):

$$\ln \frac{\text{rate}_1}{\text{rate}_2} = \ln \frac{k_1}{k_2} = \frac{A_E}{R} \left(\frac{1}{T_2} - \frac{1}{T_1} \right) \quad (\text{A-9})$$

Using experimentally determined conversions, the appropriate rate constant k values are calculated from Equation (A-5) to arrive at A_E = 8.10 x 10⁷ J/Kmol.

The values determined from the two methods can be compared to that reported by Levenspiel (1996) for typical gas phase reactions that proceed only at high temperatures of 2.0- 4.0 x 10⁸ J/Kmol. Transition-state theory based calculations performed by Morrison (1998) resulted in an A_E of 1.90 x 10⁸ J/Kmol. These values are summarized in Table A-2.

Table A-2: Comparison of Calculated Activation Energies for ZnSe Reaction

Source	A_E (J/Kmol)
Method I	2.93×10^7
Method II	8.10×10^7
Levenspiel*	3.0×10^8
Transition-State Theory**	1.90×10^7

Note: *1996, **Morrison (1998)

APPENDIX B

DESIGN BASIS CALCULATIONS

Dimensionless Parameter Calculations

The Reynolds number equation for a cylinder:

$$\text{Re} = \frac{\rho D v}{\mu} \quad (\text{B-1})$$

Where, D is the cylinder diameter, v is the velocity, ρ and μ are the fluid density and viscosity, respectively. Combining B-1 with the equations of continuity and cylinder area where V_o is the fluid volumetric flow rate:

$$v = \frac{V_o}{A} \quad (\text{B-2})$$

$$A = (\pi/4)D^2 \quad (\text{B-3})$$

Results in the following form:
$$\text{Re} = \left(\frac{4\rho}{\pi\mu} \right) \left(\frac{V_o}{D} \right) \quad (\text{B-4})$$

The mass Peclet number is given by:

$$\text{Pe}_m = \text{Re} \times \text{Sc} \quad (\text{B-5})$$

The Schmidt number, Sc , is given by:

$$\mu/\rho D_m \quad (\text{B-6})$$

Where, D_m is the mass diffusivity of the fluid components and we arrive at the final form for the mass Peclet number:

$$\text{Pe}_m = (D v)/D_m \quad (\text{B-7})$$

The volumetric flow rate, V_o , velocity, ν , and the properties of ρ , μ , and D_m can be calculated at inlet conditions or averaged for the length of the reactor to account for changes in composition and temperature. Temperature dependent property functions are available in the thesis of Morrison (1998).

Basic Flow Calculations

The above calculations for our system can be made via the following basic relations. The formulas are in spreadsheet format in Appendix C for quick calculation of operating conditions. The volumetric flow rate, V_o , of individual reactants is derived from the ideal gas law and assumes the form of:

$$V_o' = \frac{\dot{n}_i RT}{P} \quad (\text{B-8})$$

Where, the molar flow rate of component i , \dot{n}_i , is found from:

$$\dot{n}_i = \frac{\dot{m}_i}{MW_i} \quad (\text{B-9})$$

And the mass flow rate, \dot{m}_i , is determined from flowmeter calibrations in cm^3/sec as:

$$\dot{m}_i = \frac{\text{cm}^3 / \text{sec} \left(1000 \frac{\text{cm}^3}{\text{m}^3} \right) MW_i}{\delta} \quad (\text{B-10})$$

Where, δ refers to the molar volume (m^3/mol) gas constant taken from an appropriate plot or temperature dependent function.

The inlet velocities are then calculated as follows. For inlet 1, ν_1 is given by:

$$V_1 = \frac{V_o^{Zn} + V_o^{Ar}}{\pi r_{inlet}^2} \quad (B-11)$$

Inlet 2 velocity is calculated similarly:

$$V_2 = \frac{V_o^{Zn} + V_o^{Ar}}{\pi r_{inlet}^2} \quad (B-12)$$

The inlet mass fractions, X_i , required as for input boundary conditions by FLUENT are calculated in the spreadsheet as follows:

$$x_{Zn} = \frac{\dot{m}_{Zn}}{\dot{m}_{Zn} + \dot{m}_{Ar}} \quad (B-13)$$

$$x_{Se2} = \frac{\dot{m}_{Se2}}{\dot{m}_{Se2} + \dot{m}_{Ar}} \quad (B-14)$$

Conversion of FLUENT Steady State Yields to Actual Yields

The following is an example calculation that estimates a time-dependent batch product yield from the steady state output data given by the FLUENT CFD model. With the batch output set at 2.0 kgs ZnSe, the required number of moles of Zn and Se is given by:

$$\frac{\left(\frac{2.0 \text{ kg ZnSe}}{144.35 \frac{\text{kg}}{\text{kmol}}} \right)}{(\text{yield}(\%)/100 = 0.775)} = 17.88 \text{ moles Zn \& Se} \quad (B-15)$$

Based on run conditions as outlined in Chapter V and inlet flow rates calculated from the above relationships or Spreadsheets C-4 (a&b); the batch run time is calculated as:

$$\left(\frac{17.88 \text{ moles Zn}}{7.28 \times 10^{-4} \frac{\text{mol}}{\text{sec}}} \right) \left(\frac{3600 \text{ sec}}{\text{hr}} \right) = 6.82 \text{ hours} \quad (\text{B-16})$$

It is apparent from above that run times can be shortened with higher flows. Recall, however, that the higher flows will require larger nozzles to maintain proper flow characteristics given by Eqns. (5-2) and (5-3). Table B-1 gives the FLUENT species mole fractions taken from steady state integration of the reactor interior for the confirm05 run.

Table B-1: Steady State Mole Fractions from FLUENT for Confirm05 Run

Component	Mole Fraction
Zn	0.130
Se ₂	0.065
ZnSe	0.477
Ar	0.328
Total	1.000

For an ideal gas at constant pressure and temperature with a change in the number of moles in the gas phase due to reaction, the expansion coefficient, ϵ_A , is given by Eqn. (A-2). The volumetric flow rates, V_o , for Zn, Se₂, and Ar are calculated from Eqn. (B-8) and summarized in Table B-2.

Table B-2: Inlet Volumetric Flow Rates for Confirm05 Run

Component	V_o (m ³ /sec)
Zn	7.310×10^{-4}
Se ₂	3.653×10^{-5}
Ar	2.007×10^{-5}
Total	1.297×10^{-4}

The volumetric fraction of argon, V_F^{Ar} , is calculated as:

$$V_F^{Ar} = \frac{V_o^{Ar}}{V_o^{Zn+Se_2} + V_o^{Ar}} = \frac{2.007 \times 10^{-5}}{1.100 \times 10^{-4} + 2.007 \times 10^{-5}} = 0.15 \quad (\text{B-17})$$

ϵ_A is then calculated from the volume fractions as follows:

$$\epsilon_A = \frac{(1 + 0.30) - 2.3}{2.3} = -0.43 \quad (\text{B-18})$$

Levenspiel (1996) gives the conversion of reactant A as:

$$X_A = \frac{C_{A_0} - C_A}{C_{A_0} + \epsilon_A C_A} \quad (\text{B-19})$$

Alternatively, the expressions can be given in terms of y_A , mole fraction of A:

$$\frac{y_A}{y_{A_0}} = \frac{C_A}{C_{A_0}} = \frac{1 - X_A}{1 + \epsilon_A X_A} \quad (\text{B-20})$$

Where, the inlet mole fraction of A is calculated from inlet flow rates, \dot{n} , given by (B-9).

The inlet y_{A_0} , where A = Zn is then given by:

$$y_{Zn_0} = \frac{\dot{n}_{Zn}}{\dot{n}_{Zn} + \dot{n}_{Se_2} + \dot{n}_{Ar}} = \frac{7.28 \times 10^{-4}}{7.28 \times 10^{-4} + 3.64 \times 10^{-4} + 2.00 \times 10^{-4}} = 0.563 \quad (\text{B-21})$$

And, the outflow mole fraction is computed from FLUENT profiles as an area weighted average surface integral at the outflow face of the reactor geometry. The component mole fractions are given in Table B-3.

Table B-3: Outflow Mole Fractions from FLUENT for Confirm05 Run

Component	Mole Fraction
Zn	0.0227
ZnSe	0.596
Se ₂	0.0430
Ar	0.338
Total	0.9997

Values from Table B-3 and Eqn. (B-21) result in the following ratio for Zn:

$$\frac{y_{Zn}}{y_{Zn_0}} = \frac{0.0227}{0.563} = 0.0403 \quad (\text{B-22})$$

Finally, Eqn. (B-20) is solved to arrive at an estimate for the actual conversion of Zn:

$$0.0403 = \frac{(1 - X_{Zn})}{(1 - 0.43X_{Zn})} \quad (\text{B-23})$$

The conversion obtained by iteration: $X_{Zn} = 0.977$ or 97.7 %.

The X_{Zn} value is an estimate only of the actual yield that can be derived from the FLUENT steady state output model of the new reactor operated at the optimum conditions outlined in Chapter V.

APPENDIX C

FLUENT Model DOE Documentation

Contents:

I - Design Matrix Study I

II - Fluent DDN coordinates used to input physical reactor dimensions

III - Spreadsheet calculations to establish model inputs for operating parameters

IV - Operating Parameters Grid

V – Study I Run Data

VI - Factors Analysis

VII - Interactions Analysis

VIII – Study II FLUENT DDN Coordinates

IX – Study II Factor Key

X - Study II Run Data and Results (Yield)

XI - Study II Run Data and Results (Plugging Factor)

XII – RSM Data

I. Experimental Design Study I

Table C-1: Design Optimization Study I Experimental Grid

RUN NO.	PHYSICAL PARAMETERS				OPERATING	
	1 = NA	2 = ND	3 = NP	4 = RL	5 = FR	6 = ZT
1	-1	-1	-1	-1	-1	-1
2	-1	-1	1	-1	-1	-1
3	1	-1	-1	-1	-1	-1
4	1	-1	1	-1	-1	-1
5	-1	1	-1	-1	-1	-1
6	-1	1	1	-1	-1	-1
7	1	1	-1	-1	-1	-1
8	1	1	1	-1	-1	-1
9	-1	-1	-1	1	-1	-1
10	-1	-1	1	1	-1	-1
11	1	-1	-1	1	-1	-1
12	1	-1	1	1	-1	-1
13	-1	1	-1	1	-1	-1
14	-1	1	1	1	-1	-1
15	1	1	-1	1	-1	-1
16	1	1	1	1	-1	-1
17	-1	-1	-1	-1	1	-1
18	-1	-1	1	-1	1	-1
19	1	-1	-1	-1	1	-1
20	1	-1	1	-1	1	-1
21	-1	1	-1	-1	1	-1
22	-1	1	1	-1	1	-1
23	1	1	-1	-1	1	-1
24	1	1	1	-1	1	-1
25	-1	-1	-1	1	1	-1
26	-1	-1	1	1	1	-1
27	1	-1	-1	1	1	-1
28	1	-1	1	1	1	-1
29	-1	1	-1	1	1	-1
30	-1	1	1	1	1	-1
31	1	1	-1	1	1	-1
32	1	1	1	1	1	-1
33	-1	-1	-1	-1	-1	1
34	-1	-1	1	-1	-1	1
35	1	-1	-1	-1	-1	1
36	1	-1	1	-1	-1	1
37	-1	1	-1	-1	-1	1
38	-1	1	1	-1	-1	1
39	1	1	-1	-1	-1	1
40	1	1	1	-1	-1	1

Table Continued Next Page

I. Continued:

RUN NO.	PHYSICAL PARAMETERS				OPERATING	
	1 = NA	2 = ND	3 = NP	4 = RL	5 = FR	6 = ZT
41	-1	-1	-1	1	-1	1
42	-1	-1	1	1	-1	1
43	1	-1	-1	1	-1	1
44	1	-1	1	1	-1	1
45	-1	1	-1	1	-1	1
46	-1	1	1	1	-1	1
47	1	1	-1	1	-1	1
48	1	1	1	1	-1	1
49	-1	-1	-1	-1	1	1
50	-1	-1	1	-1	1	1
51	1	-1	-1	-1	1	1
52	1	-1	1	-1	1	1
53	-1	1	-1	-1	1	1
54	-1	1	1	-1	1	1
55	1	1	-1	-1	1	1
56	1	1	1	-1	1	1
57	-1	-1	-1	1	1	1
58	-1	-1	1	1	1	1
59	1	-1	-1	1	1	1
60	1	-1	1	1	1	1
61	-1	1	-1	1	1	1
62	-1	1	1	1	1	1
63	1	1	-1	1	1	1
64	1	1	1	1	1	1

Table C-3: FLUENT Nozzle Coordinates (mm)

					Nozzle Coordinates							
					Left				Right			
Block	NA	ND	NP	RL	1	2	3	4	1	2	3	4
1	-	-	-	-	0,32.5	0,35	0,55	0,57.5	10,32.5	10,35	10,55	10,57.5
2	-	-	+	-	0,12.5	0,15	0,75	0,77.5	10,12.5	10,15	10,75	10,77.5
3	+	-	-	-	0,32.5	0,35	0,55	0,57.5	7.1,39.6	7.1,42.1	7.1,47.9	7.1,50.4
4	+	-	+	-	0,12.5	0,15	0,75	0,77.5	7.1,19.6	7.1,22.1	7.1,67.9	7.1,70.4
5	-	+	-	-	0,29	0,35	0,55	0,61	10,29	10,35	10,55	10,61
6	-	+	+	-	0,9	0,15	0,75	0,81	10,9	10,15	10,75	10,81
7	+	+	-	-	0,29	0,35	0,55	0,61	7.1,36.1	7.1,42.1	7.1,47.9	7.1,53.9
8	+	+	+	-	0,9	0,15	0,75	0,81	7.1,16.1	7.1,22.1	7.1,67.9	7.1,73.9
9	-	-	-	+	0,32.5	0,35	0,55	0,57.5	10,32.5	10,35	10,55	10,57.5
10	-	-	+	+	0,12.5	0,15	0,75	0,77.5	10,12.5	10,15	10,75	10,77.5
11	+	-	-	+	0,32.5	0,35	0,55	0,57.5	7.1,39.6	7.1,42.1	7.1,47.9	7.1,50.4
12	+	-	+	+	0,12.5	0,15	0,75	0,77.5	7.1,19.6	7.1,22.1	7.1,67.9	7.1,70.4
13	-	+	-	+	0,29	0,35	0,55	0,61	10,29	10,35	10,55	10,61
14	-	+	+	+	0,9	0,15	0,75	0,81	10,9	10,15	10,75	10,81
15	+	+	-	+	0,29	0,35	0,55	0,61	7.1,36.1	7.1,42.1	7.1,47.9	7.1,53.9
16	+	+	+	+	0,9	0,15	0,75	0,81	7.1,16.1	7.1,22.1	7.1,67.9	7.1,73.9

Notes: all values in mm, NP =distance from centerline to inside edge of nozzle, all nozzles 1cm long

III. Operating Parameters Flow Calculations

Table C-4A: Flow Calculations Spreadsheet											
DOEOPT RUNS FLOW CALCULATIONS (A)											
RUN	TEMP(K)	INLET DIA (mm)	AREA (m ²)	Ar					Zn		
					@300K		@inlet T				@inlet T
SET	TEMP(K)	(mm)	(m ²)	ml/min	m ³ /sec	mol/sec	m ³ /sec	g/sec	mol/sec	g/sec	m ³ /sec
doeopt1	1223	2.5	4.909E-06	300	5.000E-06	2.000E-04	2.007E-05	0.007561	6.20E-04	4.05E-02	6.22E-05
doeopt1	1223	2.5	4.909E-06	300	5.000E-06	2.000E-04	2.007E-05	0.007561	3.30E-03	2.16E-01	3.31E-04
doeopt1	1223	6	2.827E-05	300	5.000E-06	2.000E-04	2.007E-05	0.007561	6.20E-04	4.05E-02	6.22E-05
doeopt1	1223	6	2.827E-05	300	5.000E-06	2.000E-04	2.007E-05	0.007561	3.30E-03	2.16E-01	3.31E-04
doeopt1	1323	2.5	4.909E-06	300	5.000E-06	2.000E-04	2.171E-05	0.007561	6.20E-04	4.05E-02	6.73E-05
doeopt1	1323	2.5	4.909E-06	300	5.000E-06	2.000E-04	2.171E-05	0.007561	3.30E-03	2.16E-01	3.58E-04
doeopt1	1323	6	2.827E-05	300	5.000E-06	2.000E-04	2.171E-05	0.007561	6.20E-04	4.05E-02	6.73E-05
doeopt1	1323	6	2.827E-05	300	5.000E-06	2.000E-04	2.171E-05	0.007561	3.30E-03	2.16E-01	3.58E-04
midpoint	1273	4.25	1.419E-05	300	5.000E-06	2.000E-04	2.089E-05	0.007561	1.96E-03	1.28E-01	2.05E-04
doeopt2	1223	5	1.963E-05	300	5.000E-06	2.000E-04	2.007E-05	0.007561	7.28E-04	4.76E-02	7.31E-05
doeopt2	1223	5	1.963E-05	300	5.000E-06	2.000E-04	2.007E-05	0.007561	2.01E-03	1.31E-01	2.02E-04
doeopt2	1223	5	1.963E-05	300	5.000E-06	2.000E-04	2.007E-05	0.007561	3.30E-03	2.16E-01	3.31E-04
doeopt2	1223	8.25	5.346E-05	300	5.000E-06	2.000E-04	2.007E-05	0.007561	7.28E-04	4.76E-02	7.31E-05
doeopt2	1223	8.25	5.346E-05	300	5.000E-06	2.000E-04	2.007E-05	0.007561	2.01E-03	1.31E-01	2.02E-04
doeopt2	1223	8.25	5.346E-05	300	5.000E-06	2.000E-04	2.007E-05	0.007561	3.30E-03	2.16E-01	3.31E-04
doeopt2	1223	12	1.131E-04	300	5.000E-06	2.000E-04	2.007E-05	0.007561	7.28E-04	4.76E-02	7.31E-05
doeopt2	1223	12	1.131E-04	300	5.000E-06	2.000E-04	2.007E-05	0.007561	2.01E-03	1.31E-01	2.02E-04
doeopt2	1223	12	1.131E-04	300	5.000E-06	2.000E-04	2.007E-05	0.007561	3.30E-03	2.16E-01	3.31E-04
confirm	1223	8.5	5.674E-05	300	5.000E-06	2.000E-04	2.007E-05	0.007561	0.0025	1.63E-01	2.51E-04
confirm	1223	8.5	5.674E-05	300	5.000E-06	2.000E-04	2.007E-05	0.007561	0.0030	1.96E-01	3.01E-04
confirm	1223	8.5	5.674E-05	300	5.000E-06	2.000E-04	2.007E-05	0.007561	0.0035	2.29E-01	3.51E-04

IV. FLUENT Information

Table C-5: Operating Parameters Input Grid

TEMP	DIA	Zn			Se	
		-	+		-	+
-	-	16.7635	71.5514		10.4261	38.2289
-	+	2.9103	12.4221		1.8101	6.637
+	-	18.1342	77.4019		11.2786	41.3547
+	+	3.1483	13.4378		1.9581	7.1796
MOLE FRAC :		0.8428	0.9661		0.8662	0.9721

V. Design Optimization Study I

Table C-6: Study I Run Data

RUN NO.	its	Zn	ZnSe	yield	RUN NO.	its	Zn	ZnSe	yield
1	138	0.236	0.448	65.50	33	134	0.208	0.329	61.20
2	526	0.225	0.237	51.30	34	543	0.198	0.273	58.00
3	156	0.221	0.328	59.70	35	151	0.196	0.361	64.80
4	248	0.204	0.328	61.70	36	242	0.178	0.362	67.00
5	83	0.183	0.360	66.30	37	82	0.161	0.387	70.60
6	109	0.257	0.254	49.70	38	110	0.238	0.276	53.70
7	211	0.126	0.430	77.30	39	222	0.108	0.457	80.90
8	145	0.204	0.342	62.60	40	143	0.181	0.372	67.30
9	150	0.238	0.287	54.70	41	149	0.210	0.323	60.60
10	275	0.214	0.250	53.90	42	277	0.187	0.285	60.40
11	171	0.190	0.367	65.90	43	175	0.187	0.370	66.40
12	1010	0.200	0.352	63.80	44	1000	0.176	0.382	68.50
13	89	0.156	0.394	71.60	45	84	0.139	0.416	75.00
14	102	0.228	0.284	55.40	46	101	0.210	0.307	59.40
15	135	0.133	0.444	76.90	47	135	0.115	0.468	80.30
16	113	0.122	0.446	78.50	48	105	0.107	0.466	81.30
17	131	0.457	0.209	31.40	49	128	0.416	0.268	39.20
18	1000	0.409	0.160	21.10	50	1000	0.371	0.212	36.40
19	1000	0.425	0.274	39.20	51	1127	0.386	0.330	46.10
20	227	0.403	0.272	40.30	52	222	0.364	0.329	47.50
21	119	0.352	0.319	47.50	53	118	0.313	0.374	54.40
22	347	0.350	0.275	44.00	54	351	0.320	0.318	49.80
23	181	0.304	0.457	60.00	55	177	0.273	0.502	64.80
24	235	0.378	0.360	48.80	56	245	0.347	0.404	53.80
25	138	0.441	0.222	33.50	57	135	0.402	0.278	40.90
26	265	0.399	0.173	30.20	58	250	0.360	0.228	38.80
27	190	0.409	0.297	42.10	59	187	0.371	0.352	48.70
28	1000	0.425	0.282	40.00	60	1000	0.373	0.351	48.60
29	1000	0.325	0.370	53.20	61	99	0.289	0.421	59.30
30	204	0.313	0.285	47.70	62	204	0.280	0.329	54.00
31	121	0.263	0.518	66.30	63	127	0.252	0.535	68.00
32	130	0.279	0.485	63.50	64	128	0.248	0.529	68.10

Notes: 1) "its" = number of iterations for convergence
 2) Values are Volume Integrals

VI. Data Analysis

Table C-7: Study I Factor Analysis

RUN NO.	PHYSICAL PARAMETERS				OPERATING	
	1 = NA	2 = ND	3 = NP	4 = RL	5 = FR	6 = ZT
1	-65.5	-65.5	-65.5	-65.5	-65.5	-65.5
2	-51.3	-51.3	51.3	-51.3	-51.3	-51.3
3	59.7	-59.7	-59.7	-59.7	-59.7	-59.7
4	61.7	-61.7	61.7	-61.7	-61.7	-61.7
5	-66.3	66.3	-66.3	-66.3	-66.3	-66.3
6	-49.7	49.7	49.7	-49.7	-49.7	-49.7
7	77.3	77.3	-77.3	-77.3	-77.3	-77.3
8	62.6	62.6	62.6	-62.6	-62.6	-62.6
9	-54.7	-54.7	-54.7	54.7	-54.7	-54.7
10	-53.9	-53.9	53.9	53.9	-53.9	-53.9
11	65.9	-65.9	-65.9	65.9	-65.9	-65.9
12	63.8	-63.8	63.8	63.8	-63.8	-63.8
13	-71.6	71.6	-71.6	71.6	-71.6	-71.6
14	-55.4	55.4	55.4	55.4	-55.4	-55.4
15	76.9	76.9	-76.9	76.9	-76.9	-76.9
16	78.5	78.5	78.5	78.5	-78.5	-78.5
17	-31.4	-31.4	-31.4	-31.4	31.4	-31.4
18	-21.1	-21.1	21.1	-21.1	21.1	-21.1
19	39.2	-39.2	-39.2	-39.2	39.2	-39.2
20	40.3	-40.3	40.3	-40.3	40.3	-40.3
21	-47.5	47.5	-47.5	-47.5	47.5	-47.5
22	-44.0	44.0	44.0	-44	44	-44
23	60.0	60.0	-60.0	-60	60	-60
24	48.8	48.8	48.8	-48.8	48.8	-48.8
25	-33.5	-33.5	-33.5	33.5	33.5	-33.5
26	-30.2	-30.2	30.2	30.2	30.2	-30.2
27	42.1	-42.1	-42.1	42.1	42.1	-42.1
28	40.0	-40.0	40.0	40	40	-40
29	-53.2	53.2	-53.2	53.2	53.2	-53.2
30	-47.7	47.7	47.7	47.7	47.7	-47.7
31	66.3	66.3	-66.3	66.3	66.3	-66.3
32	63.5	63.5	63.5	63.5	63.5	-63.5
33	-61.2	-61.2	-61.2	-61.2	-61.2	61.2
34	-58.0	-58.0	58.0	-58	-58	58
35	64.8	-64.8	-64.8	-64.8	-64.8	64.8
36	67.0	-67.0	67.0	-67	-67	67
37	-70.6	70.6	-70.6	-70.6	-70.6	70.6
38	-53.7	53.7	53.7	-53.7	-53.7	53.7
39	80.9	80.9	-80.9	-80.9	-80.9	80.9
40	67.3	67.3	67.3	-67.3	-67.3	67.3
41	-60.6	-60.6	-60.6	60.6	-60.6	60.6
42	-60.4	-60.4	60.4	60.4	-60.4	60.4
43	66.4	-66.4	-66.4	66.4	-66.4	66.4

Table Continued Next Page

VI. Continued

RUN NO.	PHYSICAL PARAMETERS				OPERATING	
	1 = NA	2 = ND	3 = NP	4 = RL	5 = FR	6 = ZT
44	68.5	-68.5	68.5	68.5	-68.5	68.5
45	-75.0	75.0	-75.0	75	-75	75
46	-59.4	59.4	59.4	59.4	-59.4	59.4
47	80.3	80.3	-80.3	80.3	-80.3	80.3
48	81.3	81.3	81.3	81.3	-81.3	81.3
49	-39.2	-39.2	-39.2	-39.2	39.2	39.2
50	-36.4	-36.4	36.4	-36.4	36.4	36.4
51	46.1	-46.1	-46.1	-46.1	46.1	46.1
52	47.5	-47.5	47.5	-47.5	47.5	47.5
53	-54.4	54.4	-54.4	-54.4	54.4	54.4
54	-49.8	49.8	49.8	-49.8	49.8	49.8
55	64.8	64.8	-64.8	-64.8	64.8	64.8
56	53.8	53.8	53.8	-53.8	53.8	53.8
57	-40.9	-40.9	-40.9	40.9	40.9	40.9
58	-38.8	-38.8	38.8	38.8	38.8	38.8
59	48.7	-48.7	-48.7	48.7	48.7	48.7
60	48.6	-48.6	48.6	48.6	48.6	48.6
61	-59.3	59.3	-59.3	59.3	59.3	59.3
62	-54.0	54.0	54.0	54	54	54
63	68.0	68.0	-68.0	68	68	68
64	68.1	68.1	68.1	68.1	68.1	68.1
AVG -	51.5	50.2	59.1	51.9	65.3	53.9
AVG+	61.5	62.8	53.9	58.6	47.7	59.2
DELTA	10.0	12.6	5.2	6.7	17.6	5.3
WT	0.57	0.72	0.30	0.38	1.00	0.30
RANK	3	2	5	4	1	5
SIG	YES	YES	NO	NO	YES	NO

VII. Interactions

Table C-8: Study I Interactions Analysis (Yield)

RUN	No.	12	13	14	15	16	23	24	25	26	34	35	36	45	46	56	(%)
	1	65.5	65.5	65.5	65.5	65.5	65.5	65.5	65.5	65.5	65.5	65.5	65.5	65.5	65.5	65.5	65.5
	2	51.3	-51.3	51.3	51.3	51.3	-51.3	51.3	51.3	51.3	-51.3	-51.3	-51.3	51.3	51.3	51.3	51.3
	3	-59.7	-59.7	-59.7	-59.7	-59.7	59.7	59.7	59.7	59.7	59.7	59.7	59.7	59.7	59.7	59.7	59.7
	4	-61.7	61.7	-61.7	-61.7	-61.7	-61.7	61.7	61.7	61.7	-61.7	-61.7	-61.7	61.7	61.7	61.7	61.7
	5	-66.3	66.3	66.3	66.3	66.3	-66.3	-66.3	-66.3	-66.3	66.3	66.3	66.3	66.3	66.3	66.3	66.3
	6	-49.7	-49.7	49.7	49.7	49.7	49.7	-49.7	-49.7	-49.7	-49.7	-49.7	-49.7	49.7	49.7	49.7	49.7
	7	77.3	-77.3	-77.3	-77.3	-77.3	-77.3	-77.3	-77.3	-77.3	77.3	77.3	77.3	77.3	77.3	77.3	77.3
	8	62.6	62.6	-62.6	-62.6	-62.6	62.6	-62.6	-62.6	-62.6	-62.6	-62.6	-62.6	62.6	62.6	62.6	62.6
	9	54.7	54.7	-54.7	54.7	54.7	54.7	-54.7	54.7	54.7	-54.7	54.7	54.7	-54.7	-54.7	54.7	54.7
	10	53.9	-53.9	-53.9	53.9	53.9	-53.9	-53.9	53.9	53.9	53.9	-53.9	-53.9	-53.9	-53.9	53.9	53.9
	11	-65.9	-65.9	65.9	-65.9	-65.9	65.9	-65.9	65.9	65.9	-65.9	65.9	65.9	-65.9	-65.9	65.9	65.9
	12	-63.8	63.8	63.8	-63.8	-63.8	-63.8	-63.8	63.8	63.8	63.8	-63.8	-63.8	-63.8	-63.8	63.8	63.8
	13	-71.6	71.6	-71.6	71.6	71.6	-71.6	71.6	-71.6	-71.6	-71.6	71.6	71.6	-71.6	-71.6	71.6	71.6
	14	-55.4	-55.4	-55.4	55.4	55.4	55.4	55.4	-55.4	-55.4	55.4	-55.4	-55.4	-55.4	-55.4	55.4	55.4
	15	76.9	-76.9	76.9	-76.9	-76.9	-76.9	76.9	-76.9	-76.9	-76.9	76.9	76.9	-76.9	-76.9	76.9	76.9
	16	78.5	78.5	78.5	-78.5	-78.5	78.5	78.5	-78.5	-78.5	78.5	-78.5	-78.5	-78.5	-78.5	78.5	78.5
	17	31.4	31.4	31.4	-31.4	31.4	31.4	31.4	-31.4	31.4	31.4	-31.4	31.4	-31.4	31.4	-31.4	31.4
	18	21.1	-21.1	21.1	-21.1	21.1	-21.1	21.1	-21.1	21.1	-21.1	21.1	-21.1	-21.1	21.1	-21.1	21.1
	19	-39.2	-39.2	-39.2	39.2	-39.2	39.2	39.2	-39.2	39.2	39.2	-39.2	39.2	-39.2	39.2	-39.2	39.2
	20	-40.3	40.3	-40.3	40.3	-40.3	-40.3	40.3	-40.3	40.3	-40.3	40.3	-40.3	-40.3	40.3	-40.3	40.3
	21	-47.5	47.5	47.5	-47.5	47.5	-47.5	-47.5	47.5	-47.5	47.5	-47.5	47.5	-47.5	47.5	-47.5	47.5
	22	-44.0	-44.0	44	-44.0	44.0	44.0	-44.0	44.0	-44.0	-44.0	44.0	-44.0	-44.0	44.0	-44.0	44.0
	23	60.0	-60.0	-60	60.0	-60.0	-60.0	-60.0	60.0	-60.0	60.0	-60.0	60.0	-60.0	60.0	-60.0	60.0
	24	48.8	48.8	-48.8	48.8	-48.8	48.8	-48.8	48.8	-48.8	-48.8	48.8	-48.8	-48.8	48.8	-48.8	48.8
	25	33.5	33.5	-33.5	-33.5	33.5	33.5	-33.5	-33.5	33.5	-33.5	-33.5	33.5	33.5	-33.5	-33.5	33.5
	26	30.2	-30.2	-30.2	-30.2	30.2	-30.2	-30.2	-30.2	30.2	30.2	30.2	-30.2	30.2	-30.2	-30.2	30.2
	27	-42.1	-42.1	42.1	42.1	-42.1	42.1	-42.1	-42.1	42.1	-42.1	-42.1	42.1	42.1	-42.1	-42.1	42.1
	28	-40.0	40.0	40	40.0	-40.0	-40.0	-40.0	-40.0	40.0	40.0	40.0	-40.0	40.0	-40.0	-40.0	40.0
	29	-53.2	53.2	-53.2	-53.2	53.2	-53.2	53.2	53.2	-53.2	-53.2	-53.2	53.2	53.2	-53.2	-53.2	53.2
	30	-47.7	-47.7	-47.7	-47.7	47.7	47.7	47.7	47.7	-47.7	47.7	47.7	-47.7	47.7	-47.7	-47.7	47.7
	31	66.3	-66.3	66.3	66.3	-66.3	-66.3	66.3	66.3	-66.3	-66.3	-66.3	66.3	66.3	-66.3	-66.3	66.3
	32	63.5	63.5	63.5	63.5	-63.5	63.5	63.5	63.5	-63.5	63.5	63.5	-63.5	63.5	-63.5	-63.5	63.5
	33	61.2	61.2	61.2	61.2	-61.2	61.2	61.2	61.2	-61.2	61.2	61.2	-61.2	61.2	-61.2	-61.2	61.2
	34	58.0	-58.0	58	58.0	-58.0	-58.0	58.0	58.0	-58.0	-58.0	-58.0	58.0	58.0	-58.0	-58.0	58.0
	35	-64.8	-64.8	-64.8	-64.8	64.8	64.8	64.8	64.8	-64.8	64.8	64.8	-64.8	64.8	-64.8	-64.8	64.8
	36	-67.0	67.0	-67	-67.0	67.0	-67.0	67.0	67.0	-67.0	-67.0	-67.0	67.0	67.0	-67.0	-67.0	67.0
	37	-70.6	70.6	70.6	70.6	-70.6	-70.6	-70.6	-70.6	70.6	70.6	70.6	-70.6	70.6	-70.6	-70.6	70.6
	38	-53.7	-53.7	53.7	53.7	-53.7	53.7	-53.7	-53.7	53.7	-53.7	-53.7	53.7	53.7	-53.7	-53.7	53.7
	39	80.9	-80.9	-80.9	-80.9	80.9	-80.9	-80.9	-80.9	80.9	80.9	80.9	-80.9	80.9	-80.9	-80.9	80.9
	40	67.3	67.3	-67.3	-67.3	67.3	67.3	-67.3	-67.3	67.3	-67.3	-67.3	67.3	67.3	-67.3	-67.3	67.3
	41	60.6	60.6	-60.6	60.6	-60.6	60.6	-60.6	60.6	-60.6	-60.6	60.6	-60.6	-60.6	60.6	-60.6	60.6
	42	60.4	-60.4	-60.4	60.4	-60.4	-60.4	-60.4	60.4	-60.4	60.4	-60.4	60.4	-60.4	60.4	-60.4	60.4
	43	-66.4	-66.4	66.4	-66.4	66.4	66.4	-66.4	66.4	-66.4	-66.4	66.4	-66.4	-66.4	66.4	-66.4	66.4

VIII: FLUENT Information (Study II)

Table C-9: Study II: FLUENT DDN Coordinates (mm)

Config	Physical Factors		REACTOR				NOZZLES							
	NDZ	NDS	Left		Right		Left				Right			
Block	NDZ	NDS	1	2	1	2	Se	Se	Zn	Zn	Se	Se	Zn	Zn
1	-	-	0,0	0,90	900,0	900,90	0,30	0,35	0,55	0,60	10,30	10,35	10,55	10,60
2	0	-	0,0	0,90	900,0	900,90	0,30	0,35	0,55	0,63.5	10,30	10,35	10,55	10,63.5
3	+	-	0,0	0,90	900,0	900,90	0,30	0,35	0,55	0,67	10,30	10,35	10,55	10,67
4	-	0	0,0	0,90	900,0	900,90	0,26.5	0,35	0,55	0,60	10,26.5	10,35	10,55	10,60
5	0	0	0,0	0,90	900,0	900,90	0,26.5	0,35	0,55	0,63.5	10,26.5	10,35	10,55	10,63.5
6	+	0	0,0	0,90	900,0	900,90	0,26.5	0,35	0,55	0,67	10,26.5	10,35	10,55	10,67
7	-	+	0,0	0,90	900,0	900,90	0,23	0,35	0,55	0,60	10,23	10,35	10,55	10,60
8	0	+	0,0	0,90	900,0	900,90	0,23	0,35	0,55	0,63.5	10,23	10,35	10,55	10,63.5
9	+	+	0,0	0,90	900,0	900,90	0,23	0,35	0,55	0,67	10,23	10,35	10,55	10,67

164

IX. Key to Study II Physical Factors

Table C-10: Factor Key

Factor	Symbol	Levels (mm)		
		-	0	+
Nozzle Diameter Zn	NDZ	5.0	8.5	12
Nozzle Diameter Se	NDS	5.0	8.5	12

X. Design Optimization Study II Results I

Table C-11: Study II Run Data and Results (Yield)

DESIGN MATRIX GRID: 3(4-1) Results

RUN NO.	CONFIG NO.	NDZ	NDS	FRZ	FRS	YIELD(%)
1	1	65.7	65.7	65.7	65.7	65.7
2	9	38.7	38.7	38.7	38.7	38.7
3	5	21.3	21.3	21.3	21.3	21.3
4	8	69.2	69.2	69.2	69.2	69.2
5	4	21.6	21.6	21.6	21.6	21.6
6	3	42.1	42.1	42.1	42.1	42.1
7	6	84.1	84.1	84.1	84.1	84.1
8	2	45.6	45.6	45.6	45.6	45.6
9	7	9.5	9.5	9.5	9.5	9.5
10	9	86.3	86.3	86.3	86.3	86.3
11	5	64.9	64.9	64.9	64.9	64.9
12	1	70.4	70.4	70.4	70.4	70.4
13	4	77.3	77.3	77.3	77.3	77.3
14	3	79.3	79.3	79.3	79.3	79.3
15	8	37.2	37.2	37.2	37.2	37.2
16	2	84.0	84.0	84.0	84.0	84.0
17	7	27.6	27.6	27.6	27.6	27.6
18	6	62.4	62.4	62.4	62.4	62.4
19	7	80.6	80.6	80.6	80.6	80.6
20	1	64.6	64.6	64.6	64.6	64.6
21	9	64.8	64.8	64.8	64.8	64.8
22	3	79.7	79.7	79.7	79.7	79.7
23	8	67.8	67.8	67.8	67.8	67.8
24	4	44.0	44.0	44.0	44.0	44.0
25	7	77.7	77.7	77.7	77.7	77.7
26	6	79.4	79.4	79.4	79.4	79.4
27	2	66.6	66.6	66.6	66.6	66.6
AVG	LOW	50.9	66.4	78.3	44.2	59.72
AVG	MID	59.7	59.5	54.4	65.5	
AVG	HIGH	68.5	53.2	46.5	69.5	
RANGE	H - L	17.6	-13.3	-31.8	25.3	

XI. Design Optimization Study II Results U

Table C-12: Study II Run Data and Results (Plugging Factor)

DESIGN MATRIX GRID: 3(4-1) Results						
RUN NO.	CONFIG NO.	Plugging				
		NDZ	NDS	FRZ	FRS	Factor
1	1	0.00362	0.00362	0.00362	0.00362	0.00362
2	9	0.00667	0.00667	0.00667	0.00667	0.00667
3	5	0.0156	0.0156	0.0156	0.0156	0.0156
4	8	0.00704	0.00704	0.00704	0.00704	0.00704
5	4	0.00689	0.00689	0.00689	0.00689	0.00689
6	3	0.00424	0.00424	0.00424	0.00424	0.00424
7	6	0.00502	0.00502	0.00502	0.00502	0.00502
8	2	0.00286	0.00286	0.00286	0.00286	0.00286
9	7	0.0307	0.0307	0.0307	0.0307	0.0307
10	9	0.00629	0.00629	0.00629	0.00629	0.00629
11	5	0.00456	0.00456	0.00456	0.00456	0.00456
12	1	0.00224	0.00224	0.00224	0.00224	0.00224
13	4	0.00233	0.00233	0.00233	0.00233	0.00233
14	3	0.00643	0.00643	0.00643	0.00643	0.00643
15	8	0.0133	0.0133	0.0133	0.0133	0.0133
16	2	0.00443	0.00443	0.00443	0.00443	0.00443
17	7	0.0379	0.0379	0.0379	0.0379	0.0379
18	6	0.00168	0.00168	0.00168	0.00168	0.00168
19	7	0.00495	0.00495	0.00495	0.00495	0.00495
20	1	0.00283	0.00283	0.00283	0.00283	0.00283
21	9	0.0029	0.0029	0.0029	0.0029	0.0029
22	3	0.00845	0.00845	0.00845	0.00845	0.00845
23	8	0.00306	0.00306	0.00306	0.00306	0.00306
24	4	0.00327	0.00327	0.00327	0.00327	0.00327
25	7	0.00429	0.00429	0.00429	0.00429	0.00429
26	6	0.00645	0.00645	0.00645	0.00645	0.00645
27	2	0.000821	0.000821	0.000821	0.000821	0.000821
AVG	LOW	0.01045	0.00399	0.00516	0.00918	0.007364
AVG	MID	0.00629	0.00564	0.00863	0.00880	
AVG	HIGH	0.00535	0.01246	0.00831	0.00411	
RANGE	H - L	-0.0051	0.00847	0.00315	-0.00507	

Note: Highlighted results indicates runs in excess of 0.01 plugging criteria.

VITA

Christopher D. Shay

Candidate for the Degree of

Master of Science

Thesis: DESIGN AND OPTIMIZATION OF A HIGH TEMPERATURE REACTOR FOR THE PRODUCTION OF II-VI COMPOUNDS VIA COMPUTER MODELS AND STATISTICAL EXPERIMENTATION

Major Field: Chemical Engineering

Professional Background:

Education: Received Bachelor of Science degree in Chemistry from the University of Texas at Dallas, Richardson, Texas in December 1991. Completed the requirements for the Master of Science degree in Chemical Engineering at Oklahoma State University in December 1998.

Experience: Employed as a research and teaching assistant at Oklahoma State University, School of Chemical Engineering, 1997-1998. Employed as summer (1997) engineering intern, Eagle-Picher Industries, Inc. Employed as research chemist at SACHEM, Inc., Austin, Tx., 1993-1996.

Member: American Chemical Society, The Electrochemical Society, American Institute of Chemical Engineers (student).